213-219B

701-708B 709-717B

591-594B 149-153B

595-597A

459-469A

5-12B

1281-1286A

2163-2173A

1003-1012A

1626-1631A

1339-1351A

281-288B 1099-1102A

411-419A

245-246A

101-107B

399-4024

983-994A

2221-2229

1155-1163A

2193-2203A

1855-1864A

1819-1828A

339-345A

501-510A

679-691A

250-251A

91-99B

1485-1490A

729-733A 2087-2092A

# **Combined Author Index**

Aaronson, H.I. Ahel O 729-732B Acholonu, C.C. 345-349B Adasczik C Ahman, L. Alam, M. 400-403B Altstetter, C.J. 719-728A Anello, J. Ardeil, A.J. Argyropoulos, S.A Arsenault, R.J. 47-58B Asaki, Z. Atkinson, M. 1185-1192A 1117-1127A Ayers, J.D

Baer, D.R. Baeslack, W.A. III Bain, K.R. Baker, I. Ballal N.B. Barcik, J Barrera, E.V. Bay, B. Beck, C.G.

Beckerman, L.P. Beevers, C.J. Belton, G.R.

Bensussan, P.L. Berggren, M.H. Berke, N.S. Berstein, I.M. Bertram, L.A. Beswick, J. Bhambri, S.K. Bhattacharya, D.

Biancaniello, F.S.

Bibby, M. Biss, V. Biörkman B Blackburn, D.A. Blanchard, W.K., Jr. Block-Bolten, A Bockris, J.O'M Boettinger, W.J. Boisvert, R.F. Bourgeois, T. Bowden, D.M. Bowker J Bradley, J.R. Bretz, P.E. Brewer, L.

Bridge, M.R. Brimacombe, J.K.

Brisley, R.J. Brown, J.M. Brown, L.C.

Brown, R.D. Buck, O. Buene, L. Bui, R.T. Burke, M.A. Bustos, A.A

Carlsson, G Carpenter, S.H. Carr, M.J. Carter, R.D. Castillo R Castleman, L.S. Chakrabortty, S.B.

Chakravarti, A. Chan, C. Chan, K.S.

Chang, A.Y Chang, K.M. Chang, M. Chang, P.-H. 427.435A 1287-1288A 1623-1626A 117-125B 1829-1835A 693-699A 1531-1543A 1571-1577A 127-133B

Chang, Y.A.

Charatte A

Chen, C.H. Chen, M.M.

Cheong, D.-S.

Chevey, P.M Chewey, P.M Chilton, J.M. Cho, S.-J. Chochol, M.

Choo, W.Y.

Chu, M.G. Chu, W.-Y

Chuang, Y.-Yu. Chuck, W.

Churn, K.S.

Clark, W.A.T

Cline, H.E.

Clyne, T.W. Cohen, J.B. Cohen, M.

Coltters, R.G.

Cook, J.M. Coons, W.C.

Coriell, S.R.

Cooperrider, M.W.

Charpentier, P.L.

Charrevron P.O.

853-860A 1948-1952A 381-388A 1129-1136A 71-75R 406A 1415-1430A 287-297A 23-28A 661-670A 1465-1474A 555-563A 517-521B 655-661B

1379-1387A

511-516B

639-648A

461-469B

39-46B 55-66A

1281-1286A

2117-2124A

487-492B 1687-1698A

2093-2095A

1287-1288A 369-379A

2075-2085A

581-589B

243-250B

493-509B

307-318B

135-139B

449-458A

1969-1975A 1613-1621A

147-153A 1787-1805A

487-492B

661-670A

633-640B

555-563A

229-236A

1359-1366A 511-517A

1229-1245A

299-305B 2175-2184A

1579-1588A

2097-2101A

323-329A

756-760A

337-344B

399-402A 685-694B

671-678A

73-86A

1849-1853A 347-368A

29-31A

11-22A

77-89R

67-72A

107-120A 433.440B Courtney, T.H. Craig, B.D. 393-395B 1953-1955A Cramb A W 117-125B 299-306A Crombie, E.A Crooks, M.J. Crooks, R.E. 250-251A 547-562B 547-562B Cuddy, L.J. 1987-1997A Cummings, D.L. 55-66A 299-305B

> Dai W Dandapani, B. David, S.A. Davidson, D.L. Davis, D.G. Dayananda, M.A. De Jonghe, L.C. de Malherbe, M.C.

DeArdo, A.J. Debroy, T. DeCarlo, J.L. Dell, M.B. Denholm, W.T DiGiallonardo, S.L. Dilewijns, J. Doane, R.E. Donald, J.K. Donoso, E. Dressler, B Drouven, B. Dupre, B. Dutta, V.B.

Eagar, T.W. Easterling, K.E. Ebara, R. Eckelmeyer, K.H. El-Kaddah, N.

Dwivedi RK

El-Naggar, M.M.A.A. El-Rahaiby, S.K. Eldis, G.T. Elliott, J.F Endo, T Erhart, H. Eriksson, G. Esaklul, K

Esdaile, J.D. Espiell, F Evans, J.W Eylon, D.

43-54A 1921-1930A Fang, Q.T. Fearing, V.L. Feng, C.R. 329-335B Feng. W.X 487-492B 1699-1710A Finnemore, D.K. Fitzsimons, G. 173-181B 719-728A Fix R

147-153A

693-699A

663-676B

1303-1310A

2087-2092A

1921-1930A

2125-2137A

331-338A

747.75AA

427-435A

573.586A

369-381B

819-833A

517-521B

433-440B

2109-2115A 2117-2124A

2125-2137A

1065-1074A 565-572A

23-28A 1711-1719A

1137-1145A

1367-1377A 87-98A

639-648A

319.327B

605-608B

67-72A

649-659A

685-694B

501-510A

241-243A

400-403B 641-644B

2155-2161A

277-280B 1311-1317A

121-128A

23-34B 433-440B

693-699A

235-242B

383-391B

471-478B

523-528B

217-227A

461-469B

229-233B

734-736B 623-631B

183-197A

1493-1496A

13-18B

33-41A

1193-1207A

1999-2008A

1505-1507A

1579-1588A

1931-1940A

655-661B

1623-1626A

1013-1017A

1519-1529A

1977-1986A 1741-1752A

Flemings, M.C. 1741-1752A Fletcher M.A. 1137-1145A Flewitt, P.E.J Floreen, S. 1075-1080A 1953-1955A

Fong, H.S. Ford, J.D. Fraser, H.L. Fray, D.J. Friesel, M. Froes, F.H

Fujimura, Y

Gao, M. García-Cordovilla, C. Garcia-Rocha, J. Gasior, W. Gaskell, D.R. Geiger GH Gerberich, W.W. German, R.M.

Geyling, F.T. Ghali, E. Gherardi, F.

Ghosh, A. Ghosh, A.K Gibson, E.D. Gibson, J.K. Gillis, P.P. Gingerich, K.A.

Gleitzer, C. Glicksman, M.E.

Gokhale, A.M. Goldak, J. Goldstein, J.I.

Goto, S. Gougeon, M. Gourdin, W.H. Grant, N.J. Gray, N.B. Greulich, F.A. Grob, B. Grobner, P.J. Grugel, R.N. Grushko, B

Guha, A. Guo, J. Guthrie, R.I.L. Gysler A

Hack J.F.

250-251A 1319-1330A 633-640B 183-186B Hahn, G.T. 59-70B Hajika, K. 725-726B Hall, E.L. 19-22B 1173-1183A Hamm, R. Hammond, C 663-676B Hanafee, J.E. 2029-2038A Hanawa, K. Hanna, M.D. 2241-2246A 511-516B 875-888A 889-900A 1311-1317A

Hänninen, H Hannula, S.-P. Hansen, N. Hao, S... Hara, S. Harris, R. Hart, R.G. Hattori, I. Hauk, V.M.

2117-2124A 245-246A 1571-1577A 1209-1220A 283-286A 241-243A 1837-1847A 241-243A

1303-1310A 2095-2097A 173-181B 1963-1967A 707-718A 783-792A 5-10A 1643-1651A 719-723B 149-153B 135-139B 1849-1853A 1493-1496A 183-197A

248.2494

735-746A 389-391A 939-9414 563-571B 617-622B 875-888A 889-900A 121-128A

331-338A 747-754A 1103-1110A 1963-1967A 605-608B 1331-1334A 71-75B 283-286A 2075-2085A 133-138A 2075-2085A 383-391B 2117-2124A

995-1001A 1081-1088A 1643-1651A 243-245A 391-393A 299-305B 861-865A 867-874A 1677-1685A 535-541B 383-391B 1653-1664A 1491-1493A 77-89B 1955-1958A 529-533B 1379-1387A 1003-1012A 1626-1631A 609-620A 1623-1626A 1331-1334A 47-58B 1229-1245A

11-22A 756-760A 1389-1396A 1397-1405A 947-959A 127-133B 793-811A

1597-1605A

1873-1881A

1787-1805A 813-817A 121-128A 1147-1153A 595-597A 459-469A 2205-2211A 2205-2211A 287-297A 1819-1828A 563-571B 393-395B 1731-1739A

Haunschild, P.A. Hayes, P.C.

Heldt, L.A. Hellawell A

Henein, H. Henry, M.F. Heusler, K Hickl, A.J. Hillert, M. Hirth, J.P. Hong, C.P.

Hsiao, C.-M. Huang, S.C. Hunt, J.D. Hutchings, R. Hwang, C.M. Hyspecka, L

Imbert, C. Immarigeon, J.-P. Immarigeon, J.-P.A. Inouye, H. Inouye, H. Ishida, K. Ishii. H.

Jablonski, D.A. 107-120A Jackson, A.G. 248-249A Jimbo, I. Jin, Z.-M. Jiricny, V. Jones, R.H. Jones, S.E.

535-541B 5-12B 623-631B 853-860A 129-132A 133-138A Jungling, T.L. 2231-2240A 307-312A 1515-1517A 501-510A

Kabassis, H. Kandeil A Y Kane, R.H. Kang, C.T. 5-10A 403-405A Kanome, O. Kato M Kaufmann, E.N Kawabe, H. Kawarazaki T Kay, D.A.R. Keefe, P.W Kelly, T.F. Kerans, R.J. Kestenbach, H.-J. Khan, P.A.A. Kikuchi, M. Kim, C.H. Kim. C.W. Kim, D. Kim, H.-M. Kim, H.J. Kim, J.I. Kimura, R.T. Kimura, Y Kirkaldy, J.S.

Kishimoto, N. Kiuchi, K. Klepaczko, J.R. Kleppa, O.J.

Kobayashi, K.F. Koizumi, T. Kondo, Y. Konitzer, D.G. Koria, S.C. Korzekwa, D.A. Koss, D.A.

Kou, S. Kozuka, Z. Kramer LR Krawitz, A.D.

Krehl, M.

609-615B 755-756A 1787-1805A 1273-1280A 679-6914 1865-1871A 819-833A 1721-1729A 1496-1499A 641-644B 1431-1436A 393-395A 649-659A 403-406B 395-399 2213-2219A 2213-2219A 213-219B 91-99B 101-107B 545-553A 396-400R 199-202A 901-911A 203-208A 357-368B 573-580B 307-312A 1731-1739A 127-133B 149-153B 109-116B 323-329A 1281-1286A 1165-1171A 329-335B 141-147B 1571-1577A

347-368A

1545-1554A

1111-1116A

Krzewski Kuhn, H.	A.	451-459B 1837-1847A	Mohamed, F.A. Moody, N.R.	1893-1904A 1955-1958A	Plichta, M.R. Podsiadly, H.	427-435A 451-459B	Sherman, R. Shewmon, P.	1397-1405A 487-494A
Kumar, P Kundrat.		1099-1102A 663-676B	Moore, K. Morris, D.R.	1117-1127A 645-654B	Podsiadly, J. Poirier, D.R.	451-459B 163-172B	Shewmon, P.G.	495-499A 2021-2027A
Kurose.	Υ.	141-147B	Morris, J.W., Jr.	2213-2219A	Prange, R.	281-288B	Shiflet, G.J.	1287-1288A
Kuwano, Kwon, H.		621-626A 393-395A	Morrish, K.A. Moser, Z.	2125-2137A 543-546B	Prasad, Y.V.R.K. Pratt, W.	1883-1892A 755-756A	Shingu, P.H.	471-480A 307-312A
			Mostert, R.J.	2185-2191A	Price, D.	913-922A	Shiohara, Y.	1303-1310A
			Moteff, J. Moukassi, M.	248-249A 383-391B	Price, D.W. Prioul, C.	235-242B 2193-2203A	Sick, G.	736-739B 729-732B
Lakshma	anan, V.K.	541-544A 545-553A	Muddle, B.C.	1089-1098A	Purdy, G.R.	1055-1062A	Sieradzki, K.	1941-1946A
Landsbe	erg, A.	695-700B	Mueller, R.R.	783-792A		1499-1502A	Sigworth, G.K. Silberstein, R.P.	277-282A 2147-2154A
Lanna M	/ W	732-734B 109-116B	Mukherjee, A.K.	1437-1441A 1443-1450A	Pussegoda, N.	1499-1502A	Simkovich, G.	245-246A
Lange, K Langer, v	J.S.	961-966A		1763-1767A			Simpson, M. Sinha, S.N.	2095-2097A 441-449B
Lankford	đ, J.	1579-1588A	Mukherjee, K. Mullins, F.D.	755-756A 1948-1952A	Queneau, P.B.	433-440B		595-598B
Larbales	stier, D.C.	1931-1940A 843-852A	Murakami, Y.	2029-2038A			Siviour, N.G. Sohn, H.Y.	1311-1317A 403-406B
Lark, K.A	A.	481-486A	Murray, G.T.	597-600A 261-268A	Raghavan, M.	700 7004	John, H. T.	441-449B
Larson, I Laughlin	D.J., Jr.	2147-2154A 939-941A	Murray, J.L.	201-200A	Hagnavan, M.	783-792A 1299-1302A	Colook A	595-598B 901-911A
Le. Y.		1165-1171A			Rajan, K.	339-345A	Solecki, A. Soliman, M.S.	1893-1904A
Lee, D. Y	,	1777-1779A 1415-1430A	Nagamori, M.	441-449B	Ranucci, D.	1335-1338A 1331-1334A	Solorzano, I.G. Somboonsuk, K.	1055-1062A 967-975A
Lee, E.W		511-517A	Nair, S.V.	595-598B 1865-1871A	Rao, Y.K.	396-400B	Song, YD.	1503-1505A
Lee, H-C		555-563A 734-736B	Naito, T.	1431-1436A	Rapp, R.A.	19-22B 195B	Spitzig, W.A.	1259-1264A
Lee. H.G		396-400B	Nakahara, S. Narayan, C.	1963-1967A 861-865A	парр, п.н.	2231-2240A	Sponholz, R.O. Spurling, R.A.	313-321A 813-817A
Lee, M. Lee, R.G		2241-2246A 243-250B		867-874A		2241-2246A 573-586A	Squires, D.R.	1947-1948A
L'Espera		913-922A	Nelson, J.G. Newman, R.C.	597-600A 1941-1946A		587-593A	Sridhar Rao, Ch. Srinivasan, V.	259-275B 481-486A
		923-929A	Niasong, X.	2101-2102A	Dantasi D.V	765-782A	Sriramamurthy, A.M.	1905-1919A
Leverant	t, G.H.	1389-1396A 1397-1405A	Nieh, T.G.	139-146A	Rastogi, P.K. Raynaud, G.M.	257-260A 573-586A	St. John, D.H.	701-708B 709-717B
Li, WX.		2087-2092A	Nishizawa, T. Nix, W.D.	1819-1828A 1769-1775A		587-593A	Staffansson, LI.	319-327B
Liang, W Liaw, P.I	V.W.	403-405A 693-699A	Nordgren, A.	33-41A	Reddy, R.G.	33-37B 345-349B	Stark, J.P. Starke, E.A., Jr.	1415-1430A 511-517A
Liddell, F	K.C.	213-219B	Numata, H. Núñez, C.	39-46B 229-233B	Rehm, R.G.	2125-2137A	Oldine, E.A., of.	555-563A
Lieberma Lin, FS	ann, H.H.	155-161B 1873-1881A		13-18B	Reilly, I.G. Reuben, R.L.	726-729B 639-648A		1209-1220A 1229-1245A
Lin, F.S.		1209-1220A		221-228B	Rey, P.	433-440B		1687-1698A
Lindholm	. 110	1229-1245A 2097-2101A			Richards, G.G. Richarz, W.	77-89B 529-533B		1873-1881A 1367-1377A
Lipsitt, F		481-486A	O'Brien, T.	117-125B	Ricou, R.	471-478B	Staudhammer, K.P.	1607-1612A
10.07		395-399A 701-706A	Ochiai, S.	173-181A 535-541B	Ridley, N.	1019-1036A	Steeds, J.W. Steinmetz, P.	1299-1302A 383-391B
Liu, C.T. Liu, J.M.		1247-1251A	Ogawa, O. Ogino, Y.	519-526A	Rigsbee, J.M.	1443-1450A 719-728A	Stevens, R.A.	707-718A
		1253-1258A	Ogura, T.	835-842A	Rioja, R.J.	939-941A	Steward, F.R.	645-654B
Livesey.	D.W.	1289-1292A 1443-1450A	Okabayashi, K.	1563-1570A 2247-2249A	Ritchie, R.O. Ritter, A.M.	1193-1207A 1339-1351A	Stickels, C.A. Stobbs, W.M.	2101-2102A 1977-1986A
Loberg,	В.	33-41A	Okabe, T.	609-615B	Roberts, W.T.	913-922A	Stout, M.G.	1607-1612A
Lograss- Loretto,	io, T.A. M H	1003-1012A 913-922A	Okazaki, M. Okuwaki, A.	1731-1739A 609-615B	Robertson, I.M.	923-929A 269-276A	Straver, W.T.M. Strid, J.	627-637A 33-41A
		923-929A	Olesinski, R.W.	677-680B		1353-1357A	Sue, J.J.	283-286A
Lou, M.Y	.A. v.w	1507-1509A 1491-1493A	Oliver, W.C. O'Neal, J.E.	2221-2229A 237-240A	Robinson, S.L. Rodrigues, C.A.V.	1955-1958A	Sukiennik, M.Z. Sure, G.N.	677-680B 1613-1621A
Louis, E.		389-391A	O Neal, S.L.	1451-1463A	deA.	2193-2203A	Suresh, S.	369-379A
Lu, M. Lu, SZ.		735-746A 459-469A	Osamura, K. Ostenson, J.E.	835-842A 283-286A	Rogers, G.D. Romig, A.D., Jr.	581-589B 1319-1330A	Suzuki, T.	1193-1207A 173-181A
Lütjering		1597-1605A	Otsuka, S.	329-335B	Rosén, E.	511-516B	Swaminathan, K.	259-275B
Lyudkov	vsky, G.	257-260A		141-147B	Roy, P.	1769-1775A	Szekely, J.	633-640B 183-186B
			Owen, C.V.	337-344B 147-153A	Rozendaal, H.C.F. Ruth, J.A., Jr.	627-637A 245-246A		59-70B
Mahulika	ar, D.	209-215A	Oya, Y.	173-181A	Rutter, J.W.	1515-1517A		
Makino,		1563-1570A	Ozturk, B.	245-246A	Ryan, N.D.	1855-1864A	Tahuahi C	351-356B
Maples. Marcus.		163-172B 1415-1430A					Tabuchi, S. Tähtinen, S.	2205-2211A
		209-215A	Packer, C.M.	1741-1752A	Sabatini, R.L.	1941-1946A	Takagi, H.	1273-1280A
Margolin Marra, V		155-171A 1787-1805A	Page, R.A.	11-22A 756-760A	Sadananda, K. Sagoe-Crentsil, K.K.	527-539A 1969-1975A	Takayama, T. Takeuchi, E.	1819-1828A 493-509B
Marshal	II, D.	43-54A		1389-1396A	Sakakibara, Y.	250-251A	Tan, T.C.	719-723B
Martin, Martinez		1711-1719A 246-247A	Pahl, R.G., Jr.	1397-1405A 1519-1529A	Samarasekera, I.V. Sample, A.K.	307-318B 2163-2173A	Tanabe, T. Taplin, D.M.R.	127-133B 1437-1441A
Martins,	, G.S.	1496-1499A	Pajdowski, L.	451-459B	Samuel, F.H.	1807-1817A		1763-1767A
Mason,	J.T.	967-975A 1665-1676A	Pak, C.S.L. Panda, B.	755-756A 487-494A	Sandvik, B.P.J. Sano, N.	1555-1562A 351-356B	Tarassoff, P. Tartaglia, J.M.	411-432B 1173-1183A
Massals		421-425A	Pandey, M.C.	1437-1441A	Sasaki, Y.	563-571B	Taub, A.I.	399-402A
Masumo Mataya,		1563-1570A 347-368A	Panek, Z.	1763-1767A 543-546B	Sastry, S.M.L.	1451-1463A 1465-1474A	Tazunoki, Y. Tench, D.	2029-2038A 2039-2040A
Matlock	k, D.K.	1221-1228A	Panigrahy, S.C.	23-34B	Savage, W.F.	1339-1351A	Tewari, S.N.	1905-1919A
Matson, Matthey		2241-2246A 701-708B	Park, HH.	1075-1080A	Scanlon, J.C.	1299-1302A 1977-1986A	Thomas, B.G. Thomas, M.T.	307-318B 853-860A
Matthey	w, S.F.	709-717B	Park, J.K. Park, J.S.	1531-1543A 155-171A	Scarsbrook, G. Schaefer, R.J.	1987-1997A	Thompson, A.W.	931-937A
Mazumo	der, J.	2175-2184A	Parsey, J.M., Jr.	1963-1967A		2109-2115A	Tien, J.K.	1865-1871A
McDona	ney, D.G. ald, M.L.	983-994A 1787-1805A	Parthasarathy, T.A.	1485-1490A 2021-2027A	Schmid, R.	55-66A 1921-1930A	Tiitto, K. Toksoy, C.	241-243A 755-756A
	den, G.B.	2117-2124A	Paton, N.E.	813-817A	Schnur, D.S.	1777-1779A	Tomita, Y.	2247-2249A
McGinn,	PJ	2125-2137A 1099-1102A	Pearson, D.D.	1037-1045A 1047-1054A	Schulson, E.M.	1129-1136A 701-706A	Topor, L.	203-208A 573-580B
McKelli	iget, J.	59-70B	Pelloux, R.M.	107-120A	Schulze, K.	1111-1116A	Townsend, H.E.	393-395B
McLella McNalla	an, R.B. an, M.I	199-202A 403-405A	Peng, T.C.	381-388A 1465-1474A	Schwerdtfeger, K.	736-739B 729-732B	Trivedi, R.	967-975A 977-982A
McQuee	en, H.J.	1855-1864A	Perepezko, J.H.	437-447A		281-288B		1665-1676A
Medina, Mendira	L.F. atta, M.G.	725-726B 395-399A	Perkins, J. Peters, C.R.	313-321A 2101-2102A	Scott, D.S. Scott, T.E.	726-729B 147-153A	Tsai, Y.S. Tyson, W.	495-499A 1475-1484A
Meredit	th, S.E.	243-250B	Peters, M.	1597-1605A	Seetharaman, S.	319-327B	Tyson, W.R.	1499-1502A
Mescht	ter, P.J.	237-240A 1451-1463A	Pethica, J.B.	1589-1596A 2221-2229A	Sekhar, J.A. Sellamuthu, R.	29-31A		
Meyer,		471-478B	Petzow, G.	1111-1116A	Seshan, K.	1677-1685A 617-622B	Ueda, H.	1431-1436A
Meyrick Michael	k, G.	495-499A 99-105A	Piehler, H.R.	1699-1710A	Shahinian, P.	527-539A	Ueda, H. Umeda, T.	1431-1436A 91-99B
Miller, A		99-105A 1099-1102A	Pielet, H.M.	547-562B 547-562B	Sharma, R.C. Shechtman, D.	545-553A 1987-1997A		101-107B
Mimura.	, T.	1147-1153A	Piercy, G.R.	2093-2095A		55-66A	Umeno, M.	1273-1280A
Miracle Mitra, L		481-486A 217-227A	Pinsky, D.A. Pirich, R.G.	173-181B 2139-2145A	Shen, B.W.	1247-1251A 1253-1258A		
	eijer, E.J.	627-637A		2155-2161A		1289-1292A	Vaessen, G.J.H.	1407-1414A

Van Rooyen, G.T. Vander Sande, J.B. Varma, S.K. Varschavsky, A. Vasudévan, A.K. Vaughn, G.A. Verhoeven, J.D.

2185-2191A 819-833A 1502-1503A 1999-2008A 1999-2008A 369-379A 783-792A 1037-1045A 1047-1054A 1665-1676A 283-286A

Verstraeten, P. Viñals, J. Viswanathan, R. Vives, C.

283-286A 23-34B 221-228B 23-28A 734-736B 471-478B 995-1001A Voorhees, P.W. 1081-1088A

Wadsworth, J. Wadsworth, M.E. Wagoner, R.H. Wallace, W.

Walters, K.W. Warren, G.W.

1741-1752A 289-297B 1265-1271A 339-345A 501-510A 149-153B 235-242B 289-297B 5-12B

Watanabe, S. Wayman, C.M.

357-368B 621-626A 1155-1163A 269-276A 1353-1357A 1555-1562A 406A 735-746A 681-684B

Webster, D. Wei, R.P. Weinberg, F. Weirick, L.J.

479-485B 739-741B 1319-1330A 609-620A 1493-1496A 843-852A 2039-2040A 23-28A 1753-1762A 617-622B 229-236A 99-105A

Weirick, L.J.
Weiss, B.Z.
Weiss, I.
West, A.W.
White, J.
Whitlow, G.A.
Whittenberger, J.D.
Whyte, J.R., Jr.
Willett, K.P.
Williams, D.B.
Williams, J.C.

Willits, B.L. Wilson, B.W. Wilson, D.V.

Wilson, E.A. Wilson, R.D.

Winegard, W.C. Wise, J. Wo, G. Wood, J.V. Wray, P.J.

Wycliffe, P.

1311-1317A 913-922A 923-929A 1947-1948A 695-700B 732-734B 1515-1517A 2097-2101A 1359-1366A 471-480A 2009-2019A 2041-2058A 2059-2073A 1499-1502A

931-937A 1589-1596A 1502-1503A 1311-1317A

Yacaman, M.J. Yamasaki, T. Yamauchi, I. Yamauchi, I Yang, D.-Z. Yang, M.M. Yao, J. Yoder, G.R. Yoon, D.N.

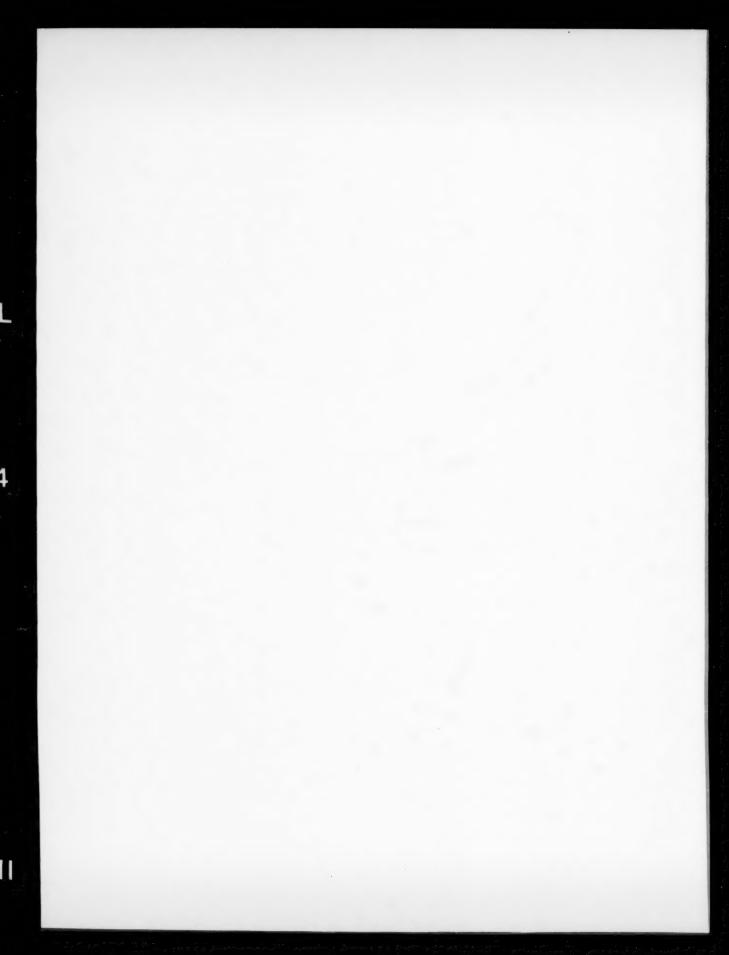
Yoshida, H. Yoshii, K. Young, M.S.S. Yu, W.

Zanner, F.J. Zhang, Y.-G. Zovas, P.E.

Yuen, J.L.

1485-1490A 519-526A 739-741B 1555-1562A 1545-1554A 729-733A 183-197A 1075-1080A 1503-1505A 396-400B 396-400B 1273-1280A 1963-1967A 875-888A 889-900A 1769-1775A

117-125B 2087-2092A 1103-1110A



# **Combined Subject Index**

Absorption (material)		Alkaline earth metals	
Distribution of Lead Between Copper and Matte and the Activity of PbS in Copper-Saturated Mattes.  Hydride Precipitation and Dislocation Substructures in Ti—5AI—2.5Sn.	441-449B 813-817A	See Beryllium Calcium Magnesium Strontium	
Acid leaching See Hydrochloric acid leaching	010-0174	Alkaline leaching See Ammonia pressure leaching	
Sulfuric acid leaching  Acoustic emission  Determination of the Sources of Acoustic Emission Generated During the Deformation of Titanium.	1849-1853A	Alloy steels  See Austenitic stainless steels Chromium molybdenum steels Chromium molybdenum vanadium steels	
Actinide metal alloys See Uranium base alloys		Chromium steels Electrical steels Ferritic staniless steels	
Activated sintering Retarded Grain Boundary Mobility in Activated Sintered Mo- lybdenum.	1103-1110A	High strength low alloy steels High strength steels Low alloy steels	
Activation energy Kinetics of Methane Bubble Growth in a 1020 Steel. Kinetics of Precipitation From Quenched Low-Carbon Steel.	487-494A	Martensitic stainless steels Nickel chromium molybdenum steels Nickel chromium steels Nickel steels	
Activity (chemical)  The Determination of the Thermodynamics of the NaF— AIF,—AI,O, System With a Solid Electrolyte Cell. Activities of Oxygen in Liquid Bi—Pb and Bi—Sb Alloys. Activity Coefficient of Oxygen in Copper—Sulfur Melts.	135-139B 141-147B 337-344B	Precipitation hardening steets Silicon steets Stainless steets  Alloying See Microalloying	
Activity Coefficient of CuO <sub>0.5</sub> in Alumina-Saturated Iron Silicate Slags.	345-349B	Surface alloying Alloys	
Thermodynamics of Phosphate and Phosphide in CaO— CaF <sub>2</sub> Melts. Activity of SnS in Copper-Saturated Matte.	351-356B 595-598B	See Dispersion hardening alloys Ferrous alloys Master alloys	
Activity coefficients See Activity (chemical)		Nonferrous alloys Precipitation hardening alloys Superalloys	
Additives See Master alloys		Alpha annealing See Annealing	
Adhesion  Ribbon—Substrate Adhesion Dynamics in Chill Block Melt- Spinning Processes.	155-161B	Alpha iron, Heat treatment Consequences of the Heterogeneous Nitriding of Alpha-Iron: Dislocation Production and Oriented Precipitation.	627-637A
Adhesivity See Adhesion		Alphatizing	021-031A
Admiralty metal, Corrosion The Influence of Deformation Path on the Slow Strain-Rate Stress Corrosion Cracking of Admiralty Brass Sheet.	1281-1286A	See Annealing Alumina See Aluminum oxide	
Adsorption, Stress effects Influence of Stress on H <sub>2</sub> S Adsorption on Iron.	853-860A	Aluminum, Alloying additive The Role of Alloy Composition on the Stability of Nitrides in Titanium-Microalloyed Steels During Weld Thermal Cycles.	33-41A
Aerospace Effect of Microstructure, Strength and Oxygen Content on Fatigue Crack Growth Rate of Ti-4.5AI-5.0Mo-1.5Cr (CORONA 5).	183-197A	Aluminum, Alloying elements Slip Directions in B2 Fe—Ai Alloys. The Structure of Extruded NiAl. A Quantitative Assessment of the Hardenability Increase Re-	395-399A 1129-1136A
Age hardening See Precipitation hardening			2185-2191A
Age hardening steels See Precipitation hardening steels		Steady Low of Liquid Aluminum in a Rectangular-Vertical Ingot Mold, Thermally or Electromagnetically Activated.	471-478B
Age softening See Overaging		Aluminum, Coatings Heat Transfer and Fluid Flow in Plasma Spraying.	59-708
Agents See Catalysts Agglomeration See Sintering (roasting)		Aluminum, Crystal growth Recrystallization in Commercially Pure Aluminum. Numerical Treatment of Rapid Solidification. Subgrain Growth in Aluminum During Static Annealing.	287-297A 369-381B 1502-1503A
Aging See Aging (artificial) Overaging		A Two-Dimensional Transient Model for Convection in Laser Melted Pool.  Aluminum, Diffusion	2175-2184A
Quench aging Aging (artificial)		The Room-Temperature Effective Diffusivity of Hydrogen in Vapor-Deposited Aluminum.	1953-1955A
Modulated Microstructures in Copper—Zinc and Copper— Aluminum—Nickel.	269-276A	Aluminum, Extraction Reactions in Hall Smelting Cell Potlining. Simulating the Process of Carbon Anode Baking Used in the	277-280B
Mechanisms of Slow Fatigue Crack Growth in High-Strength Aluminum Alloys: Role of Microstructure and Environment. Effect of Retrogression and Reaging Treatments on the Mi	369-379A	Aluminum Industry. Chlorination of Alumina in Kaolinitic Clay.	487-492B 529-533B
crostructure of Al-7075-T651.  The Stabilization of Martensite in Cu—Zn—Al Shape Mem	1531-1543A	Mössbauer Spectroscopy Used to Study the Removal of Iron From Clay.	732-734B
ory Alloys.  Agitation  See Electromagnetic stirring	1977-1986A	Aluminum, Reactions (chemical) The Determination of the Thermodynamics of the NaF— $AIF_3$ — $AI_2O_3$ System With a Solid Electrolyte Cell.	135-139B
Alkali metal compounds See also Potassium compounds Sodium chloride		Aluminum, Ternary systems  The Grain Refining of Aluminum and Phase Relationships in the Al—Ti—B System.	277-282A
Alkali metal compounds, Reactions (chemical)	d	Nickel—Aluminum—Molybdenum Phase Equilibria. The Liquidus Surface for the Al—Li—Si System From 0.20%	
The Effects of CO and CO <sub>2</sub> on the Rate of Na <sub>2</sub> CO <sub>3</sub> Catalyze Boudovard Reaction.	400-403B	Lithium and 0.20% Silicon.  Crystallization Studies in the Aluminum-Rich Corner of the Aluminum—Iron—Manganese System.	595-597A 1311-1317A
Alkali metals See Lithium Sodium		Miscibility Gap in Fe—Ni—Al and Fe—Ni—Al—Co Systems.	
Alkaline earth metal alloys See Magnesium base alloys Strontium		Aluminum base alloys, Composite materials Creep Rupture of a Silicon Carbide Reinforced Aluminum Composite. Correction to "Effect of Lithium on the Mechanical Properties	139-146A
Alkaline earth metal compounds See Magnesium oxide		and Microstructure of SiC Whisker Reinforced Aluminum Alloys".	

Aluminum base alloys, Crystal growth Convection in the Two-Phase Zone of Solidifying Alloys.	163-172B	Recovery of Elemental Sulfur During the Oxidative Ammonia- cal Leaching of Chalcopyrite.	726-729B
The Grain Refining of Aluminum and Phase Relationships in the Al—Ti—B System.	277-282A	Amorphous materials See Metallic glasses	120 120
Aluminum base alloys, Directional solidification The Solidification of Monotectic Alloys—Microstructures		Amplifiers	
and Phase Spacings. Interlamellar Spacing in Directionally Solidified Eutectic Thin	1003-1012A	See Lasers Analyzing	
Films.	1013-1017A	See Mathematical analysis Statistical analysis	
Aluminum base alloys, Heat treatment An Electron Microscope Study of the Featureless Zone Ob-		Thermal analysis X ray stress analysis	
tained During Rapid Solidification. Effect of Retrogression and Reaging Treatments on the Mi- crostructure of Al-7075-7651.	29-31A 1531-1543A	Andrade method See Crystal growth	
Aluminum base alloys, Machining		Androforming See Stretch forming	
Determination of Strain Distributions in Machined Chips.  Aluminum base alloys, Mechanical properties	1777-1779A	Angular velocity	
A Study of Creep Crack Growth in 2219-T851 Aluminum Alloy Using a Computerized Testing System. Localized Necking of Sheet at Negative Minor Strains.	107-120A 323-329A	See Rotation Annealing	
Mechanisms of Slow Fatigue Crack Growth in High-Strength Aluminum Alloys: Role of Microstructure and Environment.	369-379A	See also Continuous annealing Isothermal annealing Chromium Depletion in the Vicinity of Carbides in Sensitized	
The Effect of Microstructure and Environment on Fatigue Crack Closure of 7475 Aluminum Alloy.	555-563A	Austenitic Stainless Steels.	793-811A
Tensile Properties of a 2014 Aluminum Alloy in the Tempera- ture Range 250 to 500°C.	913-922A	Segregation of Manganese During Intercritical Annealing of Dual-Phase Steels.	1499-1502A
The Effect of Minor Alloying Elements on the Mechanical Properties of Al—Cu—Li Alloys.	1209-1220A	Subgrain Growth in Aluminum During Static Annealing.  Anodes	1502-1503A
Dislocation-Depth Distribution in High-Temperature Creep. The Influence of Crack Tip Plasticity in the Growth of Small	1571-1577A	Simulating the Process of Carbon Anode Baking Used in the Aluminum Industry.	487-492B
Fatigue Cracks.  Creep Transitions in an Al—Zn Alloy.  Existence of the Coaxing Effect and Effects of Small Artificial Holes on Fatigue Strength of an Aluminum Alloy and	1579-1588A 1893-1904A	Anodic dissolution  The Electrochemical Oxidation of Chalcopyrite in Ammoniacal Solutions.	289-297B
70-30 Brass.	2029-2038A	Antidomains See Domains	
An Analysis of Biaxial Stretching of a Flat Sheet.	133-138A	Antimony, Alloying additive	
Punch-Stretching Behavior of a 2014 Aluminum Alloy in the Temperature Range 250 to 500°C.  Aluminum base alloys, Microstructure	923-929A	Effect of Antimony on Recrystallization Behavior and Mag- netic Properties of a Nonoriented Silicon Steel.	257-260A
The Effect of Fluid Flow on the Eutectic Lamellar Spacing.	307-312A	Antimony, Dopants  Effects of the Additions of Boron, Phosphorus, Tin and Anti-	
Modification in the Aluminum—Silicon System. Ostwald Ripening and Relaxation in Dendritic Structures.	459-469A 995-1001A	mony on Oxygen-Assisted Hydrogen Embrittlement of Nick- ei.	519-526A
Aluminum base alloys, Phase transformations Interlamellar Spacing in Discontinuous Precipitation. Precipitation in Rapidly Solidified Al—Mn Alloys.	1055-1062A 1987-1997A	Antimony, Solubility Equilibria Between Silica-Saturated Iron Silicate Slags and Molten Cu—As, Cu—Sb and Cu—Bi Alloys.	535-541B
Aluminum base alloys, Powder technology The Microstructure and Tensile Properties of a Splat-		Arc welding See Gas tungsten arc welding	
Quenched Al—Cu—Li—Mg—Zr Alloy.  Local Microstructural Modification in Dynamically Consoli-	1367-1377A	Submerged arc welding	
dated Metal Powders.	1653-1664A	Arc welds See Welded joints	
Aluminum base alloys, Structural hardening Calorimetric Studies of Al—Cu Alloys: Quench Sensitivity		Argon arc welding	
and Sample Preparation.  Shape Changes During Dissolution of Theta Prime-CuAl <sub>2</sub> .  Metastable Phases in the Early Stage of Precipitation in AI—	389-391A 449-458A	See Gas tungsten arc welding  Arrhenius activation energy  See Activation energy	
Mg Alloys.  Effects of Fatigue on the G—P Zones in Al—Zn Alloys.	835-842A 1519-1529A	Arsenic, Solubility	
Dissolution Kinetics of Widmanstätten Gamma-Ag <sub>2</sub> Al Precipitates.	1969-1975A	Equilibria Between Silica-Saturated Iron Silicate Slags and Molten Cu—As, Cu—Sb and Cu—Bi Alloys.	535-541B
Aluminum base alloys, Welding Metal Vaporization From Weld Pools.	461 460P	Artificial aging See Aging (artificial)	
Heat Flow During the Autogenous GTA Welding of Pipes.	461-469B 1165-1171A	Atmospheres	
Aluminum brasses, Phase transformations The Stabilization of Martensite in Cu—Zn—Al Shape Memory Alloys.	1977-1986A	See Controlled atmospheres Inert atmospheres	
Aluminum compounds	7077 700077	Atomic diffusion See Diffusion	
See also Aluminum oxide  Aluminum compounds, Mechanical properties		Atomization See Atomizing	
Improved Strength and Ductility in Ni <sub>3</sub> Al by Boron Modifica- tion and Rapid Solidification.	399-402A	Atomizing	
Deformation in TigAl Fatigued at Room and Elevated Temper- atures.	1721-1729A	Rapidly Solidified Prealloyed Powders by Laser Spin Atomization.	149-153B
Aluminum killed steels, Casting		Attack (chemical) See Chemical attack	
Thermodynamics of Nozzle Blockage in Continuous Casting of Calcium-Containing Steels.	547-562B	Austenite, Phase transformations	
Correction to Thermodynamics of Nozzle Blockage in Contin- uous Casting of Calcium-Containing Steels.	547-562B	The Isothermal Decomposition of Austenite in Hot Rolled Microalloyed Steels.	1137-1145A
Aluminum killed steels, Diffusion Segregation of Manganese During Intercritical Annealing of		Austenite, Solubility Solubility Product for Niobium Carbide in Austenite.	541-544A
Dual-Phase Steels.	1499-1502A	Solubility of Niobium Carbide and Niobium Carbonitride in Alloved Austenite and Ferrite.	545-553A
Aluminum killed steels, Metal working An Analysis of Biaxial Stretching of a Flat Sheet.	133-138A	Austenitic stainless steels, Coatings Embrittlement of Types 316L and 347 Weld Overlay by Post-	
Aluminum oxide, Composite materials  Critical Stress Intensity for Off-Axis Fracture of Al <sub>2</sub> O <sub>3</sub> Fiber		Weld Heat Treatment and Hydrogen.	1475-1484A
Reinforced Magnesium. Tensile and Fatigue Behavior of Aluminum Oxide Fiber-	756-760A	Austenitic stainless steels, Forging The Effect of Hot Working on Structure and Strength of a Pre-	
Reinforced Magnesium Composites. I.—Fiber Fraction and Orientation.	1389-1396A	cipitation Strengthened Austenitic Stainless Steel.	347-368A
Tensile and Fatigue Behavior of Aluminum Oxide Fiber Reinforced Magnesium Composites. II. — Alloying Effects.		Austenitic stainless steels, Heat treatment Chromium Depletion in the Vicinity of Carbides in Sensitized	
Aluminum oxide, Reactions (chemical)		Austenitic Stainless Steels.  Austenitic stainless steels, Mechanical properties	793-811A
Chlorination of Alumina in Kaolinitic Clay.  Ammonia pressure leaching	529-533 <b>B</b>	Behavior of Fe—Ni—Cr Alloys in a Complex Multioxidant En- vironment Under Conditions of Dynamic Straining.	
The Electrochemical Oxidation of Chalcopyrite in Ammonia cal Solutions.	289-297B	Hydrogen-Induced Slow Crack Growth in Stable Austenitic Stainless Steels.	11-22A 729-733A

The Effect of One Slow—Fast Strain Cycle on the Fatigue Crack Growth Behavior of SUS 304 Stainless Steel at Ele-		Billets, Crystal growth Fluid Flow From a Low to a Higher Density Liquid.	681-684B
vated Temperature. Influence of Nitrogen Alloying on Hydrogen Embrittlement in	1731-1739A	Binary systems, Phase transformations Solute Stabilization for H.C.PF.C.C. Transitions: Co-Mo.	67-72A
AISI 304 Type Stainless Steels. The Wear Behavior of Nitrogen-Implanted Metals.	2205-2211A 2221-2229A	Binary systems, Phases (state of matter)	67-72A
Austenitic stainless steels, Phases (state of matter) Correction to "The Kinetics of Sigma-Phase Precipitation in		Calculations of Stable and Metastable Equilibrium Diagrams of the Ag—Cu and Cd—Zn Systems.  A Generalized Approach to the Flood—Knapp Structure	261-268A
AISI 310 and AISI 316 Steels".  High-Temperature Phase Chemistries and Solidification Mode Prediction in Nitrogen-Strengthened Austenitic	406A	Based Model for Binary Liquid Silicates: Application and Update for the PbO—SiO <sub>2</sub> System.	511-516B
Stainless Steels.	1339-1351A	Thermodynamic Analysis of the Iron—Copper System.  I.—The Stable and Metastable Phase Equilibria.	1921-1930A
Austenitic stainless steels, Powder technology Rapid Solidification of a Droplet-Processed Stainless Steel.	819-833A	Binary systems, Physical properties Thermochemistry of Binary Liquid Gold Alloys: the Systems	
Austenitic stainless steels, Reactions (chemical) Hydrogen Attack in an Austenitic Stainless Steel.	1485-1490A	Gold—Copper and Gold—Silver at 1379K.  Bismuth, Diffusion	203-208A
Austenitic stainless steels, Welding Alloying Element Vaporization and Weld Pool Temperature During Laser Welding of AISI 202 Stainless Steel.	641-644B	An Analytical Electron Microscope Study of the Kinetics of the Equilibrium Segregation of Bismuth in Copper.	99-105A
Austenitizing Effect of Prior Cold Work on the Martensite Transformation in		Bismuth, Solubility Equilibria Between Silica-Saturated Iron Silicate Slags and Molten Cu—As, Cu—Sb and Cu—Bi Alloys.	535-541B
SAE 52100. The Effect of Furnace Atmosphere Carbon Potential on the	299-306A	Bismuth base alloys, Crystal growth	300 0410
Development of Residual Stresses in 52100 Bearing Steel. A Quantitative Assessment of the Hardenability Increase Re-	2101-2102A	Studies of Directionally Solidified Eutectic Bi/MnBi at Low Growth Velocities. Thermoelectric and Morphological Effects of Peltier Pulsing	2139-2145A
sulting From a Superhardenability Treatment.  Auto oxidation	2185-2191A	on Directional Solidification of Eutectic Bi/Mn.  Effect of Applied Magnetic Fields During Directional Solidifi-	2147-2154A
See Oxidation			2155-2161A
Autoclaving Control of Autoclave Scaling During Acid Pressure Leaching of Nickeliferous Laterite Ore.	433-440B	Activities of Oxygen in Liquid Bi—Pb and Bi—Sb Alloys.  Bismuth compounds, Single crystals	141-147B
Autodiffusion	400 4400	Bismuth Precipitation in "Monocrystalline" InBi.	1963-1967A
See Diffusion Automatic control		Blades See Turbine blades	
See Computer control  Axial stress		Blades (cutting), Mechanical properties Microstructure and Its Effect on Toughness and Wear Resis-	
Biaxial Deformation of 70-30 Brass: Flow Behaviors, Tex- ture, Microstructures.	1607-1612A	tance of Laser Surface Melted and Post-Heat Treated High-Speed Steel.	1829-1835A
Baking		Blankets (atmospheres) See Controlled atmospheres	
Simulating the Process of Carbon Anode Baking Used in the Aluminum Industry.	487-492B	Blast furnace chemistry Phase Relationships in the System Fe—Na—O.	319-327B
Band theory Thermodynamics of Several Lewis-Acid-Base Stabilized		Reduction of Silica in Coke With Ash of Increased Basicity.	729-732B
Transition Metal Alloys.  Banded structure	2075-2085A	Blast furnaces Exergy Analysis of a Chemical Metallurgical Process.	645-654B
Structural Effects and Band Segregate Formation During the Electromagnetic Stirring of Strand-Cast Steel. Magnetization Measurement Associated With Gamma → Alpha Martensitic Transformation of Iron Parti-	581-589B	Blocking Thermodynamics of Nozzle Blockage in Continuous Casting of Calcium-Containing Steels. Correction to Thermodynamics of Nozzle Blockage in Contin-	547-562B
cles in a Cu-1.59Fe Alloy.	755-756A	uous Casting of Calcium-Containing Steels.	547-562B
Basic converters See LD converters		Blowing A New Approach to Investigate the Drop Size Distribution in Basic Oxygen Steelmaking.	109-116B
Basic oxygen processes See Oxygen steel making		Boiler scale	100 1100
Basic oxygen steel making See Oxygen steel making		See Scale (corrosion)  Boron, Alloying elements	
Batch type furnaces See Bottom blown converters		Improved Strength and Ductility in Ni <sub>3</sub> Al by Boron Modifica- tion and Rapid Solidification.  Boron, Composite materials	399-402A
Copper converters LD converters		Environmentally Influenced Mixed Mode Fatigue Crack Propagation of Titanium Metal/Matrix Composites.	209-215A
Bauschinger effect The Role of Alpha and Beta Phases in Fatigue Crack Propa-		Boron, Dopants Effects of the Additions of Boron, Phosphorus, Tin and Anti-	
gation of Ti—Mn Alloys.  Yielding Anisotropy From the Bauschinger Effect and Crys-	155-171A 1699-1710A	mony on Oxygen-Assisted Hydrogen Embrittlement of Nick- el.	519-526A
tallographic Texture in Drawn HSLA Steel Sheet.  Bearing steels, Heat treatment		Boron, Ternary systems	
The Effect of Furnace Atmosphere Carbon Potential on the Development of Residual Stresses in 52 100 Bearing Steel.		The Grain Refining of Aluminum and Phase Relationships in the Al—Ti—B System.	277-282A
Bearing steels, Mechanical properties  The Wear Behavior of Nitrogen-Implanted Metals.	2221-2229A	Boron, Trace elements Segregation and Influence of Boron on the Impact Toughness to Ti-6AI-2Nb-1Ta-0.8Mo Welds and Castings.	1505-1507A
Bearing steels, Phase transformations Effect of Prior Cold Work on the Martensite Transformation in SAE 52100.	299-306A	Boron carbide, Composite materials Environmentally Influenced Mixed Mode Fatigue Crack Propagation of Titanium Metal / Matrix Composites.	209-215A
Bendability See Formability		Boron compounds	
Beryllium, Alloying elements The Gamma Phase Boundary of CuBe Alloys.	939-941A	See Boron carbide BOS process	
Beryllium, Irradiation Metastable Alloys of Beryllium Prepared by Ion Implantation		See Oxygen steel making Bottom blown converters	
Beryllium, Melting		Mixing of Concentric Gas Jets Issuing Vertically Into a Liquid.  Boundaries	71-75B
Heat and Fluid Flow Phenomena in a Levitation Melter Sphere Under Zero Gravity.	183-186B	See Grain boundaries Grain sub boundaries	
Biaxial stress See Axial stress		Phase boundary Brasses	
Bicrystals, Mechanical properties  Dependence of Dynamic Fracture Resistance on Crack Ve	1253-1258A	See also Admiralty metal Aluminum brasses	
locity in Tungsten. II.—Bicrystals and Polycrystals.  Billet casting  Structural Effects and Band Segregate Formation During the Electromagnetic Stirring of Strand-Cast Steel.		Brasses, Mechanical properties  Localized Necking of Sheet at Negative Minor Strains.  Biaxial Detormation of 70-30 Brass: Flow Behaviors, Texture, Microstructures.	323-329A 1607-1612A

Existence of the Coaxing Effect and Effects of Small Artifi- cial Holes on Fatigue Strength of an Aluminum Alloy and		Carbon steets See also Aluminum killed steets	
70-30 Brass.	2029-2038A	Carbon steels, Crystal growth Numerical Models for Casting Solidification. I.—The Cou-	
Brazed joints, Microstructure Structure of Vacuum Brazed BNi-5 Joint of Inconel 718.	609-620A	pling of the Boundary Element and Finite Difference Meth- ods for Solidification Problems.	91-99B
See Vacuum brazing		Effect of Composition and Initial Grain Size on the Dynamic Recrystallization of Austenite in Plain Carbon Steels.	2009-2019A
Bridgman method See Crystal growth		Carbon steels, Diffusion Kinetics of Methane Bubble Growth in a 1020 Steel.	487-494A
Brine		The Effect of a Tin Barrier on the Permeability of Hydrogen	A2602-E602
See Salt water Brittle fracture		Carbon steels, Heat treatment Temper-Aging of Continuously Annealed Low-Carbon Dual-	
Influence of Nitrogen Alloying on Hydrogen Embrittlement in AISI 304 Type Stainless Steels.	2205-2211A	Phase Steel.  Carbon steels, Mechanical properties	73-86A
Brittle fracture, Microstructural effects The Influence of Microstructure on Brittle Fracture Toughness.	947-959A	Effects of Prior Cold Rolling and Post-Temper Rolling on the Properties of Continuously Annealed Low-Carbon Dual- Phase Steel.	671-678A
Brittleness See also Temper brittleness		The Influence of Microstructure on Brittle Fracture Toughness.	947-959A
Brittleness, Microstructural effects A Microstructural Investigation of the Origin of Brittle Behavior in the Transverse Direction in Molybdenum-Based Alloy		Strain Hardening Behavior of Polycrystalline Iron and Low- Carbon Steels—a Statistical Analysis. Effect of Shape of Sulfide Inclusions on Anisotropy of Inclu- sion Spacings and on Directionality of Ductility in Hot	1185-1192A
Bars. Bubbles	1741-1752A	Rolled C-Mn Steels.  Residual Stress Evaluation With X-Rays in Steels Having Preferred Orientation.	1259-1264A 1407-1414A
Kinetics of Methane Bubble Growth in a 1020 Steel.  Cadmium, Binary systems	487-494A	High-Temperature Plastic-Flow Behavior of Mixtures of Aus- tenite, Cementite, Ferrite and Pearlite in Plain-Carbon	
Calculations of Stable and Metastable Equilibrium Diagrams of the Ag—Cu and Cd—Zn Systems.	261-268A	Steels. Tensile Failure Behavior of Plain Carbon Steels at Elevated Temperatures.	2041-2058A 2059-2073A
Cadmium, Ternary systems Thermodynamic Properties of Liquid Mg—In—Cd Ternary Solutions.	543-546B	Carbon steels, Microstructure Dislocation Substructure as a Function of Strain in a Dual- Phase Steel.	1221-1228A
Cadmium base alloys, Directional solidification Interlamellar Spacing in Directionally Solidified Eutectic Thin Films.	1013-1017A	Grain Boundary Widmanstätten Ferrite Spacings in 0.2% Carbon Steel.	1643-1651A
Cakes (metal)	1013-10174	Carbon steels, Structural hardening Kinetics of Precipitation From Quenched Low-Carbon Steel.	1147-1153A
See Ingots Calcining		Carbonates, Reactions (chemical) The Effects of CO and CO <sub>2</sub> on the Rate of Na <sub>2</sub> CO <sub>3</sub> Catalyzed	
See Roasting  Calcium, Alloying additive  Thermodynamics of Nozzle Blockage in Continuous Casting		Boudovard Reaction.  Carbonitrides, Solubility  Solubility of Niobium Carbide and Niobium Carbonitride in Al-	400-403B
of Calcium-Containing Steels.  Correction to Thermodynamics of Nozzle Blockage in Contin- uous Casting of Calcium-Containing Steels.	547-562B 547-562B	loyed Austenite and Ferrite.  Carbothermic reactions  A Study of the Mechanisms of the Salt Catalyzed Carbo-	545-553A
Calorimeters Calorimetric Studies of Al—Cu Alloys: Quench Sensitivity and Sample Preparation.	389-391A	chlorination of Kaolin.  Establishment of Product Morphology During the Initial Stages of Wustite Reduction.	695-700B 709-717B
Carbides	303-33 IN	Carburization	100 / 110
See also Boron carbide Chromium carbide		See Carburizing Carburizing	
Metal carbides Niobium carbide		Discussion of "Self-Diffusion Coefficients of Carbon in Fe <sub>3</sub> C at 723K Via the Kinetics of Formation of This Compound	
Silicon carbide		(and Authors' Reply).	245-246A
Carbides, Diffusion Discussion of "Self-Diffusion Coefficients of Carbon in Fe <sub>3</sub> C		Core Hardenability Calculations for Carburizing Steels. Fatigue Behavior of Carburized Steel With Internal Oxides	1173-1183A
at 723K Via the Kinetics of Formation of This Compound (and Authors' Reply).	245-246A	and Nonmartensitic Microstructure Near the Surface.  The Effect of Furnace Atmosphere Carbon Potential on the	1431-1436A
Carbon, Alloying elements Forced Velocity Pearlite in High-Purity Fe—C Alloys I.— Experimental.	1037-1045A	Development of Residual Stresses in 52100 Bearing Steel.  Case carburizing  See Carburizing	2101-2102A
Carbon, Diffusion		Case hardening	
Discussion of "Self-Diffusion Coefficients of Carbon in Fe <sub>3</sub> C at 723K Via the Kinetics of Formation of This Compound		See Carburizing Nitriding	
(and Authors' Reply).	245-246A	Cast iron See Gray iron	
Carbon, Reactions (chemical)  Discussion of "Calculation Method of Equilibrium Composi-		Nodular iron	
tion in the Carbon—Hydrogen—Oxygen System and Its Application to Environments of a High-Temperature Gas		See Billet casting	
Cooled Reactor"; Authors Reply.  The Effects of CO and CO <sub>2</sub> on the Rate of Na <sub>2</sub> CO <sub>3</sub> Catalyzed	396-400B	Continuous casting Ingot casting	
Boudovard Reaction.	400-403B	Melt spinning Slab casting	
Carbon, Ternary systems  Phase Relationships in the Fe—Cr—C System at Solidification Temperatures.	663-676B	Casting defects Structural Effects and Band Segregate Formation During the	
Carbon compounds See Boron carbide		Electromagnetic Stirring of Strand-Cast Steel.  Strain Induced Cracking in Partially Solidified Tin—Lead	
Carbides Carbon dioxide		Alloy.	739-741B
Carbon dioxide Carbonitrides Chromium carbide		Castings See also Continuous cast shapes	
Niobium carbide		Ingots Castings, Crystal growth	
Carbon dioxide, Environment Isotope Exchange Studies of the Rate of Dissociation of CO on Liquid Iron Oxides and CaO-Saturated Calcium Ferrites		Numerical Models for Casting Solidification. I.—The Cou- pling of the Boundary Element and Finite Difference Meth- ods for Solidification Problems.	
Carbon dioxide, Reactions (chemical) The Effects of CO and CO <sub>2</sub> on the Rate of Na <sub>2</sub> CO <sub>3</sub> Catalyzed		Numerical Models for Casting Solidification. II.—Application of the Boundary Element Method to Solidification Prob-	
Boudovard Reaction.  The Interfacial Kinetics of the Reaction of CO <sub>2</sub> With Liquid	400-403B	lems. Castings, Microstructure	101-107B
Nickel.	655-661B	Ostwald Ripening and Relaxation in Dendritic Structures.	995-1001A
Carbon dioxide, Solubility Interactions of Gases in Molten Salts: Carbon Dioxide and Oxygen in Cryolite Alumina Melts.	d 39-46B	Catalysis The Effects of CO and CO <sub>2</sub> on the Rate of Na <sub>2</sub> CO <sub>3</sub> Catalyzed Boudovard Reaction.	400-403B

Catalysts The Effects of CO and CO <sub>2</sub> on the Rate of Na <sub>2</sub> CO <sub>3</sub> Catalyzed		Chromium, Oxidation The High-Temperature Oxidation of Metals Forming Cation-	
Boudovard Reaction.	400-403B	Diffusing Scales.  The High-Temperature Oxidation of Metals Forming Cation-Diffusing Scales.	195B 765-782A
See also Fluidized bed cathodes			103-102M
Cathodes, Chemical analysis Reactions in Hall Smelting Cell Potlining.	277-280B	Chromium, Ternary systems Phase Relationships in the Fe—Cr—C System at Solidifica- tion Temperatures. Determination of Inchinated Sections of Michael Birth Regions	663-676B
Cavitation  Punch-Stretching Behavior of a 2014 Aluminum Alloy in the Temperature Range 250 to 500°C.	923-929A	Determination of Isothermal Sections of Nickel-Rich Portion of Ni—Cr—Mo System by Analytical Electron Microscopy.  Chromium carbide, Thermal properties	783-792A
Cavitation, Deformation effects  Effect of Cavitation on Post-Deformation Tensile Properties of a Superplastic Copper-Base Alloy.	1443-1450A	High-Temperature Thermodynamic Properties of the Chro- mium Carbides Cr <sub>2</sub> C <sub>2</sub> and Cr <sub>2</sub> C <sub>2</sub> Determined Using a Gal- vanic Cell Technique.	517-5218
Cavities	1440 14001	Chromium compounds See Chromium carbide	
See Holes Cells		Chromium molybdenum nickel steels See Nickel chromium molybdenum steels	
See Electrolytic cells Cellular precipitates		Chromium molybdenum steels See also Chromium molybdenum vanadium steels	
Chromium Depletion in the Vicinity of Carbides in Sensitized Austenitic Stainless Steels. Interlamellar Spacing in Discontinuous Precipitation.	793-811A 1055-1062A	Nickel chromium molybdenum steels  Chromium molybdenum steels. Coating	
CGF forging process See Forging	1033-10024	Embrittlement of Types 316L and 347 Weld Overlay by Post- Weld Heat Treatment and Hydrogen.	1475-1484A
Chalcogenides		Chromium molybdenum steels, Corrosion Effect of Tempering on the Carbon Activity and Hydrogen At-	
See Sulfides Chalcopyrite, Reactions (chemical)		tack Kinetics of 2.25Cr—1Mo Steel.  Investigation of Stress Corrosion Cracking of Cast and Forged Steel in Water.	2021-2027A 2087-2092A
The Electrochemical Oxidation of Chalcopyrite in Ammonia- cal Solutions.	289-297B	Chromium molybdenum steels, Diffusion A Grain Boundary Etching Method for the Analysis of Inter-	2007 20027
Chalcopyrite, Reduction (chemical)  A Mathematical Model for Calculation of Equilibrium Solution  Secretarios for the Foot - Court - Cuch - Cu		granular Phosphorus-Segregation in Iron-Based Alloys.	1563-1570A
Speciations for the FeCl <sub>3</sub> —FeCl <sub>2</sub> —CuCl <sub>2</sub> —CuCl—HCl— NaCl—H <sub>2</sub> O System at 25°C.	213-219B	Chromium molybdenum steels, Mechanical properties Grain Boundary Composition and Associated Hydrogen Cracking of Modified 4130 Steels.	565-572A
Recovery of Elemental Sulfur During the Oxidative Ammonia- cal Leaching of Chalcopyrite.	726-7298	Core Hardenability Calculations for Carburizing Steels. Fatigue Behavior of Carburized Steel With Internal Oxides	1173-1183A
Chapmanizing See Nitriding		and Nonmartensitic Microstructure Near the Surface.  Chromium molybdenum vanadium steels, Mechanical	1431-1436A
Charge density Electron Microscopy Studies of Charge Density Wave (CDW) Transitions in a Ti <sub>50 x</sub> Ni <sub>3x 5</sub> Al <sub>3x</sub> Alloy.	1155-1163A	properties  Recovery of Creep Properties of a Vanadium-Strengthened	707-718A
Charge transfer	7700 77007	Steel (1Cr1Mo0.75VTiB) by Reheat Treatment.  Chromium nickel molybdenum steels	707-710A
Charge Transfer at Fe/FeO(CaF <sub>2</sub> ) Electrodes at 1450°C: Exchange Current Density, Electrode Capacitance, Diffu- sivity.	281-288B	See Nickel chromium molybdenum steels Chromium nickel steels	
Chemical attack	201-2008	See Nickel chromium steels	
Hydrogen Attack in an Austenitic Stainless Steel.  Chemical composition, Welding effects	1485-1490A	Chromium steels See also Austenitic stainless steels	
Alloying Element Vaporization and Weld Pool Temperature During Laser Welding of AISI 202 Stainless Steel.	641-644B	Chromium molybdenum steels Chromium molybdenum vanadium steels Ferritic stainless steels Mattensitie stainless steels	
Chemical equilibrium  The Determination of the Thermodynamics of the NaF—		Martensitic stainless steels Nickel chromium molybdenum steels Nickel chromium steels	
AIF,—AI <sub>2</sub> O <sub>3</sub> System With a Solid Électrolyte Cell. Discussion of "Calculation Method of Equilibrium Composition in the Carbon—Hydrogen—Oxygen System and Its	135-139B	Stainless steels	
Application to Environments of a High-Temperature Gas Cooled Reactor"; Authors Reply.	396-400B	Chromium steels, Heat treatment Discussion of "The Effect of Heat Treatments on the Corro- sion Fatigue Properties of 13% Chromium Stainless Steel	
Chemical etching		in 3% NaCl Aqueous Solution" (and Authors' Reply).	250-251A
A Grain Boundary Etching Method for the Analysis of Inter- granular Phosphorus-Segregation in Iron-Based Alloys.	1563-1570A	Chromium steels, Mechanical properties Effect of Tempering on Quasistatic and Impact Fracture Toughness and Mechanical Properties for 5140 H Steel.	901-911A
Chemical finishing See Chemical etching		Chromium vanadium steels See Chromium molybdenum vanadium steels	
Chemical kinetics See Reaction kinetics		Clay minerals	
Chemical properties See Heat of formation		See Kaolinite Closing	
Chemistry See Surface chemistry		See Blocking Coating	
Thermochemistry Chip formation		See Copper plating Duplex plating	
Determination of Strain Distributions in Machined Chips.	1777-1779A	Nickel plating Coatings	
Chipless machining See Electric discharge machining		See Diffusion coatings Electroplates	
Chlorides See Hydrochloric acid Sodium chloride		Hot dip coatings Weld deposited coatings	
Chloridizing		Cobalt, Binary systems Solute Stabilization for H.C.PF.C.C. Transitions: Co—Mo.	67-72A
Chloridization Beneficiation of Ilmenite.  Chlorination	259-275B	Cobalt, Corrosion Chlorination of Cobalt in an Argon—1% Oxygen—1% Chlorine Mixture at 1000K.	403-405A
Chlorination of Cobalt in an Argon—1% Oxygen—1% Chlo- rine Mixture at 1000K. Chlorination of Alumina in Kaolinitic Clay.	403-405A 529-533B	Cobalt, Extraction	
A Study of the Mechanisms of the Salt Catalyzed Carbo- chlorination of Kaolin.	695-700B	Control of Autoclave Scaling During Acid Pressure Leaching of Nickeliterous Laterite Ore.	433-440B
Mossbauer Spectroscopy Used to Study the Removal of Iron From Clay.	732-734B	Cobalt, Quaternary systems  Miscibility Gap in Fe—Ni—Al and Fe—Ni—Al—Co Systems.	1819-1828A
Chlorine, Environment Chlorination of Cobalt in an Argon—1% Oxygen—1% Chlo- rine Mixture at 1000K.	403-405A	Cobalt, Thermal properties Thermochemistry of Binary Liquid Gold Alloys: the Systems	
Chromium Chromium Depletion in the Vicinity of Carbides in Sensitized		Au—Ni, Au—Co, Au—Fe and Au—Mn.  Cobalt base alloys, Crystal growth	573-590B
Austenitic Stainless Steels.	793-811A	Nucleation of Recrystallization in a Co-Cr-Mo Alloy.	1335-1338A

## Cobalt base alloys

Cobalt base alloys, Mechanical properties  The Effects of a Liquid Sulfate /Chloride Environment on Superalloy Stress Rupture Properties at 704°C.	23-28A	Compressive properties, Temperature effects Elevated-Temperature Compressive Steady State Deformation and Failure in the Oxide Dispersion Strengthened Alloy	1753-1762A
Cobalt base alloys, Metal working Flow and Fracture of a Multiphase Alloy MP35N for Study of Workability.	1837-1847A	MA 6000E.  Compressive strength, Microstructural effects The Mechanical Behavior of Nonstoichiometric Compounds	
Cobalt base alloys, Microstructure Microstructural Changes During Isothermal Forging of a	220.2454	Ni <sub>3</sub> Si, Ni <sub>3</sub> Ge and Fe <sub>3</sub> Ga.  Compressive yield strength See Compressive strength	173-181A
Co—Cr—Mo Alloy.  Structure of Interphase Boundaries in a Eutectic Co—Al Alloy.	339-345A 1623-1626A	Computer control A Study of Creep Crack Growth in 22 19-T851 Aluminum Alloy	
Cobalt base alloys, Powder technology Carbide Composition Change During Liquid Phase Sintering of a Wear Resistant Alloy.	1099-1102A	Using a Computerized Testing System.  Computer programs Convection in the Two-Phase Zone of Solidifying Alloys.	107-120A 163-172B
Cobalt compounds, Mechanical properties The Fracture of Ordered (Fe, Co) <sub>3</sub> V.	701-706A	Discussion of "Calculation Method of Equilibrium Composi- tion in the Carbon—Hydrogen—Oxygen System and Its	103-1720
Cobalt compounds, Reduction (chemical) Whisker Growth in Reduction of Oxides.	685-694B	Application to Environments of a High-Temperature Gas Cooled Reactor"; Authors Reply.  Computer simulation	396-400B
Coefficient of expansion See Thermal expansion		Simulating the Process of Carbon Anode Baking Used in the Aluminum Industry.	487-492B
Coefficient of thermal expansion See Thermal expansion		Interlamellar Spacing in Directionally Solidified Eutectic Thin Films. Ostwald Ripening During Liquid Phase Sintering—Effect of	1013-1017A
Coke See also Metallurgical coke		Volume Fraction on Coarsening Kinetics.  Concast	1081-1088A
Coke, Oxidation The Effects of CO and CO <sub>2</sub> on the Rate of Na <sub>2</sub> CO <sub>3</sub> Catalyzed Boudovard Reaction.	400-403B	See Continuous casting Concentration (composition)	
Coke breeze See Coke		High-Temperature Phase Chemistries and Solidification Mode Prediction in Nitrogen-Strengthened Austenitic Stainless Steels.	1339-1351A
Cold ductility See Ductility		Concentration (stress) See Stress concentration	
Cold formability See Formability		Conducting See Conduction	
Cold forming See Cold working		Conducting sheet analog See Heat transmission	
Cold reduction See Cold working		Conduction Comparison of Numerical Modeling Techniques for Complex,	207 2100
Cold rolling  Effects of Prior Cold Rolling and Post-Temper Rolling on the  Properties of Continuously Annealed Low-Carbon Dual- Phase Steel.	671-678A	Two-Dimensional, Transient Heat-Conduction Problems.  Consolidation  Local Microstructural Modification in Dynamically Consolidated Metal Powders.	307-318B
Cold shortness See Brittleness	0710704	Constitutional diagrams See Phase diagrams	
Cold working See also Cold rolling		Consumption See Energy consumption	
Stretch forming  Effect of Prior Cold Work on the Martensite Transformation in  SAE 52100.	299-306A	Continuous annealing Temper-Aging of Continuously Annealed Low-Carbon Dual-Phase Steel.	73-86A
Microstructural Changes Produced in a Multifilamentary Nb / Ti Composite by Cold Work and Heat Treatment. Crystallographic and Morphological Characteristics of Oxi- dation Growth Pits in Wustite Grown at 1200°C.	843-852A 2241-2246A	Effects of Prior Cold Rolling and Post-Temper Rolling on the Properties of Continuously Annealed Low-Carbon Dual- Phase Steel.	671-678A
Columbium See Niobium	2241 224011	Continuous cast shapes, Crystal growth Fluid Flow From a Low to a Higher Density Liquid.	681-684B
Columbium base alloys See Niobium base alloys		Continuous casting The Formation of Oscillation Marks in the Continuous Cast-	100 5000
Columbium compounds See Niobium compounds		ing of Steel Slabs. Thermodynamics of Nozzle Blockage in Continuous Casting of Calcium-Containing Steels.	493-509B 547-562B
Compacting See also Hot isostatic pressing		Correction to Thermodynamics of Nozzle Blockage in Contin- uous Casting of Calcium-Containing Steels.	547-562B
On the Effect of NaCl on Porosity in Elemental-Blend Powder Metallurgy Ti—5AI—2.5Sn.	248-249A	Structural Effects and Band Segregate Formation During the Electromagnetic Stirring of Strand-Cast Steel. Strain Induced Cracking in Partially Solidified Tin—Lead	581-589B
Compacts See Powder compacts		Alloy.  Controllability	739-741B
Compliance (elasticity) See Modulus of elasticity		See Stability Controlled atmospheres	
Composite materials See also Fiber composites		See also Inert atmospheres Sintering Atmosphere Effects on the Ductility of W—Ni—Fe Heavy Metals.	747-754A
Composite materials, Mechanical properties  Creep Rupture of a Silicon Carbide Reinforced Aluminum	139-146A	The Effect of Furnace Atmosphere Carbon Potential on the Development of Residual Stresses in 52100 Bearing Steel.	
Composite.  Correction to "Effect of Lithium on the Mechanical Properties and Microstructure of SiC Whisker Reinforced Aluminum Alloys".		Controlled rolling Grain Refinement of Niobium Steels by Control of Recrystall- ization During Hot Rolling.	87-98A
Composite materials, Superconductivity  Effect of Tantalum Additions Upon In Situ Prepared Nb <sub>3</sub> Sn—		Convection Thermosolutal Convection During Directional Solidification.	2125-2137A
Cu Superconducting Wire.  Compositions See Chemical composition	283-286A	Converters See Bottom blown converters Copper converters LD converters	
Compressing Precipitation of Nb(CN) During High-Strain Rate Compression Testing of a 0.07% Niobium-Bearing Austenite.	241-243A	Cooling See Splat cooling	
Compression See Compressing	E-17-E-10A	Supercooling Cooling rate Longitude Mariation With Tool Toppositive and Cooling	
Compressing See Compressive strength		Toughness Variation With Test Temperature and Cooling Rate for Liquid Phase Sintered W—3.5Ni—1.5Fe. The Effect of Quench Rate on the Microstructure, Mechani-	121-128A
Compressive modulus See Modulus of elasticity		cal Properties and Corrosion Behavior of U—6 Wt.% Nb. Estimating Hardness Response of Hot Rolled Steel by Simulating Cooling Cycles Via Jominy Bar Testing.	1319-1330A

Cooling Rate Effects in Ti—6AI—2Sn—4Zr—2Mo Weld- ments. A Two-Dimensional Transient Model for Convection in Laser	1948-1952A	Copper base alloys, Phase transformations Stress-Induced Martensitic Transformation Cycling and Two- Way Shape Memory Training in Cu—Zn—Al Alloys.	313-321A
Melted Pool. Isothermal Martensitic Transformation in Fe—Ni and	2175-2184A	Growth Kinetics and Mechanism of the Massive Transformation.	437-447A
Fe-Ni-C Alloys at Subzero Temperatures.  Copper, Alloying elements An Electron Microscope Study of the Featureless Zone Ob-	2193-2203A	The Effect of Processing Conditions and Subsequent Heat Treatment on the Transformation Behavior of Some Rap- idly Solidified Copper-Base Shape Memory Alloys.	471-480A
tained During Rapid Solidification.  Densification and Structural Development in Liquid Phase	29-31A	Some Effects of Parent Phase Aging on the Martensitic Transformation in a Cu—Al—Ni Shape Memory Alloy. Magnetization Measurement Associated With	621-626A
Sintering.  Pore Filling Process in Liquid Phase Sintering.	1065-1074A 1075-1080A	Magnetization Measurement Associated With Gamma • Alpha Martensitic Transformation of Iron Parti- cles in a Cu—1.59Fe Alloy.	755-756A
Copper, Binary systems Thermochemistry of Binary Liquid Gold Alloys: the Systems Gold—Copper and Gold—Silver at 1379K.	203-208A	Copper base alloys, Phases (state of matter) The Gamma Phase Boundary of CuBe Alloys. Identification of Cu <sub>2</sub> Zr Phase in Cu—Zr Alloys.	939-941A
Calculations of Stable and Metastable Equilibrium Diagrams of the Ag—Cu and Cd—Zn Systems.  Thermodynamic Analysis of the Iron—Copper System.	261-268A	Copper base alloys, Powder technology	1491-1493A
I.—The Stable and Metastable Phase Equilibria.  Copper, Composite materials	1921-1930A	Ostwald Ripening During Liquid Phase Sintering—Effect of Volume Fraction on Coarsening Kinetics.	1081-1088A
Effect of Tantalum Additions Upon In Situ Prepared Nb <sub>3</sub> Sn— Cu Superconducting Wire.	283-286A	Copper base alloys, Structural hardening Age Hardening in Cu—2.5%Ti.	931-937A
Microstructural Changes Produced in a Multifilamentary Nb./ Ti Composite by Cold Work and Heat Treatment. Tensile Strength of Ni/Cu/(001)Ni Triple Layer Films.	843-852A 1273-1280A	Copper converters Injection Phenomena in Nonferrous Processes. High-Pressure Injection of Air Into a Peirce—Smith Copper	77-89B
Copper, Corrosion Stress-Corrosion Cracking of Copper Single Crystals.	1941-1946A	Converter. Copper converters, Design	243-250B
Copper, Dopants Metastable Alloys of Beryllium Prepared by Ion Implantation.	1787-18054	Process R & D—the Noranda Process.	411-432B
Copper, Extraction		Copper mattes Activity Coefficient of Oxygen in Copper—Sulfur Melts.	337-344B
A Mathematical Model for Calculation of Equilibrium Solution Speciations for the FeCl <sub>3</sub> —FeCl <sub>2</sub> —CuCl <sub>2</sub> —CuCl—Hcl— NaCl—H <sub>2</sub> O System at 25°C.	213-219B	Copper mattes, Diffusion Activity of SnS in Copper-Saturated Matte.	595-598B
High-Pressure Injection of Air Into a Peirce—Smith Copper Converter.	243-250B	Copper mattes, Sorption Distribution of Lead Between Copper and Matte and the Ac-	441 440P
The Electrochemical Oxidation of Chalcopyrite in Ammonia- cal Solutions. Activity Coefficient of CuO <sub>0.5</sub> in Alumina-Saturated Iron Sili-	289-297B	tivity of PbS in Copper-Saturated Mattes.  Copper ores	441-449B
cate Slags. Process R & D—the Noranda Process.	345-349B 411-432B	See Chalcopyrite Copper plating	
Distribution of Lead Between Copper and Matte and the Activity of PbS in Copper-Saturated Mattes.	441-449B	Enhanced Tensile Strength for Electrodeposited Nickel / Copper Multilayer Composites.	2039-2040A
Electrochemical Determination of Thiourea and Glue in the Industrial Copper Electrolyte. Equilibria Between Silica-Saturated Iron Silicate Slags and	451-459B	Core hardenability Core Hardenability Calculations for Carburizing Steels.	1173-1183A
Molten Cu—As, Cu—Sb and Cu—Bi Alloys. Activity of SnS in Copper-Saturated Matte.	535-541B 595-598B	Core hardness See Hardness	
The Nature and Source of Copper Smelter Particulate Emissions.	617-622B	Corrosion See Corrosion fatigue	
Copper, Oxidation The High-Temperature Oxidation of Metals Forming Cation-		Corrosion mechanisms Hot gas corrosion	
Diffusing Scales. In Situ Observation of Copper Oxidation at High Temperatures.	195B 573-586A	Scale (corrosion) Sulfurization	
A Collision Model for Fume Formation in Metal Oxidation. The High-Temperature Oxidation of Metals Forming Cation-	587-593A	Corrosion cracking See Stress corrosion cracking	
Diffusing Scales. Copper, Reactions (chemical)	765-782A	Corrosion effects	
A Contribution to the Thermodynamics of High-Temperature Digenite Cu <sub>2-y</sub> —S.	736-739B	See Scale (corrosion)  Corrosion fatigue  Near-Threshold Corrosion Fatigue Crack Growth Behavior of	
Copper, Refining Vacuum Refining Copper Melts to Remove Bismuth, Arsenic		Type 422 Stainless Steel at Controlled Maximum Stress In- tensities.	693-699A
and Antimony.  Copper, Ternary systems	251-257B	Effect of Oxidation Kinetics on the Near Threshold Fatigue Crack Growth Behavior of a Nickel-Base Superalloy.	1769-1775A
Zero-Flux Planes and Flux Reversals in the Cu—Ni—Zn System at 775°C.  Copper, Thermal properties	649-659A	Corrosion fatigue, Heating effects Discussion of "The Effect of Heat Treatments on the Corrosion Fatigue Properties of 13% Chromium Stainless Steel	
Thermochemistry of Alloys of Transition Metals. IV.—Alloys of Copper With Scandium, Yttrium, Lanthanum and Lute tium.		in 3% NaCl Aqueous Solution" (and Authors' Reply).  Corrosion mechanisms	250-251A
Copper base alloys	337-3666	See also Scale (corrosion) In Situ Observation of Copper Oxidation at High Temperatures.	573-586A
See also Admiralty metal Aluminum brasses Brasses		A Collision Model for Fume Formation in Metal Oxidation.	587-593A
Copper base alloys, Crystal lattices		Corrosion products See Scale (corrosion)	
Heating Rate Dependence of Disordering in Alpha-Cu — Al Al loys.	1999-2008A	Corrosion rate Chlorination of Cobalt in an Argon—1% Oxygen—1% Chlorine Mixture at 1000K.	403-405A
Copper base alloys, Diffusion An Analytical Electron Microscope Study of the Kinetics o the Equilibrium Segregation of Bismuth in Copper. Surface Relief Produced by Diffusion-Induced Boundary Mi	99-105A	Corrosion rate, Composition effects The Effects of a Liquid Sulfate / Chloride Environment on Su-	
gration in Cu—Zn.	495-499A	peralloy Stress Rupture Properties at 704°C.  Corrosion rate, Stress effects	23-28A
Copper base alloys, Directional solidification  The Solidification of Monotectic Alloys—Microstructures and Phase Spacings.	1003-1012A	Behavior of Fe—Ni—Cr Alloys in a Complex Multioxidant En- vironment Under Conditions of Dynamic Straining.	11-22A
Copper base alloys, Mechanical properties  Effect of Cavitation on Post-Deformation Tensile Properties		Corrosion resistance, Cooling effects The Effect of Quench Rate on the Microstructure, Mechanical Properties and Corrosion Behavior of U—6 Wt. % Nb.	1319-1330A
of a Superplastic Copper-Base Alloy.  The Mechanical Properties of Grain-Refined Beta-CuAIN Strain-Memory Alloys.	1443-1450A li 1613-1621A	Crack closure Fatigue Threshold Studies in Iron, Fe—Si and HSLA Steel.	
Copper base alloys, Melting Distribution of Nickel Between Copper—Nickel and Alumina Saturated Iron Silicate Slags.	33-37B	I. — Effect of Strength and Surface Asperities on Closure.  Crack closure, Environmental effects     Environmentally Influenced Mixed Mode Fatigue Crack Prop-	875-888A
Copper base alloys, Microstructure Modulated Microstructures in Copper—Zinc and Copper—		agation of Titanium Metal/Matrix Composites.  Crack closure, Microstructural effects	209-215A
Aluminum—Nickel. A Review of the Data on the Interlamellar Spacing of Pearlite	269-276A	The Effect of Microstructure and Environment on Fatigue Crack Closure of 7475 Aluminum Alloy.	555-563A

(	Crack growth See Crack propagation		Creep rate A Study of Creep Crack Growth in 2219-T851 Aluminum Alloy	
-	Crack propagation A Study of Creep Crack Growth in 2219-T851 Aluminum Alloy		Using a Computerized Testing System.  Creep rate, Composition effects	107-120A
	Using a Computerized Testing System.  Envelopes of Crack-Like Surfaces for Modeling Cavity Growth.	107-120A 246-247A	Creep Rupture of a Silicon Carbide Reinforced Aluminum Composite.	139-146A
	Fracture Behavior of W-Ni-Fe Heavy Alloys. Fatigue Crack Growth Behavior of an Oxide Dispersion-	331-338A 527-539A	Creep rate, Deformation effects Prior Deformation Effects on Creep and Fracture in Inconel Alloy X-750.	1437-1441A
	Strengthened MA 956 Alloy.  Hydrogen-Induced Slow Crack Growth in Stable Austenitic Stainless Steels.  Fatigue Threshold Studies in Iron, Fe—Si and HSLA Steel.  II.—Thermally Activated Behavior of the Effective Stress	729-733A	Creep rate, Microstructural effects Structure and Properties of Rapidly Solidified Dispersion- Strengthened Titanium Alloys. II.—Tensile and Creep Properties.	1465-1474A
	Intensity at Threshold.  Dependence of Dynamic Fracture Resistance on Crack Ve-	889-900A 1247-1251A	Creep recovery	1571-1577A
	Dependence of Dynamic Fracture Resistance on Crack Velocity in Tungsten. II.—Bicrystals and Polycrystals.  The Effect of One Slow—Fast Strain Cycle on the Fatigue	1253-1258A	Creep recovery, Heating effects Recovery of Creep Properties of a Vanadium-Strengthened Steel (1Cr1Mo0.75VTiB) by Reheat Treatment.	707-718A
	Crack Growth Behavior of SUS 304 Stainless Steel at Ele- vated Temperature. Fatigue Crack Growth Mechanics for Ti—6AI—4V (RA) in	1731-1739A	Creep resistance See Creep strength	
	Vacuum and Humid Air.  Crack propagation, Alloying effects	1931-1940A	Creep rupture strength Fatigue Crack Growth Behavior of an Oxide Dispersion-	
	Fatigue in Binary Alloys of B.C.C. Iron.  Crack propagation, Corrosion effects	679-691A	Strengthened MA 956 Álloy. Hydrogen-Induced Slow Crack Growth in Stable Austenitic Stainless Steels.	527-539A 729-733A
	The Sulfidation Attack of a Nickel-Base Alloy at Intermediate Temperatures.  Effect of Oxidation Kinetics on the Near Threshold Fatigue	5-10A	Creep rupture strength, Coating effects The Effect of Protective Coatings on the High-Temperature	729-733A
	Crack Growth Behavior of a Nickel-Base Superalloy.  Crack propagation, Diffusion effects	1769-1775A	Properties of a Gamma Prime-Strengthened Nickel-Base Superalloy.	229-236A
	Hydrogen-Induced Interior Crack-Tip Morphologies in High- Strength Steel.	1865-1871A	Creep rupture strength, Corrosion effects The Sulfidation Attack of a Nickel-Base Alloy at Intermediate Temperatures.	5-10A
	Crack propagation, Environmental effects Environmentally Influenced Mixed Mode Fatigue Crack Propagation of Titanium Metal / Matrix Composites.	209-215A	The Effects of a Liquid Sulfate / Chloride Environment on Su- peralloy Stress Rupture Properties at 704°C.	23-28A
	Mechanisms of Slow Fatigue Crack Growth in High-Strength Aluminum Alloys: Role of Microstructure and Environment. Effect of Environment on Creep Crack Growth in PM/HIP	369-379A	Creep rupture strength, Deformation effects Prior Deformation Effects on Creep and Fracture in Inconel Alloy X-750.	1437-1441A
	René-95. Crack propagation, Heating effects	381-388A	Creep rupture strength, Environmental effects Behavior of Fe—Ni—Cr Alloys in a Complex Multioxidant En-	
	Discussion of "The Effect of Heat Treatments on the Corro- sion Fatigue Properties of 13% Chromium Stainless Steel		vironment Under Conditions of Dynamic Straining. Effect of Environment on Creep Crack Growth in PM/HIP	11-22A
	in 3% NaCl Aqueous Solution" (and Authors' Reply).  Crack propagation, Microstructural effects	250-251A	René-95.  Creep strength, Composition effects	381-388A
	The Role of Alpha and Beta Phases in Fatigue Crack Propa- gation of Ti—Mn Alloys. Effect of Microstructure, Strength and Oxygen Content on	155-171A	Creep Rupture of a Silicon Carbide Reinforced Aluminum Composite.	139-146A
	Fatigue Crack Growth Rate of Ti—4.5AI—5.0Mo—1.5Cr (CORONA 5). Fatigue Crack Propagation in Dual-Phase Steels: Effects of	183-197A	Creep strength, Environmental effects Tensile Behavior of Inconel Alloy X-750 in Air and Vacuum at Elevated Temperatures.	1763-1767A
	Ferritic—Martensitic Microstructures on Crack Path Mor- phology.	1193-1207A	Creeping See Creep (materials)	
	Influence of Texture on Fatigue Properties of Ti—6AI—4V.  Crack propagation, Size effects	1597-1605A	Critical current (superconductivity), Alloying effects Effect of Tantalum Additions Upon In Situ Prepared Nb <sub>3</sub> Sn—	
	The Influence of Crack Tip Plasticity in the Growth of Small Fatigue Cracks.	1579-1588A	Cu Superconducting Wire.  Critical field (superconductivity), Alloying effects	283-286A
	Crack propagation, Stress effects The Effect of Overload on the Fatigue Crack Propagation in Metastable Beta Ti—V Alloys.	511-517A	Effect of Tantalum Additions Upon In Situ Prepared Nb <sub>3</sub> Sn— Cu Superconducting Wire.	283-286A
	Existence of the Coaxing Effect and Effects of Small Artifi- cial Holes on Fatigue Strength of an Aluminum Alloy and 70-30 Brass.		Critical temperature The Effect of Processing Conditions and Subsequent Heat Treatment on the Transformation Behavior of Some Rap-	
	Crack propagation, Temperature effects Crack Growth in a Single-Crystal Superalloy at Elevated		idly Solidified Copper-Base Shape Memory Alloys.  Cross tension test	471-480A
	Temperature.  Crack resistance	1711-1719A	See Tension tests Crushing strength	
	See Crack propagation Cracking (fracturing)		See Compressive strength  Cryogenic temperature	
	See also Stress corrosion cracking Stress cracking		See Cryogenics Cryogenics	
	Strain Induced Cracking in Partially Solidified Tin—Lead Alloy. Prior Deformation Effects on Creep and Fracture in Incone	739-741B	The Role of the Constituent Phases in Determining the Low Temperature Toughness of 5.5Ni Cryogenic Steel.	2213-2219A
	Alloy X-750.  Cracking (fracturing), Microstructural effects	1437-1441A	Cryolite, Reactions (chemical)  The Determination of the Thermodynamics of the NaF—  AIF <sub>3</sub> —AI <sub>2</sub> O <sub>3</sub> System With a Solid Electrolyte Cell.	135-139B
	The Influence of Hydrogen and the Interface Phase on Frac- ture in Ti Code 12.  Creep (materials)	1955-1958A	Cryolite, Solubility Interactions of Gases in Molten Salts: Carbon Dioxide and Oxygen in Cryolite Alumina Melts.	39-46B
	See also Creep life Creep rate		Crystal defects See also Dislocations	
	Creep recovery Creep rupture strength Creep strength Dislocation-Depth Distribution in High-Temperature Creep.	1571-1577A	Edge dislocations Screw dislocations Structure of Interphase Boundaries in a Eutectic Co—Al	
	Creep Transitions in an Al—Zn Alloy.  Creep life	1893-1904A	Alloy.  Crystal growth	1623-1626A
	Recovery of Creep Properties of a Vanadium-Strengthened Steel (1Cr1Mo0.75VTiB) by Reheat Treatment.	707-718A	Distinguishing Features of Massive Transformations. Convection-Induced Distortion of a Solid/Liquid Interface. Morphological Stability in the Presence of Fluid Flow in the	421-425A 2109-2115A
	Creep life, Corrosion effects The Effects of a Liquid Sulfate / Chloride Environment on Su peralloy Stress Rupture Properties at 704°C.	23-28A	Melt. Thermosolutal Convection During Directional Solidification. Studies of Directionally Solidified Eutectic Bi/MnBi at Low	2117-2124A 2125-2137A
	Creep limit See Creep (materials)		Growth Velocities.  Thermoelectric and Morphological Effects of Peltier Pulsing	2139-2145A
	Creep properties See Creep (materials)		on Directional Solidification of Eutectic Bi / Mn. A Two-Dimensional Transient Model for Convection in Laser Melted Pool.	2147-2154A 2175-2184A

Crystal growth, Diffusion effects Growth Kinetics and Mechanism of the Massive Transforma-	427 4478	Descaling Control of Autoclave Scaling During Acid Pressure Leaching of Nickeliferous Laterite Ore.	433-440B
tion.  Crystal growth, Field effects  Effect of Applied Magnetic Fields During Directional Solidifi-	437-447A	Desulfurizing A Contribution to the Thermodynamics of High-Temperature	
cation of Eutectic Bi / Mn.  Crystal lattices	2155-2161A	Digenite Cu <sub>2-y</sub> —S.  Diagrams	736-739B
See Superlattices Crystal orientation		See Phase diagrams S N diagrams	
See Crystal structure		Dielectric properties See Dielectrics	
Crystal structure See also Substructures (crystalline) The Nucleation Kinetics, Crystallography and Mechanism of the Massive Transformation. Rapid Solidification of a Droplet-Processed Stainless Steel. Formation of Metal Carbide Powder by Spark Machining of Reactive Metals.	427-435A 819-833A	Dielectrics, Reactions (chemical) Formation of Metal Carbide Powder by Spark Machining of Reactive Metals.  Diffraction See also Diffraction patterns Electron diffraction	1117-1127A
Use of Reciprocal Lattice Layer Spacing in Convergent Beam Electron Diffraction Analysis.	1299-1302A	Modulated Microstructures in Copper—Zinc and Copper— Aluminum—Nickel.	269-276A
Crystallinity See Crystal structure		Diffraction patterns "Premartensitic" Phase in Nickel—Aluminum Thin Foils.	1353-1357A
Crystallization See also Recrystallization		Diffractometry See Diffraction	
Numerical Treatment of Rapid Solidification.  Crystallization Studies in the Aluminum-Rich Corner of the Aluminum—Iron—Manganese System.	369-381B 1311-1317A	Diffusion Distinguishing Features of Massive Transformations. Kinetics of Methane Bubble Growth in a 1020 Steel. The Effect of Pressure Modulation on the Flow of Gas	421-425A 487-494A
Crystallography On the Substructure of Athermal and Isothermal Martensites Formed in an Fe—21Ni—4Mn Alloy.	1555-1562A	Through a Solid Membrane: Permeation and Diffusion of Hydrogen Through Nickel.	639-648A
Crystals		Zero-Flux Planes and Flux Reversals in the Cu—Ni—Zn System at 775°C.	649-659A
See Bicrystals Polycrystals Single crystals		Forced Velocity Pearlite in High-Purity Fe—C Alloys. II.— Theoretical. Ternary Diffusion. Solutions With Diffusion Coefficients Lin-	1047-1054A
Whiskers (metals)		early Dependent on Concentrations.	1359-1366A
Currents See Critical current (superconductivity) Curves		Diffusion coatings The Effect of Protective Coatings on the High-Temperature Properties of a Gamma Prime-Strengthened Nickel-Base Superalloy.	229-236A
See Stress strain curves Cutting		Diffusion coefficient See Diffusion	
See Electric discharge machining Cutting tools		Diffusion couples	
See Hack saws High speed steel tools		See Diffusion  Diffusion rate Segregation of Manganese During Intercritical Annealing of	
Czochralski process See Crystal growth		Dual-Phase Steels.  Diffusivity	1499-1502A
Decarburizing The Interfacial Kinetics of the Reaction of CO <sub>2</sub> With Liquid Nickel.	655-661B	Discussion of "Self-Diffusion Coefficients of Carbon in Fe <sub>3</sub> C at 723K Via the Kinetics of Formation of This Compound (and Authors' Reply).	245-246A
Decomposition See Phase decomposition		Oxygen Solubility in Liquid Indium and Oxygen Diffusivity in Liquid Indium and Tin. Thermodynamics of the Massive Transformation.	329-335B 411-419A
Deep carburizing See Carburizing		Surface Relief Produced by Diffusion-Induced Boundary Mi- gration in Cu—Zn.  The Room-Temperature Effective Diffusivity of Hydrogen in	495-499A
See Casting defects Crystal defects		Vapor-Deposited Aluminum.  Diffusivity, Coating effects Prevention of Hydrogen Embrittlement by a TiO <sub>2</sub> Surface	1953-1955A
Dislocations Edge dislocations Screw dislocations Surface defects		Layer.  Diffusivity, Environmental effects Isotope Exchange Studies of the Rate of Dissociation of CO <sub>2</sub>	597-600A
Deformability See Formability		on Liquid Iron Oxides and CaO-Saturated Calcium Ferrites.  Dimensions	
Dendrite See Dendritic structure		See Particle size Thickness	
Dendritic structure		Dioxides See Carbon dioxide	
Fluid Flow From a Low to a Higher Density Liquid. Pattern Selection in Solidification.	681-684B 961-966A	Silicon dioxide Titanium dioxide	
Interdendritic Spacing. I.—Experimental Studies. Interdendritic Spacing. II.—A Comparison of Theory and Experiment.	967-975A 977-982A	Dip coatings See Hot dip coatings	
A Numerical Finite Difference Model of Steady State Cellula and Dendritic Growth.		Direct reduction	
Ostwald Ripening and Relaxation in Dendritic Structures. Solidification of Highly Undercooled Sn—Pb Alloy Droplets Primary Dendrite Spacing. II.—Experimental Studies of Pb—	995-1001A	See also Hydrogen reduction Cell Measurements of the Reduction Potentials of Gas- Phase Emanating From PbS/CaO/C at Elevated Tempera- tures.	
Pd and Pb—Au Alloys.  Effects of Gravity on Interdendritic Flow: an Analytical Ap		The Breakdown of Dense Iron Layers on Wustite in CO/CO <sub>2</sub> and H <sub>2</sub> /H <sub>2</sub> O Systems.	
proach.  The Mechanisms of Formation and Prevention of Channel		Establishment of Product Morphology During the Initial Stages of Wustite Reduction.	
Segregation During Alloy Solidification.  Densification	2163-2173A	Directional solidification Pattern Selection in Solidification.	961-966A
Densification and Structural Development in Liquid Phas Sintering.	e 1065-1074A	Interdendritic Spacing, I.—Experimental Studies, Interdendritic Spacing, II.—A Comparison of Theory and Ex	967-975A
Densification, Environmental effects Sintering Atmosphere Effects on the Ductility of W—Ni—F	е	periment.  Primary Dendrite Spacing, II.—Experimental Studies of Pb—	977-982A
Heavy Metals.  Dephosphorizing Thermodynamics of Phosphate and Phosphide in CaO-	747-754A	Pd and Pb—Au Alloys.  Thermosolutal Convection During Directional Solidification.  Studies of Directionally Solidified Eutectic Bi/MnBi at Low Growth Velocities.	1665-1676A 2125-2137A v 2139-2145A
CaF <sub>2</sub> Melts.	351-356B	Thermoelectric and Morphological Effects of Peltier Pulsing on Directional Solidification of Eulectic Bi / Mn.	
Deposition See Copper plating Duplex plating Nickel plating		Directional solidification, Field effects  Effect of Applied Magnetic Fields During Directional Solidification of Fitteric RIVMs	

#### **Directionally solidified eutectics**

Directionally solidified eutectics Intertamellar Spacing in Directionally Solidified Eutectic Thin Films.	1013-1017A	Ductile brittle transition, Cooling effects Toughness Variation With Test Temperature and Cooling Rate for Liquid Phase Sintered W—3.5Ni—1.5Fe.	121-128A
Directionally solidified eutectics, Crystal growth The Breakdown of Fibrous Structures in Directionally Grown	1626-1631A	Ductile brittle transition, Heating effects The Role of the Constituent Phases in Determining the Low Temperature Toughness of 5.5Ni Cryogenic Steel.	2213-2219A
Directionally solidified eutectics, Mechanical		Ductile iron See Nodular iron	
properties Deformation and Fracture Behavior of Ni Mo Al (Gamma Gamma Prime-Alpha) In Situ Composite.	1905-1919A	Ductility Fracture Behavior of WNiFe Heavy Alloys.	331-338A
Directionally solidified eutectics, Microstructure The Effect of Fluid Flow on the Eutectic Lamellar Spacing.	307-312A	The Fracture of Ordered (Fe. Co) <sub>3</sub> V.  Hot Workability of Three Grades of Tool Steels.	701-706A 1855-1864A
The Solidification of Monotectic Alloys—Microstructures and Phase Spacings.	1003-1012A	Ductility, Alloying effects  Effects of Hydrogen on Mechanical Properties of	
Structure of Interphase Boundaries in a Eutectic Co-Al Alloy.	1623-1626A	Vanadium—Niobium Alloys. Improved Strength and Ductility in Ni <sub>3</sub> Al by Boron Modifica- tion and Rapid Solidification.	147-153A 399-402A
Discontinuous precipitates See Cellular precipitates		Ductility, Anisotropy Effect of Shape of Sulfide Inclusions on Anisotropy of Inclu-	
Dislocation density  Consequences of the Heterogeneous Nitriding of Alpha-Iron: Dislocation Production and Oriented Precipitation.	627-637A	sion Spacings and on Directionality of Ductility in Hot Rolled C—Mn Steels.	1259-1264A
	1571-1577A	Ductility, Coating effects The Effect of Protective Coatings on the High-Temperature Properties of a Gamma Prime-Strengthened Nickel-Base	
Crystallographic and Morphological Characteristics of Oxi-	2241-2246A	Superalloy.  Ductility, Heating effects	229-236A
Dislocation density, Stress effects Dislocation Substructure as a Function of Strain in a Dual- Phase Steel.	1221-1228A	Low-Temperature Improvement of the Mechanical Properties of 4340-Type Ultra-High-Strength Steel With Heat Treating	2247-2249A
Dislocations See also Edge dislocations		Ductility, High temperature effects Tensile Failure Behavior of Plain Carbon Steels at Elevated	
Screw dislocations Tensile Strength of Ni/Cu/(001)Ni Triple Layer Films.	1273-1280A	Temperatures.  Ductility, Microstructural effects	2059-2073A
Dislocations, Deformation effects The Structure of Extruded NiAl.	1129-1136A	The Effect of Microstructure on the Deformation Modes and Mechanical Properties of Ti—6AI—2Nb—1Ta—0.8Mo.	
Dispersion hardening Rapid Solidification Processing of Magnesium—Lithium Al-		I.—Widmanstätten Structures. The Effect of Microstructure and Deformation Behavior on the Hot Ductility of Ti—6AI—2Nb—1Ta—0.8Mo.	1229-1245A 1687-1698A
loys.	237-240A	Duomeit process	1007-1030A
Dispersion hardening, Heating effects Structure and Properties of Rapidly Solidified Dispersion-		See Vacuum arc melting	
Strengthened Titanium Alloys. I.—Characterization of Dis- persoid Distribution, Structure and Chemistry.	1451-1463A	Duplex chromium plating See Duplex plating	
Dispersion hardening alloys, Mechanical properties Fatigue Crack Growth Behavior of an Oxide Dispersion-		Duplex nickel plating See Duplex plating	
Strengthened MA 956 Alloy.  Structure and Properties of Rapidly Solidified Dispersion- Strengthened Titanium Alloys. II.—Tensile and Creep	527-539A	Duplex plating Enhanced Tensile Strength for Electrodeposited Nickel / Copper Multilayer Composites.	2039-2040A
Properties. Elevated Temperature Compressive Steady State Deforma-	1465-1474A	Dur Ni process	
tion and Failure in the Oxide Dispersion Strengthened Alloy MA 6000E.	1753-1762A	See Duplex plating  Dust	
Dissociation energy See Free energy of formation		See Smelter dust  Dynamics	
Dissolution See also Anodic dissolution		See Fluid dynamics Kinetics	
The Dissolution of Titanium in Liquid Steel.  Shape Changes During Dissolution of Theta Prime-CuAl <sub>2</sub> .  Metastable Phases in the Early Stage of Precipitation in Al—	47-58B 449-458A	Edge dislocations High-Temperature Oxidation of Iron at 1200°C in a Hot Stage Environmental Scanning Electron Microscope.	2231-2240A
Mg Alloys.  Dissolution Kinetics of Widmanstätten Gamma-Ag <sub>2</sub> Al Precipitates.	835-842A 1969-1975A	Elastic constants See Modulus of elasticity	
Dissolving	1909-1975M	Elastic modulus See Modulus of elasticity	
See Dissolution  Doehler double plating		Electric arc melting	
See Duplex plating  Domains		See Vacuum arc melting Electric conductors (materials)	
Some Effects of Parent Phase Aging on the Martensitic Transformation in a Cu—Al—Ni Shape Memory Alloy.	621-626A	See Electrolytes Electric discharge machining	
Drawing (heat treatment) See Tempering		Formation of Metal Carbide Powder by Spark Machining of Reactive Metals.	1117-1127A
Drill steels See Tool steels		See Electric discharge machining	
Dual nickel plating See Duplex plating		Electric welding See Electron beam welding	
Dual phase steels, Diffusion Segregation of Manganese During Intercritical Annealing of Dual-Phase Steels.	1499-1502A	Electroslag welding Gas tungsten arc welding Submerged arc welding	
Dual phase steels, Heat treatment		Electrical conductance See Electrical resistance	
Temper-Aging of Continuously Annealed Low-Carbon Dual Phase Steel.	73-86A	Electrical impedance See Electrical resistance	
Dual phase steels, Mechanical properties Effects of Prior Cold Rolling and Post-Temper Rolling on the Properties of Continuously Annealed Low-Carbon Dual	9	Electrical properties See Thermoelectricity	
Phase Steel.  Fatigue Crack Propagation in Dual-Phase Steels: Effects o Ferritic—Martensitic Microstructures on Crack Path Mor	671-678A f	Electrical resistance, Temperature effects Electron Microscopy Studies of Charge Density Wave (CDW, Transitions in a Ti <sub>58 7</sub> Ni <sub>37 5</sub> Al <sub>3 8</sub> Alloy.	) 1155-1163A
phology.  Dual phase steels, Microstructure  Dislocation Substructure as a Function of Strain in a Dual	1193-1207A	Electrical steels, Microstructure A Review of the Data on the Interlamellar Spacing of Pearlite	. 1019-1036A
Phase Steel.  Dual phase steels, Rolling	1221-1228A	Electrocoatings See Electroplates	
Grain Refinement of Niobium Steels by Control of Recrystall ization During Hot Rolling.	87-98A	Electrodeposition See Duplex plating	
	;		

Electrodes		Heat of formation	
See Anodes Cathodes Fluidized bed cathodes		Heat of mixing Heat of solution Surface energy	
Electroerosion (machining) See Electric discharge machining		Energy conservation Exergy Analysis of a Chemical Metallurgical Process.	645-654B
Electrolysis See Electrowinning		Energy consumption Exergy Analysis of a Chemical Metallurgical Process.	645-654B
Electrolytes, Chemical analysis Electrochemical Determination of Thiourea and Glue in the	15. 1505	Energy of activation See Activation energy	043-034B
Industrial Copper Electrolyte.  Electrolytic cells Reactions in Hall Smelting Cell Pottining.	451-459B 277-280B	Energy of dissociation See Free energy of formation	
Electrolytic dissolution See Anodic dissolution	277-2808	Energy of formation See Free energy of formation	
Electromagnetic stirring		Energy of fracture See Toughness	
The Effect of Fluid Flow on the Eutectic Lamellar Spacing. Steady Low of Liquid Aluminum in a Rectangular-Vertical Ingot Mold, Thermally or Electromagnetically Activated.	307-312A 471-478B	Environment See Space environment	
Structural Effects and Band Segregate Formation During the Electromagnetic Stirring of Strand-Cast Steel.	581-589B	Equilibrium	
Fluid Flow and Mass Transfer in an Inductively Stirred Four- Ton Melt of Molten Steel: a Comparison of Measurements and Predictions.	633-640B	See Chemical equilibrium  Equilibrium constants	
Electron beam melting The Effect of Rapid Solidification Velocity on the Microstruc-		See Chemical equilibrium  Equilibrium diagrams See Phase diagrams	
ture of Ag—Cu Alloys.  Electron beam vacuum melting See Electron beam melting	55-66A	Erosion resistance, Heating effects Laser Processing of Cast Iron for Enhanced Erosion Resis-	
Electron beam welding		tance.	719-728A
A New Finite Element Model for Welding Heat Sources.  Metal Vaporization From Weld Pools.	299-305B 461-469B	See Chemical etching	
Electron diffraction Use of Reciprocal Lattice Layer Spacing in Convergent Beam Electron Diffraction Analysis.	1299-1302A	Eutectic composition Microstructure of One of the Ternary Eutectic Alloys in the Bi—In—Sn System.	1515-1517A
"Premartensitic" Phase in Nickel—Aluminum Thin Foils.  Electron microscopy	1353-1357A	Eutectics See also Directionally solidified eutectics	
See also Scanning electron microscopy An Analytical Electron Microscope Study of the Kinetics of		Eutectics, Crystal growth Modification in the Aluminum—Silicon System.	450 4604
the Equilibrium Segregation of Bismuth in Copper.  Electroplates, Mechanical properties	99-105A	Eutectoid reactions	459-469A
Enhanced Tensile Strength for Electrodeposited Nickel/ Copper Multilayer Composites.	2039-2040A	A Review of the Data on the Interlamellar Spacing of Pearlite. Further Considerations on the Thermodynamics of the Proeutectoid Ferrite Reaction in Fe—C Alloys.	1019-1036A 1287-1288A
See Duplex plating		Exhaust gases See Flue gases	
Electroreduction See Electrowinning		Expansion See Thermal expansion	
Electrorefining See Electroslag refining		Extractive metallurgy	
Electroslag process See Electroslag refining		See Hydrometallurgy  Extrusion compacting	
Electroslag refining Charge Transfer at Fe/FeO(CaF <sub>2</sub> ) Electrodes at 1450°C:		See Compacting  Extrusions, Microstructure  The Structure of Extruded NiAl.	1129-1136A
Exchange Current Density, Electrode Capacitance, Diffusivity.	281-288B	Fatigue (materials)	1129-1136A
Electroslag welding The Role of Alloy Composition on the Stability of Nitrides in Titanium-Microalloyed Steels During Weld Thermal Cycles.	33-41A	See also Corrosion fatigue Fatigue life Fatigue limit	
Electrowinning Electrochemical Determination of Thiourea and Glue in the	45 + 450B	Fatigue strength Low cycle fatigue Fatigue Crack Growth Behavior of an Oxide Dispersion-	
Industrial Copper Electrolyte. Electrodissolution of Lead Sulfide in Different Acidic Media. Fluidized-Bed Electrodeposition of Zinc.	451-459B 605-608B 623-631B	Strengthened MA 956 Alloy.  The Effect of Microstructure and Environment on Fatigue Crack Closure of 7475 Aluminum Alloy.	527-539A 555-563A
Elongation Tensile Properties of a 2014 Aluminum Alloy in the Tempera-		Fatigue Threshold Studies in Iron, Fe—Si and HSLA Steel.  II.—Thermally Activated Behavior of the Effective Stress Intensity at Threshold.	889-900A
ture Range 250 to 500°C.  Embrittlement See also Hydrogen embrittlement	913-922A	Fatigue (materials), Alloying effects The Effect of Minor Alloying Elements on the Mechanical	
Interphase Boundary Precipitation in Liquid Phase Sintered W—Ni—Fe and W—Ni—Cu Alloys.	1089-1098A	Properties of Al—Cu—Li Alloys.  Fatigue (materials), Microstructural effects	1209-1220A
Embrittlement, Alloying effects The Influence of Alloying Elements on Impurity-Induced Grain Boundary Embrittlement.	1415-1430A	Fatigue Crack Propagation in Dual-Phase Steels: Effects of Ferritic—Martensitic Microstructures on Crack Path Mor- obology	1193-1207A
Embrittlement, Cooling effects Toughness Variation With Test Temperature and Cooling		Fatigue Behavior of Carburized Steel With Internal Oxides and Nonmartensitic Microstructure Near the Surface.	1431-1436A
Rate for Liquid Phase Sintered W—3.5Ni—1.5Fe.  Embrittlement, High temperature effects Tensile Failure Behavior of Plain Carbon Steels at Elevated	121-128A	Fatigue (materials), Stress effects  The Effect of Overload on the Fatigue Crack Propagation in Metastable Beta Ti—V Alloys.	511-517A
Temperatures.  Emission	2059-2073A	Fatigue (materials), Temperature effects Fatigue Threshold Studies in Iron, Fe—Si and HSLA Steel.	075 005
See Acoustic emission End quenching		<ul> <li>I.—Effect of Strength and Surface Asperities on Closure.</li> <li>Fatigue cracking</li> </ul>	875-888A
See Jominy test		See Fatigue failure Fatigue failure, Corrosion effects	
Endurance (testing) See Fatigue tests		The Sulfidation Attack of a Nickel-Base Alloy at Intermediate Temperatures.	5-10/
Endurance limit See Fatigue limit		Fatigue failure, Microstructural effects Effect of Microstructure, Strength and Oxygen Content or	
Energy See Activation energy Free energy		Fatigue Crack Growth Rate of Ti—4.5Al—5.0Mo—1.5Ci (CORONA 5).  Mechanisms of Slow Fatigue Crack Growth in High-Strength	183-197A
Free energy of formation		Aluminum Alloys: Role of Microstructure and Environment	369-379

Fatigue failure, Temperature effects Crack Growth in a Single-Crystal Superalloy at Elevated		The Nucleation Kinetics, Crystallography and Mechanism of the Massive Transformation.	427-435A
Temperature.  Deformation in Ti <sub>3</sub> Al Fatigued at Room and Elevated Temper-	1711-1719A 1721-1729A	Further Considerations on the Thermodynamics of the Proeutectoid Ferrite Reaction in Fe—C Alloys. Isothermal Martensitic Transformation in Fe—Ni and	1287-1288A
Fatigue fracture See Fatigue failure		Ferrous alloys, Phases (state of matter)	2193-2203A
Fatigue life The High-Temperature Low-Cycle Fatigue Behavior of the		Nucleation of Intragranular Ferrite in Fe—Ni—P Alloys. Growth of Intragranular Ferrite in Fe—Ni—P Alloys. On the Substructure of Athermal and Isothermal Martensites	861-865A 867-874A
Nickel-Base Alloy IN-617.  The Effect of One Slow—Fast Strain Cycle on the Fatigue Crack Growth Behavior of SUS 304 Stainless Steel at Ele-	661-670A	Formed in an Fe—21Ni—4Mn Alloy.  Ferrous alloys, Powder technology	1555-1562A
	1731-1739A	Densification and Structural Development in Liquid Phase Sintering.  Pore Filling Process in Liquid Phase Sintering.	1065-1074A 1075-1080A
Fatigue in Binary Alloys of B.C.C. Iron. Fatigue life, Temperature effects	679-691A	Ostwald Ripening During Liquid Phase Sintering—Effect of Volume Fraction on Coarsening Kinetics.	1081-1088A
Deformation in Ti <sub>3</sub> Al Fatigued at Room and Elevated Temper-	1721-1729A	Ferrous alloys, Solubility Solubility Product for Niobium Carbide in Austenite.	541-544A
Fatigue limit, Stress effects Existence of the Coaxing Effect and Effects of Small Artifi-		Ferrous alloys, Structural hardening Kinetics of Aging in an Fe—12Ni—6Mn Maraging Alloy.	1947-1948A
cial Holes on Fatigue Strength of an Aluminum Alloy and	2029-2038A	Ferrous alloys, Thermal properties On the Relationship Between Interaction Coefficients.	677-680B
Fatigue properties See Fatigue (materials)		Ferrous compounds See Iron compounds	
Fatigue strength, Heating effects Discussion of "The Effect of Heat Treatments on the Corro-		Ferrous metals See Ferrous alloys	
sion Fatigue Properties of 13% Chromium Stainless Steel in 3% NaCl Aqueous Solution" (and Authors' Reply).	250-251A	Fiber composites, Forging The Fracture Behavior of Tungsten Wire-Reinforced Superal-	
Fatigue strength, Microstructural effects Tensile and Fatigue Behavior of Aluminum Oxide Fiber- Tensile and Magnetium Composition 1. Fiber Fronting and		loy Composites During Isothermal Forging.  Fiber composites, Mechanical properties	501-510A
Reinforced Magnesium Composites. I.—Fiber Fraction and Orientation. Influence of Texture on Fatigue Properties of Ti—6AI—4V.	1389-1396A 1597-1605A	Environmentally Influenced Mixed Mode Fatigue Crack Propagation of Titanium Metal / Matrix Composites.	209-215A
Fatigue strength, Stress effects Existence of the Coaxing Effect and Effects of Small Artifi-		Critical Stress Intensity for Off-Axis Fracture of Al <sub>2</sub> O <sub>3</sub> Fiber- Reinforced Magnesium. Tensile and Fatigue Behavior of Aluminum Oxide Fiber-	756-760A
cial Holes on Fatigue Strength of an Aluminum Alloy and 70-30 Brass.	2029-2038A	Reinforced Magnesium Composites. I. — Fiber Fraction and Orientation.	1389-1396A
Fatigue tests Effects of Fatigue on the G—P Zones in AI—Zn Alloys.	1519-1529A	Tensile and Fatigue Behavior of Aluminum Oxide Fiber- Reinforced Magnesium Composites. II.—Alloying Effects.	1397-1405A
Ferric compounds See Iron compounds		Fiber composites, Microstructure Microstructural Changes Produced in a Multifilamentary Nb/ Ti Composite by Cold Work and Heat Treatment.	843-852A
Ferrite, Crystal growth Nucleation of Intragranular Ferrite in Fe—Ni—P Alloys. Growth of Intragranular Ferrite in Fe—Ni—P Alloys.	861-865A 867-874A	Fiber metallurgy See Fiber composites	010 0027
Ferrite, Solubility Solubility of Niobium Carbide and Niobium Carbonitride in Al-		Fibers See Whiskers (metals)	
loyed Austenite and Ferrite. Ferrites, Reduction (chemical)	545-553A	Fibrous structure The Solidification of Monotectic Alloys—Microstructures	
Kinetics of Leaching of Zinc Ferrite in Aqueous Hydrochloric Acid Solutions.  Whisker Growth in Reduction of Oxides.	221-228B 685-694B	and Phase Spacings.  Fields (physics)  See Critical field (superconductivity)	1003-1012A
Ferritic stainless steels, Diffusion The Effect of a Tin Barrier on the Permeability of Hydrogen Through Mild Steel and Ferritic Stainless Steel.	2093-2095A	Magnetic fields  Filler metal Structure of Vacuum Brazed BNi-5 Joint of Inconel 718.	609-620A
Ferrous alloys	2033-2035A	Films See Thin films	
See also Steels Ferrous alloys, Casting		Finishing	
Ribbon—Substrate Adhesion Dynamics in Chill Block Melt- Spinning Processes.	155-161B	See Surface finishing Finite element method	
Ferrous alloys, Diffusion Measurement and Analysis of Distribution Coefficients in		A Numerical Finite Difference Model of Steady State Cellular and Dendritic Growth.	983-994A
Fe—Ni Alloys Containing Sulfur and/or Phosphorus. I.—K <sub>Ni</sub> and K <sub>p</sub> .	1677-1685A	Finsider process See Direct reduction	
Ferrous alloys, Directional solidification Forced Velocity Pearlite in High-Purity Fe—C Alloys. I.— Experimental.	1037-1045A	Flame descaling See Descaling	
Forced Velocity Pearlite in High-Purity Fe—C Alloys. II.— Theoretical.	1047-1054A	Flame reduction process See Direct reduction	
Ferrous alloys, Heat treatment Resistometric Study of Fe—V and Fe—Mo Nitrided by		Flexural vibration See Fatigue (materials)	
Constant Activity Aging.  Ferrous alloys, Mechanical properties	1545-1554A	Flow See Fluid flow	
The Sulfidation Attack of a Nickel-Base Alloy at Intermediate Temperatures.	5-10A	Gas flow Mass flow Plastic flow	
Behavior of Fe—Ni—Cr Alloys in a Complex Multioxidant En- vironment Under Conditions of Dynamic Straining. Fatigue Crack Growth Behavior of an Oxide Dispersion	11-22A	Flow Stress See Yield strength	
Strengthened MA 956 Alloy. Fatigue in Binary Alloys of B.C.C. Iron.	527-539A 679-691A	Flue gases	
Fatigue Threshold Studies in Iron, Fe—Si and HSLA Steel  I.—Effect of Strength and Surface Asperities on Closure.  Fatigue Threshold Studies in Iron, Fe—Si and HSLA Steel	875-888A	A Contribution to the Thermodynamics of High-Temperature Digenite Cu <sub>2-y</sub> —S.	736-739B
II.—Thermally Activated Behavior of the Effective Stress Intensity at Threshold.	889-900A	Fluid dynamics The Movement of Particles in Liquid Metals Due to Gravity.	479-485B
The Influence of Alloying Elements on Impurity Induced Grain Boundary Embrittlement.	1415-1430A	Fluid flow See also Gas flow	
Tensile Failure Behavior of Plain Carbon Steels at Elevated Temperatures.	2059-2073A	Heat Transfer and Fluid Flow in Plasma Spraying. The Effect of Fluid Flow on the Eulectic Lamellar Spacing. Steady Low of Liquid Aluminum in a Postocaular Vertice.	59-70B 307-312A
Ferrous alloys, Microstructure Slip Directions in B2 Fe—Al Alloys. A Review of the Data on the Interlamellar Spacing of Pearlite	395-399A 1019-1036A	Steady Low of Liquid Aluminum in a Rectangular-Vertica Ingot Mold, Thermally or Electromagnetically Activated. Fluid Flow and Mass Transfer in an Inductively Stirred Four Ton Melt of Molten Steel: a Comparison of Measurement	471-478B
Ferrous alloys, Phase transformations Thermodynamics of the Massive Transformation.	411-419A	and Predictions.  Fluid Flow From a Low to a Higher Density Liquid	633-640B 681-684B

	734-736B 2109-2115A	Fracture toughness The Effect of Microstructure on the Deformation Modes and Mechanical Properties of Ti-6AI-2Nb-1Ta-0.8Mo.	
	2117-2124A	Dependence of Dynamic Fracture Resistance on Crack Ve-	1229-1245A
A Two-Dimensional Transient Model for Convection in Laser	2125-2137A 2175-2184A	Dependence of Dynamic Fracture Resistance on Crack Ve-	1247-1251A 1253-1258A
Fluid mechanics		Fracture toughness, Alloying effects	1255-1256A
See Fluid dynamics Fluidized bed cathodes		The Effect of Minor Alloying Elements on the Mechanical Properties of Al—Cu—Li Alloys.	1209-1220A
Fluidized-Bed Electrodeposition of Zinc.  Fluidized bed electrodes  See Fluidized bed cathodes	623-631B	Fracture toughness, Heating effects Effect of Tempering on Quassistatic and Impact Fracture Toughness and Mechanical Properties for 5140 H Steel.	901-911A
Fluxes		Fracture toughness, Microstructural effects	
Influence of MgO Addition on Mineralogy of Iron Ore Sinter.  Fluxes, Reactions (chemical)  Slag Metal Reactions During Submerged Arc Welding of	23-34B	Effect of Microstructure, Strength and Oxygen Content on Fatigue Crack Growth Rate of Ti—4.5AI—5.0Mo—1.5Cr (CORONA 5).	183-197A
Alloy Steels.  Foil (metal), Phases (state of matter)	217-227A	The Influence of Microstructure on Brittle Fracture Tough- ness.  The Effect of Microstructure on the Deformation Modes and	947-959A
"Premartensitic" Phase in Nickel—Aluminum Thin Foils. Force	1353-1357A	Mechanical Properties of Ti-6Al-2Nb-0.8Mo. II.—Equiaxed Structures.	1873-1881A
See also Loads (forces) The Driving Force for Chemically Induced Migration of Molten		Fracturing See also Brittle fracture	
Nickel Films Between Tungsten Grains.	1503-1505A	Intergranular fracture Fracture Behavior of W—Ni—Fe Heavy Alloys.	331-338A
Forecasting High-Temperature Phase Chemistries and Solidification Mode Prediction in Nitrogen-Strengthened Austenitic		Direct Measurement of the Work of Fracture for Grain Bound- aries of Twist Misorientation About (100) in Tungsten.	1289-1292A
Stainless Steels.	1339-1351A	Fracturing, Microstructural effects Slip Directions in B2 Fe—Al Alloys.	395-399A
Forging See also Hot forging Microstructural Changes During Isothermal Forging of a		Free energy See also Activation energy	
Co-Cr-Mo Alloy.	339-345A	Free energy of formation Growth Kinetics and Mechanism of the Massive Transforma-	
Formability A Generalized Quadratic Flow Law for Sheet Metals.	129-132A	tion.  Direct Measurement of the Work of Fracture for Grain Bound-	437-447A
An Analysis of Biaxial Stretching of a Flat Sheet. Localized Necking of Sheet at Negative Minor Strains. The Fracture Behavior of Tungsten Wire-Reinforced Superal-	133-138A 323-329A	aries of Twist Misorientation About (100) in Tungsten. The Driving Force for Chemically Induced Migration of Molten	1289-1292A
loy Composites During Isothermal Forging.	501-510A	Nickel Films Between Tungsten Grains.	1503-1505A
Formability, Temperature effects Punch-Stretching Behavior of a 2014 Aluminum Alloy in the	222 2224	Free energy of activation See Activation energy	
Temperature Range 250 to 500°C. Forming	923-929A	Free energy of dissociation See Free energy of formation	
See also Cold rolling Controlled rolling		Free energy of formation High-Temperature Thermodynamic Properties of the Chro-	
Forging Hot isostatic pressing		mium Carbides Cr <sub>7</sub> C <sub>3</sub> and Cr <sub>3</sub> C <sub>2</sub> Determined Using a Gal- vanic Cell Technique.	517-521B
Hot rolling Punching Stretch forming		Thermodynamics of Several Lewis-Acid-Base Stabilized Transition Metal Alloys.	2075-2085A
A Generalized Quadratic Flow Law for Sheet Metals. An Analysis of Biaxial Stretching of a Flat Sheet.	129-132A 133-138A	Fuels See Coke	
Fossil fuels		Metallurgical coke Sour gas	
See Sour gas Fouling		Fumes A Collision Model for Fume Formation in Metal Oxidation.	587-593A
Injection Phenomena in Nonferrous Processes. Control of Autoclave Scaling During Acid Pressure Leaching	77-89B	Fuming (slag)	007 0007
of Nickeliferous Laterite Ore. Fracture mechanics	433-440B	See Stag furning Furnaces	
A Study of Creep Crack Growth in 2219-T851 Aluminum Alloy Using a Computerized Testing System.	107-120A	See Blast furnaces Bottom blown converters	
The Role of Alpha and Beta Phases in Fatigue Crack Propa- gation of Ti-Mn Alloys.	155-171A	Copper converters LD converters	
Effect of Microstructure, Strength and Oxygen Content or Fatigue Crack Growth Rate of Ti-4.5AI-5.0Mo-1.5Ci	1	Reverberatory furnaces Smelting furnaces	
(CORONA 5). Fatigue Crack Growth Behavior of an Oxide Dispersion. Strengthened MA 956 Alloy.	527-539A	Fused salts, Environment The Effects of a Liquid Sulfate / Chloride Environment on Superalloy Stress Rupture Properties at 704 °C.	23-28A
The Effect of Microstructure and Environment on Fatigue Crack Closure of 7475 Aluminum Alloy. The Fracture of Ordered (Fe, Co).\V.	555-563A 701-706A	Fusion welding	
Hydrogen-Induced Slow Crack Growth in Stable Austenition Stainless Steels.		See Electron beam welding Electroslag welding Gas tungsten arc welding	
Crack Paths and Hydrogen-Assisted Crack Growth Re sponse in AISI 4340 Steel.		Laser beam welding Submerged arc welding	
Critical Stress Intensity for Off-Axis Fracture of Al <sub>2</sub> O <sub>3</sub> Fiber Reinforced Magnesium.		Gallium compounds, Mechanical properties	
Fatigue Threshold Studies in Iron, Fe—Si and HSLA Steel I.—Effect of Strength and Surface Asperities on Closure.	875-888A	The Mechanical Behavior of Nonstoichiometric Compounds Ni <sub>3</sub> Si, Ni <sub>3</sub> Ge and Fe <sub>3</sub> Ga.	173-181A
Fatigue Threshold Studies in Iron, Fe—Si and HSLA Steel II.—Thermally Activated Behavior of the Effective Stress Intensity at Threshold.		Galvanic cells See Electrolytic cells	
Effect of Tempering on Quasistatic and Impact Fracture Toughness and Mechanical Properties for 5140 H Steel.		Galvanizing See Hot dip galvanizing	
The Influence of Deformation Path on the Slow Strain-Rate Stress Corrosion Cracking of Admiralty Brass Sheet.		Galvannealing See Annealing	
Fatigue Behavior of Carburized Steel With Internal Oxide: and Nonmartensitic Microstructure Near the Surface.	1431-1436A	Gas cooled reactors	
Effect of Cavitation on Post-Deformation Tensile Properties of a Superplastic Copper-Base Alloy.	1443-1450A	Discussion of "Calculation Method of Equilibrium Composi- tion in the Carbon—Hydrogen—Oxygen System and Its	
Fatigue Crack Growth Mechanics for Ti-6Al-4V (RA) in Vacuum and Humid Air.	1931-1940A	Application to Environments of a High-Temperature Gas Cooled Reactor"; Authors Reply.	396-400B
Fracture mechanics, Deformation effects The Fracture Behavior of Tungsten Wire-Reinforced Superal loy Composites During Isothermal Forging.	501-510A	Gas flow, Pressure effects  The Effect of Pressure Modulation on the Flow of Gas  Through a Solid Membrane: Permeation and Diffusion o  Hydrogen Through Nickel.	
Fracture mechanics, Microstructural effects Interrelations of Cooling Rate, Microstructure and Mechan	j.	Gas permeability	

Gas tungsten arc welding Heat Flow During the Autogenous GTA Welding of Pipes.	1165-1171A	Gray iron See also Nodular iron	
Cooling Rate Effects in Ti—6AI—2Sn—4Zr—2Mo Weld- ments.	1948-1952A	Gray iron, Heat treatment Laser Processing of Cast Iron for Enhanced Erosion Resis-	
Germanium compounds, Mechanical properties The Mechanical Behavior of Nonstoichiometric Compounds Ni,Si, Ni <sub>3</sub> Ge and Fe <sub>3</sub> Ga.	173-181A	tance.  Grey iron See Gray iron	719-728A
Gibbs free energy See Free energy		Growth	
Glass		See Crystal growth Grain growth Growth rate	
See Metallic glasses Gold, Binary systems		Growth rate	
Thermochemistry of Binary Liquid Gold Alloys: the Systems Gold—Copper and Gold—Silver at 1379K.	203-208A	Estimation of the Parabolic Growth Rate From the Stereological Counting Measurements. Kinetics of Methane Bubble Growth in a 1020 Steel.	391-393A 487-494A
Gold, Thermal properties Thermochemistry of Binary Liquid Gold Alloys: the Systems Au—Ni, Au—Co, Au—Fe and Au—Mn.	573-580B	Interdendritic Spacing. I.—Experimental Studies.  A Numerical Finite Difference Model of Steady State Cellular and Dendritic Growth.	967-975A 983-994A
GP zone See Guinier Preston zone		Ostwald Ripening and Relaxation in Dendritic Structures.  A Review of the Data on the Interlamellar Spacing of Pearlite.	995-1001A 1019-1036A
Grain boundaries		Forced Velocity Pearlite in High-Purity Fe—C Alloys. I.— Experimental.	1037-1045A
See also Grain sub boundaries An Analytical Electron Microscope Study of the Kinetics of the Equilibrium Segregation of Bismuth in Copper.	99-105A	Forced Velocity Pearlite in High-Purity Fe—C Alloys. II.— Theoretical. Ostwald Ripening During Liquid Phase Sintering—Effect of	1047-1054A
Consideration on the Intergranular Tempered Martensite Em- brittlement.	393-395A	Volume Fraction on Coarsening Kinetics.  Morphological Stability in the Presence of Fluid Flow in the	1081-1088A
Direct Measurement of the Work of Fracture for Grain Bound- aries of Twist Misorientation About (100) in Tungsten.	1289-1292A	Melt.	2117-2124A 2125-2137A
The Influence of Alloying Elements on Impurity-Induced Grain Boundary Embrittlement.	1415-1430A	Studies of Directionally Solidified Eutectic Bi/MnBi at Low Growth Velocities.	2139-2145A
Revealing Deformed and Recrystallized Structures in Beta Titanium Alloys.	1493-1496A	Growth rate, Diffusion effects Growth of Intragranular Ferrite in Fe—Ni—P Alloys.	867-874A
Grain boundaries, Chemical analysis  A Grain Boundary Etching Method for the Analysis of Intergranular Phosphorus-Segregation in Iron-Based Alloys.	1563-1570A	Growth rate, Field effects Effect of Applied Magnetic Fields During Directional Solidifi-	
Grain boundaries, Diffusion Surface Relief Produced by Diffusion-Induced Boundary Mi-		cation of Eutectic Bi / Mn.  Growth rate, Heating effects	2155-2161A
gration in Cu—Zn.  Grain boundary sliding	495-499A	Correction to "The Kinetics of Sigma-Phase Precipitation in AISI 310 and AISI 316 Steels".	406A
The High-Temperature Low-Cycle Fatigue Behavior of the Nickel-Base Alloy IN-617. The Fracture of Ordered (Fe, Co) <sub>3</sub> V.	661-670A 701-706A	Guinier Preston zone Metastable Phases in the Early Stage of Precipitation in Al— Mg Alloys.	835-842A
Grain growth Subgrain Growth in Aluminum During Static Annealing.	1502-1503A	Guinier Preston zone, Stress effects  Effects of Fatigue on the G—P Zones in Al—Zn Alloys.	1519-1529A
High-Temperature Oxidation of Iron at 1200°C in a Hot Stage Environmental Scanning Electron Microscope.	2231-2240A	Gyration See Rotation	
Crystallographic and Morphological Characteristics of Oxi- dation Growth Pits in Wustite Grown at 1200°C.	2241-2246A	Hack saws	
Grain growth, Alloying effects The Role of Alloy Composition on the Stability of Nitrides in Titanium-Microalloyed Steels During Weld Thermal Cycles.	33-41A	Microstructure and its Effect on Toughness and Wear Resis- tance of Laser Surface Melted and Post-Heat Treated High-Speed Steel.	1829-1835A
Retarded Grain Boundary Mobility in Activated Sintered Mo- lybdenum.	1103-1110A	Halides See Hydrochloric acid	
Grain growth, Heating effects The Effect of Processing Conditions and Subsequent Heat		lodides Sodium chloride	
Treatment on the Transformation Behavior of Some Rapidly Solidified Copper-Base Shape Memory Alloys.	471-480A	Halogenation See Chlorination	
Grain refinement Grain Refinement of Niobium Steels by Control of Recrystall-		Halogens See Chlorine	
ization During Hot Rolling. Rapid Solidification Processing of Magnesium—Lithium Al-	87-98A	Hardenability	
loys. The Grain Refining of Aluminum and Phase Relationships in		See also Core hardenability Jominy hardenability	
the AI—Ti—B System.  The Role of the Constituent Phases in Determining the Low Temperature Toughness of 5.5Ni Cryogenic Steel.	277-282A 2213-2219A	Hardenability, Alloying effects A Quantitative Assessment of the Hardenability Increase Resulting From a Superhardenability Treatment.	2185-2191A
Grain size Recrystallization in Commercially Pure Aluminum.	287-297A	Hardening	210021014
The Effect of Microstructure and Environment on Fatigue Crack Closure of 7475 Aluminum Alloy.	555-563A	See Aging (artificial) Carburizing	
Recovery of Creep Properties of a Vanadium-Strengthened Steel (1Cr1Mo0.75VTiB) by Reheat Treatment.	707-718A	Dispersion hardening Laser beam hardening Nitriding	
The Influence of Microstructure on Brittle Fracture Toughness.	947-959A	Precipitation hardening Solution strengthening	
Pore Filling Process in Liquid Phase Sintering. Strain Hardening Behavior of Polycrystalline Iron and Low-	1075-1080A	Strain hardening Hardness	
Carbon Steels—a Statistical Analysis. Fatigue Crack Propagation in Dual-Phase Steels: Effects of Ferritic—Martensitic Microstructures on Crack Path Mor-		Estimating Hardness Response of Hot Rolled Steel by Simulating Cooling Cycles Via Jominy Bar Testing.	1507-1509A
phology. Residual Stress Evaluation With X-Rays in Steels Having	1193-1207A	Hardness, Alloying effects	
Preferred Orientation.  The Mechanical Properties of Grain-Refined Beta-CuAIN	1407-1414A	The Wear Behavior of Nitrogen-Implanted Metals.  Hardness, Microstructural effects	2221-2229A
Strain-Memory Alloys.  Effect of Composition and Initial Grain Size on the Dynamic		Cooling Rate Effects in Ti-6AI-2Sn-4Zr-2Mo Weld- ments.	1948-1952A
Recrystallization of Austenite in Plain Carbon Steels. Isothermal Martensitic Transformation in Fe—Ni and Fe—Ni—C Alloys at Subzero Temperatures.	2009-2019A 2193-2203A	Hazelett process See Continuous casting	
Grain size, Alloying effects		Heat affected zone A New Finite Element Model for Welding Heat Sources.	299-305B
Grain Refinement of Niobium Steels by Control of Recrystall ization During Hot Rolling.	87-98A	Heat affected zone, Microstructure	299-3058
Grain structure Steady Low of Liquid Aluminum in a Rectangular-Vertica Ingot Mold, Thermally or Electromagnetically Activated.	471-478B	The Role of Alloy Composition on the Stability of Nitrides in Titanium-Microalloyed Steels During Weld Thermal Cycles. Microstructure and Mechanical Properties of a Welded	33-41A
Grain sub boundaries Subgrain Growth in Aluminum During Static Annealing.	1502-1503A	(Alpha → Beta) Titanium Alloy.  Cooling Rate Effects in Ti—6AI—2Sn—4Zr—2Mo Weldments.	1589-1596A 1948-1952A
Gray con See Gray iron	.002 1000A	Heat conduction	1940-1932A

Heat flow See Heat transmission		Yielding Anisotropy From the Bauschinger Effect and Crystallographic Texture in Drawn HSLA Steel Sheet.	1699-1710A
Heat flux See Heat transmission		High strength low alloy steels, Microstructure Interrelations of Cooling Rate, Microstructure and Mechani-	
Heat of decomposition		cal Properties in Four HSLA Steels.	1807-1817A
See Heat of formation  Heat of dissociation		High strength low alloy steels, Rolling Grain Refinement of Niobium Steels by Control of Recrystall- ization During Hot Rolling.	87-98A
See Heat of formation  Heat of dissolution See Heat of solution		High strength low alloy steels, Solubility Solubility of Niobium Carbide and Niobium Carbonitride in Al- loyed Austenite and Ferrite.	545-553A
Heat of formation Thermochemistry of Alloys of Transition Metals. IV. — Alloys of Copper With Scandium, Yttrium, Lanthanum and Lute-		High strength low alloy steels, Steel making A Quantitative Assessment of the Hardenability Increase Re-	2185-2191A
tium.  Heat of mixing Thermochemistry of Binary Liquid Gold Alloys: the Systems	357-368B	High strength low alloy steels, Structural hardening The Isothermal Decomposition of Austenite in Hot Rolled	
Gold—Copper and Gold—Silver at 1379K.  Thermochemistry of Alloys of Transition Metals. IV. — Alloys of Copper With Scandium, Yttrium, Lanthanum and Lute-	203-208A	Microalloyed Steels.  High strength low alloy steels, Welding The Role of Alloy Composition on the Stability of Nitrides in	1137-1145A
tium.  Thermochemistry of Binary Liquid Gold Alloys: the Systems  Au—Ni, Au—Co, Au—Fe and Au—Mn.	357-368B 573-580B	Titanium Microalloyed Steels During Weld Thermal Cycles.  High strength steels, Mechanical properties  Yield Loci of HY80, HY100 Steels and	33-41A
Heat of solution Thermochemistry of Alloys of Transition Metals. IV.—Alloys of Copper With Scandium, Yttrium, Lanthanum and Lute-	257.220	Ti-6Al-2Nb-1Ta-0.8Mo.  HIP  See Hot isostatic pressing	2097-2101A
tium. Heat resistant alloys	357-368B	Holes	
See Superalloys Heat transfer		Envelopes of Crack-Like Surfaces for Modeling Cavity Growth. Existence of the Coaxing Effect and Effects of Small Artifi-	246-247A
Comparison of Numerical Modeling Techniques for Complex, Two-Dimensional, Transient Heat-Conduction Problems	307-318B	cial Holes on Fatigue Strength of an Aluminum Alloy and 70-30 Brass.	2029-2038A
A Two-Dimensional Transient Model for Convection in Laser Melted Pool.	2175-2184A	Hot brittleness See Brittleness	
Heat transmission, Welding effects Heat Flow During the Autogenous GTA Welding of Pipes.	1165-1171A	Hot compacting See Compacting	
Heat treatment See also Aging (artificial)		Hot cracking See Cracking (fracturing)	
Annealing Austenitizing Carburizing		Hot dip coating See Hot dip galvanizing	
Continuous annealing Grain refinement Isothermal annealing		Hot dip coatings, Crystal growth  The Effects of Water Vapor on Solidification of Galvanized Coatings.	393-395B
Nitriding Overaging Precipitation hardening Quench aging		Hot dip galvanizing The Effects of Water Vapor on Solidification of Galvanized Coatings.	393-395B
Tempering Recovery of Creep Properties of a Vanadium-Strengthened	202 2.01	Hot ductility See Ductility	
Steel (1Cr1Mo0.75VTiB) by Reheat Treatment. Embrittlement of Types 316L and 347 Weld Overlay by Post- Weld Heat Treatment and Hydrogen.	707-718A 1475-1484A	Hot forging Modeling of Dynamic Material Behavior in Hot Deformation:	
Heating See Superheating		Forging of Ti-6242.  Hot gas corrosion, Coating effects	1883-1892A
Heating rate Heating Rate Dependence of Disordering in Alpha-Cu—Al Alloys.	1999-2008A	The Effects of a Liquid Sulfate Chloride Environment on Su- peralloy Stress Rupture Properties at 704°C.  Hot hardness	23-28A
Heats (energies) See Heat of formation		See Hardness	
Heat of mixing Heat of solution		Hot isostatic pressing On the Effect of NaCl on Porosity in Elemental-Blend Powder Metallurgy Ti—5Al—2.5Sn.	248-249A
Heavy metals See Antimony Bismuth		Hot pressing See Hot isostatic pressing	
Cadmium Lead (metal) Mercury (metal) Tin		Hot rolling Effect of Shape of Sulfide Inclusions on Anisotropy of Inclusion Spacings and on Directionality of Ductility in Hot Rolled C—Mn Steels. Estimating Hardness Response of Hot Rolled Steel by Simu-	1259-1264A
Heliarc welding See Gas tungsten arc welding		lating Cooling Cycles Via Jominy Bar Testing.	1507-1509A
Helmholtz free energy See Free energy		Hot roughing See Hot rolling	
High alloy steels See Austenitic stainless steels		Hot shortness See Brittleness	
Ferritic stainless steels Martensitic stainless steels		Hot strength See Tensile strength	
Stainless steels High speed steel tools, Mechanical properties		Hot stretch forming See Stretch forming	
Microstructure and its Effect on Toughness and Wear Resis- tance of Laser Surface Melted and Post-Heat Treated High-Speed Steel.	1829-1835A	Hot tensile strength See Tensile strength	
High speed tool steels, Mechanical properties Microstructure and Its Effect on Toughness and Wear Resis- tance of Laser Surface Melted and Post-Heat Treated High-Speed Steel.		Hot workability Flow and Fracture of a Multiphase Alloy MP35N for Study of Workability. Hot Workability of Three Grades of Tool Steels.	1837-1847A 1855-1864A
High strength low alloy steels, Crystal growth Precipitation of Nb(CN) During High-Strain Rate Compres-		Hot working See Hot forging Hot rolling	
sion Testing of a 0.07% Niobium-Bearing Austenite.  High strength low alloy steels, Mechanical properties Fatigue Threshold Studies in Iron, Fe—Si and HSLA Steel I.—Effect of Strength and Surface Asperities on Closure.		Hydrides, Crystal growth Hydride Precipitation and Dislocation Substructures in Ti— 5AI—2.5Sn.	813-817A
Fatigue Threshold Studies in Iron, Fe—Si and HSLA Steel II.—Thermally Activated Behavior of the Effective Stress Intensity at Threshold	875-888A	Hydrochloric acid, Reactions (chemical) Kinetic Study of Nonoxidative Leaching of Cinnabar Ore in Agreeus Hydrochloric Acid—Potassium Indide Solutions	13-18B

Hydrochloric acid leaching Reaction Kinetics of the Ferric Chloride Leaching of Sphalerite—an Experimental Study. Kinetics of Leaching of Zinc Ferrite in Aqueous Hydrochloric	5-12B	Impact strength, Microstructural effects Effect of Shape of Sulfide Inclusions on Anisotropy of Inclusion Spacings and on Directionality of Ductility in Hot Rolled C—Mn Steels.	1259-1264A
Acid Solutions.  New Hydrometallurgical Process for Obtaining Mercury From	221-228B	Impact toughness See Impact strength	
Cinnabar Ore.  Hydrogen, Alloying elements	229-233B	Impedance	
Effects of Hydrogen on Mechanical Properties of Vanadium—Niobium Alloys.	147-153A	See Electrical resistance Impermeability See Permeability	
$ \begin{array}{c} \textbf{Hydrogen, Diffusion} \\ \textbf{Prevention of Hydrogen Embrittlement by a TiO}_2 \ \textbf{Surface} \end{array} $	E07 600A	Inclusions See Nonmetallic inclusions	
Layer.  The Effect of Pressure Modulation on the Flow of Gas Through a Solid Membrane: Permeation and Diffusion of Hydrogen Through Nickel.	597-600A 639-648A	Indium, Solubility Oxygen Solubility in Liquid Indium and Oxygen Diffusivity in Liquid Indium and Tin.	329-335B
The Room-Temperature Effective Diffusivity of Hydrogen in Vapor-Deposited Aluminum.  The Influence of Hydrogen and the Interface Phase on Frac-	1953-1955A	Indium, Ternary systems Thermodynamic Properties of Liquid Mg—In—Cd Ternary	029 000D
ture in Ti Code 12.  The Effect of a Tin Barrier on the Permeability of Hydrogen	1955-1958A 2093-2095A	Solutions. Indium base alloys, Phases (state of matter)	543-546B
Through Mild Steel and Ferritic Stainless Steel.  Hydrogen, Reactions (chemical)  Discussion of "Calculation Method of Equilibrium Composi-	2093-2095A	Microstructure of One of the Ternary Eutectic Alloys in the Bi—In—Sn System.	1515-1517A
tion in the Carbon—Hydrogen—Oxygen System and Its Application to Environments of a High-Temperature Gas		Indium compounds, Single crystals Bismuth Precipitation in "Monocrystalline" InBi.	1963-1967A
Cooled Reactor"; Authors Reply. Hydrogen Attack in an Austenitic Stainless Steel.	396-400B 1485-1490A	Inert atmospheres The Influence of Gas Atmospheres on the First-Stage Sintering of High-Purity Niobium Powders.	1111-1116A
Hydrogen, Sorption Kinetics of Methane Bubble Growth in a 1020 Steel. Hydride Precipitation and Dislocation Substructures in Ti—	487-494A	Inert gas welding See Gas tungsten arc welding	
5AI—2.5Sn.  Hydrogen compounds	813-817A	Ingot casting Steady Low of Liquid Aluminum in a Rectangular-Vertical	
See also Hydrochloric acid Hydrogen sulfide		Ingot Mold, Thermally or Electromagnetically Activated.  Ingots, Crystal growth	471-478B
Hydrogen compounds, Diffusion Kinetics of Methane Bubble Growth in a 1020 Steel.	487-494A	Fluid Flow From a Low to a Higher Density Liquid. Effects of Gravity on Interdendritic Flow: an Analytical Ap- proach.	681-684B 2095-2097A
Hydrogen embrittlement Effects of Hydrogen on Mechanical Properties of Vanadium—Niobium Alloys. Hydrogen-Induced Slow Crack Growth in Stable Austenitic	147-153A	Ingots, Heat treatment Comparison of Numerical Modeling Techniques for Complex, Two-Dimensional, Transient Heat-Conduction Problems.	307-318B
Stainless Steels. Crack Paths and Hydrogen-Assisted Crack Growth Re-	729-733A	Injection Injection Phenomena in Nonferrous Processes.	77-89B
sponse in AISI 4340 Steel. Embrittlement of Types 316L and 347 Weld Overlay by Post-	735-746A	Inorganic acids	
Weld Heat Treatment and Hydrogen. Hydrogen-Induced Interior Crack-Tip Morphologies in High-	1475-1484A	See Hydrochloric acid Instability	
Strength Steel. Investigation of Stress Corrosion Cracking of Cast and	1865-1871A	See Stability	
Forged Steel in Water.  Hydrogen embrittlement, Alloying effects	2087-2092A	Intensity See Stress intensity	
Influence of Nitrogen Alloying on Hydrogen Embrittlement in AISI 304 Type Stainless Steels.	2205-2211A	Intercrystalline structure See Intergranular structure	
Hydrogen embrittlement, Coating effects Prevention of Hydrogen Embrittlement by a TiO <sub>2</sub> Surface Layer.	597-600A	Interfaces The Nucleation Kinetics, Crystallography and Mechanism of the Massive Transformation. Growth Kinetics and Mechanism of the Massive Transforma-	427-435A
Hydrogen embrittlement, Heating effects Effect of Tempering on the Carbon Activity and Hydrogen At- tack Kinetics of 2.25Cr—1Mo Steel.	2021-2027A	tion. Structure of Interphase Boundaries in a Eutectic Co—Al Alloy.	437-447A 1623-1626A
Hydrogen embrittlement, Impurity effects Grain Boundary Composition and Associated Hydrogen		Interfaces, Diffusion Distinguishing Features of Massive Transformations.	421-425A
Cracking of Modified 4130 Steels.  Hydrogen embrittlement, Mechanical properties Effects of the Additions of Boron, Phosphorus, Tin and Anti-	565-572A	Interfaces, Diffusion effects The Influence of Hydrogen and the Interface Phase on Fracture in Ti Code 12.	1955-1958A
mony on Oxygen-Assisted Hydrogen Embrittlement of Nick- el.	519-526A	Interfacial energy See Surface energy	1300 1300A
Hydrogen reduction Hydrogen Reduction of Wustite Single Crystals Doped With Magnesium, Manganese, Calcium, Aluminum and Silicon. The Law of Additive Reaction Time Applied to the Hydrogen	383-391B	Intergranular fracture, High temperature effects Tensile Failure Behavior of Plain Carbon Steels at Elevated Temperatures.	2059-2073A
Reduction of Porous Nickel-Oxide Pellets. Hydrogen Reduction Kinetics of Nickel Sulfide in the Pres- ence of Calcium Oxide	403-406B 719-723B	Intergranular structure  Effects of the Additions of Boron, Phosphorus, Tin and Anti- mony on Oxygen-Assisted Hydrogen Embrittlement of Nick-	
Hydrogen sulfide, Environment Crack Paths and Hydrogen-Assisted Crack Growth Response in AISI 4340 Steel.		<ul> <li>el.</li> <li>Grain Boundary Composition and Associated Hydrogen Cracking of Modified 4130 Steels.</li> </ul>	565-572A
Hydrogen sulfide, Sorption Influence of Stress on H <sub>2</sub> S Adsorption on Iron.	853-860A	Nucleation of Intragranular Ferrite in Fe—Ni—P Alloys. Growth of Intragranular Ferrite in Fe—Ni—P Alloys.	861-865A 867-874A
Hydrometallurgy		Intermetallic compounds See Intermetallics	
Relationships Between the Pourbaix Diagram for Ag—S— H <sub>2</sub> O and Electrochemical Oxidation and Reduction o Ag <sub>2</sub> S.	235-242B	Intermetallics, Crystal growth Crystallization Studies in the Aluminum Rich Corner of the Aluminum—Iron—Manganese System.	1311-1317A
Ilmenite, Reduction (chemical) Chloridization Beneficiation of Ilmenite.	259-275B	Intermetallics, Solubility Shape Changes During Dissolution of Theta Prime-CuAl <sub>2</sub> .	449-458A
Immersion coating See Hot dip galvanizing		Intermetallics, X ray analysis Identification of Cu <sub>5</sub> Zr Phase in Cu—Zr Alloys.	1491-1493A
Impact strength, Cooling effects Toughness Variation With Test Temperature and Cooling Rate for Liquid Phase Sintered W—3.5Ni—1.5Fe.	121-128A	Internal friction Isothermal Martensitic Transformation in Fe—Ni and Fe—Ni—C Alloys at Subzero Temperatures.	2193-2203A
Impact strength, Impurity effects Segregation and Influence of Boron on the Impact Toughnes		Internal stress See Residual stress	
to Ti—6AI—2Nb—1Ta—0.8Mo Welds and Castings.  Impact strength, Low temperature effects The Role of the Constituent Phases in Determining the Lov Temperature Toughness of 5.5Ni Cryogenic Steel.	1505-1507A w 2213-2219A	Interrupted quenching  Low-Temperature Improvement of the Mechanical Properties of 4340-Type Ultra-High-Strength Steel With Heat Treating Techniques Using Interrupted Quenching Method.	3 2247-2249A

lodides, Reactions (chemical) Kinetic Study of Nonoxidative Leaching of Cinnabar Ore in Aqueous Hydrochloric Acid—Potassium lodide Solutions.	13-18B	Jominy hardenability Core Hardenability Calculations for Carburizing Steels.  Jominy test	173-1183A
ion implantation Metastable Alloys of Beryllium Prepared by Ion Implantation. 1	787-1805A	Estimating Hardness Response of Hot Rolled Steel by Simu-	1507-1509A
Iron See also Alpha iron		Junghans Rossi casting See Continuous casting	
Gray iron Nodular iron		Kaldo process See Oxygen steel making	
Iron, Alloying elements Magnetization Measurement Associated With		Kaolin, Reactions (chemical)	
Gamma → Alpha Martensitic Transformation of Iron Parti- cles in a Cu—1.59Fe Alloy. Iron, Binary systems	755-756A	A Study of the Mechanisms of the Salt Catalyzed Carbo- chlorination of Kaolin.  Mössbauer Spectroscopy Used to Study the Removal of Iron From Clay.	695-700B 732-734B
Thermodynamic Analysis of the Iron-Copper System.	921-1930A	Kaolinite, Reactions (chemical) Chlorination of Alumina in Kaolinitic Clay.	529-533B
Iron, Impurities Mössbauer Spectroscopy Used to Study the Removal of Iron From Clay.	732-734B	Killed steels See Aluminum killed steels	
Iron, Mechanical properties	102 1040	Kinetics	
Strain Hardening Behavior of Polycrystalline Iron and Low- Carbon Steels—a Statistical Analysis.  Iron, Oxidation	1185-1192A	See also Reaction kinetics Observations of Melt Rate as a Function of Arc Power, CO Pressure and Electrode Gap During Vacuum Consumable Arc Remelting of Inconel 718.	117-125B
The High-Temperature Oxidation of Metals Forming Cation- Diffusing Scales.	195B	Kinetics of Precipitation From Quenched Low-Carbon Steel.  Ladle additions	1147-1153A
The High-Temperature Oxidation of Metals Forming Cation- Diffusing Scales.	765-782A	Thermodynamics of Nozzle Blockage in Continuous Casting of Calcium-Containing Steels.	547-562B
	2231-2240A	Correction to Thermodynamics of Nozzle Blockage in Contin- uous Casting of Calcium-Containing Steels.	547-562B
	2241-2246A	Ladle metallurgy Fluid Flow and Mass Transfer in an Inductively Stirred Four-	
Iron, Solubility Surface Interactions in the Iron—Nitrogen System.	199-202A	Ton Melt of Molten Steel: a Comparison of Measurements and Predictions.	633-640B
Iron, Sorption Influence of Stress on H <sub>2</sub> S Adsorption on Iron.	853-860A	Lamellar structure The Effect of Fluid Flow on the Eutectic Lamellar Spacing.	307-312A
Iron, Ternary systems Phase Relationships in the System Fe—Na—O.	319-327B	Pattern Selection in Solidification. Interlamellar Spacing in Directionally Solidified Eutectic Thin	961-966A
Phase Relationships in the Fe—Cr—C System at Solidification Temperatures.	663-676B	Films.  A Review of the Data on the Interlamellar Spacing of Pearlite.	1013-1017A 1019-1036A
Crystallization Studies in the Aluminum-Rich Corner of the	1311-1317A	Interlamellar Spacing in Discontinuous Precipitation.	1055-1062A
Miscibility Gap in Fe-Ni-Al and Fe-Ni-Al-Co Sys-	1819-1828A	Lamina See Laminates	
Iron, Thermal properties	1010 102011	Laminates, Mechanical properties Tensile Strength of Ni/Cu/(001)Ni Triple Layer Films.	1273-1280A
Thermochemistry of Binary Liquid Gold Alloys: the Systems Au—Ni, Au—Co, Au—Fe and Au—Mn.  Iron and steel making	573-580B	Lanthanide metals, Thermal properties Thermochemistry of Alloys of Transition Metals. IV.—Alloys	
See Ironmaking Oxygen steel making		of Copper With Scandium, Yttrium, Lanthanum and Lute- tium.  Laser beam hardening	357-3688
Iron base alloys See Ferrous alloys		An Electron Microscope Study of the Featureless Zone Obtained During Rapid Solidification.	29-31A
Iron compounds See also Iron oxides Wustite		Laser Processing of Cast Iron for Enhanced Erosion Resis- tance.  Microstructure and its Effect on Toughness and Wear Resis-	719-728
Iron compounds, Diffusion		tance of Laser Surface Melted and Post-Heat Treated High-Speed Steel.	1829-1835A
Discussion of "Self-Diffusion Coefficients of Carbon in Fe <sub>3</sub> C at 723K Via the Kinetics of Formation of This Compound (and Authors' Reply).	245-246A	Laser beam welding A New Finite Element Model for Welding Heat Sources. Alloying Element Vaporization and Weld Pool Temperature	299-3058
Iron compounds, Mechanical properties The Mechanical Behavior of Nonstoichiometric Compounds		During Laser Welding of AISI 202 Stainless Steel.  A Two-Dimensional Transient Model for Convection in Laser	641-644E
Ni <sub>3</sub> Si, Ni <sub>3</sub> Ge and Fe <sub>3</sub> Ga. The Fracture of Ordered (Fe, Co) <sub>3</sub> V.	173-181A 701-706A	Melted Pool.  Laser welding	2175-2184/
Iron compounds, Reduction (chemical)		See Laser beam welding	
Whisker Growth in Reduction of Oxides.  The Breakdown of Dense Iron Layers on Wustite in CO/CO <sub>2</sub> and H <sub>2</sub> /H <sub>2</sub> O Systems.	685-694B 701-708B	Lasers Rapidly Solidified Prealloyed Powders by Laser Spin Atomization.	149-153E
Iron constituents See Alpha iron		Laterites, Reactions (chemical)	
Iron ores, Reduction (chemical) Influence of MgO Addition on Mineralogy of Iron Ore Sinter.	23-34B	The Precipitation of Ni <sub>3</sub> S <sub>2</sub> From Sulfate Solutions. <b>Lattice constant</b> See Lattice parameters	609-615E
Reduction of Silica in Coke With Ash of Increased Basicity.  Iron oxides	729-732B	See Lattice parameters  Lattice defects	
See also Wustite		See Crystal defects  Lattice parameters	
Iron oxides, Reduction (chemical) The Effect of Emergent Dislocations on the Kinetics of De- composition of Solid Surfaces Under Conditions of Chemi-		The Mechanical Behavior of Nonstoichiometric Compounds Ni <sub>3</sub> Si, Ni <sub>3</sub> Ge and Fe <sub>3</sub> Ga. Use of Reciprocal Lattice Layer Spacing in Convergent	173-181/
cal Reaction Control.	591-594B	Beam Electron Diffraction Analysis.	1299-1302
Iron powder See Iron		Lattices See Superlattices	
Ironmaking Hydrogen Reduction of Wustite Single Crystals Doped With Magnesium, Manganese, Calcium, Aluminum and Silicon.	383-391B	Layers See Surface layer	
Isostatic pressing See Hot isostatic pressing	555-58-18	LD converters  A New Approach to Investigate the Drop Size Distribution in	100 110
Oce not isostatic pressing		Basic Oxygen Steelmaking.  Leaching	109-116
Isothermal annealing		See also Ammonia pressure leaching	
Isothermal annealing Correction to "The Kinetics of Sigma-Phase Precipitation in AISI 310 and AISI 316 Steels".	406A	Hydrochloric acid leaching Sulfuric acid leaching	
Isothermal annealing Correction to "The Kinetics of Sigma-Phase Precipitation in		Hydrochloric acid leaching	13-18

An Alternative Method for the Recovery of Lithium From Spodumene.	725-726B	Lithium, Ternary systems The Liquidus Surface for the Al—Li—Si System From 0.20%	FOE FO74
Lead (metal), Alloying elements Solidification of Highly Undercooled Sn—Pb Alloy Droplets.	1303-1310A	Lithium and 0.20% Silicon.  Lixiviation	595-597A
Lead (metal), Extraction Cell Measurements of the Reduction Potentials of Gas-		See Leaching  Load distribution See Loads (forces)	
Phase Emanating From PbS/CaO/C at Elevated Tempera- tures.  Electrodissolution of Lead Sulfide in Different Acidic Media.	19-22B 605-608B	Loads (forces) The Effect of Overload on the Fatigue Crack Propagation in	511-517A
Lead (metal), Impurities  Distribution of Lead Between Copper and Matte and the Activity of PbS in Copper-Saturated Mattes.	441-449B	Metastable Beta Ti—V Alloys.  Low alloy steels  See also Electrical steels	511-51/A
Lead (metal), Reduction (chemical)  Exergy Analysis of a Chemical Metallurgical Process.	645-654B	Silicon steels  Low alloy steels, Mechanical properties	
Lead (metal), Ternary systems Constitution of the Lead—Tin—Strontium. System Up to 36 Atomic Percent Strontium.	43-54A	The Influence of Microstructure on Brittle Fracture Tough- ness. Estimating Hardness Response of Hot Rolled Steel by Simu-	947-959A
Lead base alloys, Crystal growth		lating Cooling Cycles Via Jominy Bar Testing.  Low cycle fatigue	1507-1509A
The Movement of Particles in Liquid Metals Due to Gravity.  Primary Dendrite Spacing. II. — Experimental Studies of Pb— Pd and Pb—Au Alloys.	479-485B 1665-1676A	Fatigue Crack Growth Mechanics for Ti—6AI—4V (RA) in Vacuum and Humid Air.	1931-1940A
The Mechanisms of Formation and Prevention of Channel Segregation During Alloy Solidification.	2163-2173A	Low cycle fatigue, High temperature effects The High-Temperature Low-Cycle Fatigue Behavior of the Nickel-Base Alloy IN-617.	661-670A
Lead base alloys, Directional solidification Interdendritic Spacing. II.—A Comparison of Theory and Ex- periment.	977-982A	Machining See Electric discharge machining	
Interlamellar Spacing in Directionally Solidified Eutectic Thin Films.	1013-1017A	Macrostructure Modification in the Aluminum—Silicon System.	459-469A
Lead base alloys, Reactions (chemical) Activities of Oxygen in Liquid Bi—Pb and Bi—Sb Alloys.	141-147B	Magnesia See Magnesium oxide	
Lead compounds, Binary systems		Magnesium, Composite materials	
A Generalized Approach to the Flood—Knapp Structure Based Model for Binary Liquid Silicates: Application and Update for the PbO—SiO <sub>2</sub> System.	511-516B	Critical Stress Intensity for Off-Axis Fracture of Al <sub>2</sub> O <sub>3</sub> Fiber- Reinforced Magnesium.  Tensile and Fatigue Behavior of Aluminum Oxide Fiber-	756-760A
Lead compounds, Sorption Distribution of Lead Between Copper and Matte and the Ac-		Reinforced Magnesium Composites. I.—Fiber Fraction and Orientation.  Tensile and Fatigue Behavior of Aluminum Oxide Fiber-	1389-1396A
tivity of PbS in Copper-Saturated Mattes.  Levitation melting	441-449B	Reinforced Magnesium Composites. II. — Alloying Effects.	1397-1405A
Heat and Fluid Flow Phenomena in a Levitation Melted Sphere Under Zero Gravity.	183-186B	Magnesium, Ternary systems Thermodynamic Properties of Liquid Mg—In—Cd Ternary Solutions.	543-546B
See Fatigue life Tool life		Magnesium base alloys, Composite materials Tensile and Fatigue Behavior of Aluminum Oxide Fiber- Reinforced Magnesium Composites. II.—Alloying Effects.	1397-1405A
Light metals See Aluminum		Magnesium base alloys, Phase transformations	
Aluminum base alloys Beryllium		Interlamellar Spacing in Discontinuous Precipitation.  Magnesium base alloys, Powder technology	1055-1062A
Magnesium Magnesium base alloys Titanium		Rapid Solidification Processing of Magnesium—Lithium Alloys.  Magnesium compounds	237-240A
Titanium base alloys Line defects		See Magnesium oxide	
See Dislocations		Magnesium oxide, Reactions (chemical) Influence of MgO Addition on Mineralogy of Iron Ore Sinter.	23-34B
Liquid metals  Velocity Measurement in Wood's Metal Using an Incorporated Magnet Probe.	734-736B	Magnetic effects See Magnetic properties	
Liquid metals, Reactions (chemical) Activities of Oxygen in Liquid Bi—Pb and Bi—Sb Alloys.	141-147B	Magnetic fields See also Critical field (superconductivity) Effect of Applied Magnetic Fields During Directional Solidifi-	
Liquid metals, Solubility The Dissolution of Titanium in Liquid Steel. Oxygen Solubility in Liquid Indium and Oxygen Diffusivity in	47-58B	cation of Eutectic Bi/Mn.  Magnetic force	2155-2161A
Liquid Indium and Tin.	329-335B	See Magnetic fields  Magnetic properties, Alloying effects	
Con the Relationship Between Interaction Coefficients.	677-680B	Effect of Antimony on Recrystallization Behavior and Mag- netic Properties of a Nonoriented Silicon Steel.	257-260A
Liquid phase diffusion See Diffusion		Magnetization Measurement Associated With	
Liquid phase sintering Toughness Variation With Test Temperature and Cooling		Gamma → Alpha Martensitic Transformation of Iron Particles in a Cu — 1.59Fe Alloy.	755-756A
Rate for Liquid Phase Sintered W — 3.5Ni — 1.5Fe. Fracture Behavior of W — Ni — Fe Heavy Alloys. Sintering Atmosphere Effects on the Ductility of W — Ni — Fe	121-128A 331-338A	Malcomizing See Nitriding	
Heavy Metals.  Densification and Structural Development in Liquid Phase	747-754A	Manganese, Alloying effects Thermoelectric and Morphological Effects of Peltier Pulsing	
Sintering.  Pore Filling Process in Liquid Phase Sintering.  Ostwald Ripening During Liquid Phase Sintering—Effect of	1065-1074A 1075-1080A	on Directional Solidification of Eutectic Bi/Mn.  Manganese, Alloying elements	2147-2154A
Volume Fraction on Coarsening Kinetics. Interphase Boundary Precipitation in Liquid Phase Sintered	1081-1088A	Studies of Directionally Solidified Eutectic Bi/MnBi at Low Growth Velocities.	2139-2145A
W—Ni—Fe and W—Ni—Cu Alloys.  Carbide Composition Change During Liquid Phase Sintering	1089-1098A	Effect of Applied Magnetic Fields During Directional Solidifi- cation of Eutectic Bi / Mn.	2155-2161A
of a Wear Resistant Alloy.  The Driving Force for Chemically Induced Migration of Molter	1099-1102A	A Quantitative Assessment of the Hardenability Increase Re- sulting From a Superhardenability Treatment.	2185-2191A
Nickel Films Between Tungsten Grains.  Liquidus The Liquidus Surface for the Al—Li—Si System From 0.20%	1503-1505A	Manganese, Diffusion Segregation of Manganese During Intercritical Annealing of Dual-Phase Steels.	1499-1502A
Lithium and 0.20% Silicon.  Lithium, Alloying elements	595-597A	Manganese, Solubility Precipitation in Rapidly Solidified AI—Mn Alloys.	1987-1997A
Correction to "Effect of Lithium on the Mechanical Properties and Microstructure of SiC Whisker Reinforced Aluminum Alloys".	406A	Manganese, Ternary systems Crystallization Studies in the Aluminum-Rich Corner of the Aluminum—Iron—Manganese System.	
Lithium, Recovering An Alternative Method for the Recovery of Lithium From	1	Manganese, Thermal properties Thermochemistry of Binary Liquid Gold Alloys: the Systems	F70 F657

Martensite, Crystal lattices On the Substructure of Athermal and Isothermal Martensites		Forced Velocity Pearlite in High-Purity Fe—C Alloys. II.— Theoretical.	1047-1054A
Formed in an Fe-21Ni-4Mn Alloy.	1555-1562A		1165-1171A
Martensitic stainless steels, Corrosion Near-Threshold Corrosion Fatigue Crack Growth Behavior of		The Influence of Alloying Elements on Impurity-Induced Grain	1335-1338A
Type 422 Stainless Steel at Controlled Maximum Stress In-			1415-1430A 2125-2137A
tensities.	693-699A	Mathematics	2120-213/A
Martensitic stainless steels, Mechanical properties The Wear Behavior of Nitrogen-Implanted Metals.	2221-2229A	See Finite element method	
Martensitic transformations		Mathematical analysis Mathematical models	
Stress-Induced Martensitic Transformation Cycling and Two-	212 2211	Mattes	
Way Shape Memory Training in Cu—Zn—Al Alloys.  The Effect of Processing Conditions and Subsequent Heat	313-321A	See Copper mattes	
Treatment on the Transformation Behavior of Some Rapidly Solidified Copper-Base Shape Memory Alloys.	471.4904	Nickel mattes	
Some Effects of Parent Phase Aging on the Martensitic	471-480A	Measuring instruments	
Transformation in a Cu—Al—Ni Shape Memory Alloy.  Magnetization Measurement Associated With	621-626A	See Calorimeters Probes	
Gamma . Alpha Martensitic Transformation of Iron Parti-		Mechanical properties	
cles in a Cu—1.59Fe Alloy.  The Effect of Microstructure on the Deformation Modes and	755-756A	See also Brittleness	
Mechanical Properties of Ti-6Al-2Nb-1Ta-0.8Mo.		Compressive properties Compressive strength	
<ul> <li>I.—Widmanstätten Structures.</li> <li>"Premartensitic" Phase in Nickel—Aluminum Thin Foils.</li> </ul>	1229-1245A 1353-1357A	Creep (materials)	
The Stabilization of Martensite in Cu-Zn-Al Shape Mem-	1977-1986A	Creep life Creep rate	
ory Alloys. Isothermal Martensitic Transformation in Fe—Ni and	1977-1960A	Creep recovery	
Fe-Ni-C Alloys at Subzero Temperatures.  Influence of Nitrogen Alloying on Hydrogen Embrittlement in	2193-2203A	Creep rupture strength Creep strength	
AISI 304 Type Stainless Steels.	2205-2211A	Ductile brittle transition	
Martensitic transformations, Cooling effects		Ductility Elongation	
The Effect of Quench Rate on the Microstructure, Mechani- cal Properties and Corrosion Behavior of U—6 Wt.% Nb.	1319-1330A	Fatigue (materials) Fatigue life	
Martensitic transformations, Deformation effects	1010 100011	Fatigue limit	
Effect of Prior Cold Work on the Martensite Transformation in	200 2004	Fatigue strength Fracture toughness	
SAE 52100.	299-306A	Hardness	
Martensitic transformations, Microstructural effects The Mechanical Properties of Grain-Refined Beta-CuAlNi		Hydrogen embrittlement Impact strength	
Strain-Memory Alloys.	1613-1621A	Internal friction	
Mass flow, Environmental effects		Modulus of elasticity Plastic flow	
Heat and Fluid Flow Phenomena in a Levitation Melted Sphere Under Zero Gravity.	183-186B	Residual stress	
Mass transfer		Shear stress Superplasticity	
Vacuum Refining Copper Melts to Remove Bismuth, Arsenic and Antimony.	251-257B	Temper brittleness	
Fluid Flow and Mass Transfer in an Inductively Stirred Four-		Tensile properties Tensile strength	
Ton Melt of Molten Steel: a Comparison of Measurements and Predictions.	633-640B	Toughness	
Massive type transformation		Wear resistance Yield strength	
Thermodynamics of the Massive Transformation.	411-419A	Mechanical properties, Alloying effects	
Distinguishing Features of Massive Transformations.  The Nucleation Kinetics, Crystallography and Mechanism of	421-425A	Correction to "Effect of Lithium on the Mechanical Properties	
the Massive Transformation.  Growth Kinetics and Mechanism of the Massive Transforma-	427-435A	and Microstructure of SiC Whisker Reinforced Aluminum Alloys".	406A
tion.	437-447A	Mechanical properties, Welding effects	
Master alloys		Microstructure and Mechanical Properties of a Welded (Alpha + Beta) Titanium Alloy.	1589-1596A
The Grain Refining of Aluminum and Phase Relationships in the Al—Ti—B System.	277-282A	Mechanical tests	1309-1330A
Mathematical analysis		See Fatigue tests	
A Generalized Quadratic Flow Lavy for Sheet Metals.	129-132A	Tension tests	
An Analysis of Biaxial Stretching & a Flat Sheet.  A Test for Randomness of Spatial Distribution of Particles	133-138A	Mechanics See Fluid dynamics	
During Phase Transformations.  Localized Necking of Sheet at Negative Minor Strains.	243-245A 323-329A	Fracture mechanics	
The Law of Additive Reaction Time Applied to the Hydrogen		Kinetics	
Reduction of Porous Nickel-Oxide Pellets. Ternary Diffusion. Solutions With Diffusion Coefficients Lin-	403-406B	Melt spinning Ribbon—Substrate Adhesion Dynamics in Chill Block Melt-	
early Dependent on Concentrations.	1359-1366A	Spinning Processes.	155-161B
Subgrain Growth in Aluminum During Static Annealing. Effects of Gravity on Interdendritic Flow: an Analytical Ap	1502-1503A	The Effect of Processing Conditions and Subsequent Heat Treatment on the Transformation Behavior of Some Rap-	
proach.	2095-2097A	idly Solidified Copper-Base Shape Memory Alloys.	471-480A
Mathematical models	50 705	Melting	
Heat Transfer and Fluid Flow in Plasma Spraying. Numerical Models for Casting Solidification. I.—The Cou	59-70B	See Electron beam melting Levitation melting	
pling of the Boundary Element and Finite Difference Meth ods for Solidification Problems.		Vacuum arc melting	
Numerical Models for Casting Solidification. II Application	1	Melting furnaces	
of the Boundary Element Method to Solidification Problems.	101-107B	See Bottom blown converters Copper converters	
A Mathematical Model for Calculation of Equilibrium Solution	1	LD converters Reverberatory furnaces	
Speciations for the FeCl <sub>3</sub> —FeCl <sub>2</sub> —CuCl <sub>2</sub> —CuCl—HCl— NaCl—H <sub>2</sub> O System at 25°C.	213-219B	The manufacture of the same	
Envelopes of Crack-Like Surfaces for Modeling Cavity	1	Memory (shape) See Shape memory	
Growth.  A New Finite Element Model for Welding Heat Sources.	246-247A 299-305B	Mercury (metal), Extraction	
Comparison of Numerical Modeling Techniques for Complex Two-Dimensional, Transient Heat-Conduction Problems.	307-318B	Kinetic Study of Nonoxidative Leaching of Cinnabar Ore in	13-18B
Estimation of the Parabolic Growth Rate From the	•	Aqueous Hydrochloric Acid—Potassium Iodide Solutions. New Hydrometallurgical Process for Obtaining Mercury From	
Stereological Counting Measurements.  Discussion of "Calculation Method of Equilibrium Composi	391-393A	Cinnabar Ore.	229-233B
tion in the Carbon-Hydrogen-Oxygen System and Its	3	Mercury compounds, Reduction (electrolytic) New Hydrometallurgical Process for Obtaining Mercury From	
Application to Environments of a High-Temperature Gas Cooled Reactor"; Authors Reply.	396-400B	Cinnabar Ore.	229-233B
A Collision Model for Fume Formation in Metal Oxidation.	587-593A	Metal carbides	
On the Relationship Between Interaction Coefficients.  Growth of Intragranular Ferrite in Fe—Ni—P Alloys.	677-680B 867-874A	See also Boron carbide Chromium carbide	
Pattern Selection in Solidification. Interdendritic Spacing, II.—A Comparison of Theory and Ex	961-966A	Niobium carbide	
periment.	977-982A	Metal carbides, Crystal growth	
A Numerical Finite Difference Model of Steady State Cellula and Dendritic Growth.	983-994A	Formation of Metal Carbide Powder by Spark Machining of Reactive Metals.	1117-1127A

## Metal working

****		Charming Poplation in the Vinisity of Carbidge in Sensitived	
Metal working See Cold rolling		Chromium Depletion in the Vicinity of Carbides in Sensitized Austenitic Stainless Steels.	793-811A
Cold working Controlled rolling		Tensile Properties of a 2014 Aluminum Alloy in the Tempera- ture Range 250 to 500°C.	913-922A
Forging Hot rolling		Effect of Retrogression and Reaging Treatments on the Mi-	531-1543A
Stretch forming		Microstructure, Impurity effects	
Metallic glasses, Casting Ribbon—Substrate Adhesion Dynamics in Chill Block Melt- Spinning Processes.	155-161B	Segregation and Influence of Boron on the Impact Toughness to TI—6AI—2Nb—1Ta—0.8Mo Welds and Castings.	505-1507A
Metallic glasses, Phase transformations Precipitation in Rapidly Solidified Al—Mn Alloys.	987-1997A	Microstructure, Welding effects Microstructure and Mechanical Properties of a Welded (Alpha + Beta) Titanium Alloy.	589-1596A
Metallographic structures See Microstructure		Mill scale	
Metallography		See Scale (corrosion) Miscibility	
See Chemical etching Specimen preparation		Miscibility Gap in Fe-Ni-Al and Fe-Ni-Al-Co Sys-	819-1828A
Metalloid compounds See Silicon carbide Silicon compounds		Modification Modification in the Aluminum—Silicon System.	459-469A
Silicon dioxide Metalloids		Modulus of elasticity The High-Temperature Low-Cycle Fatigue Behavior of the	
See Arsenic Boron		Nickel-Base Alloy IN-617.  Moisture	661-670A
Silicon  Metallurgical coke, Reactions (chemical)		See Water Molality	
Reduction of Silica in Coke With Ash of Increased Basicity.	729-732B	See Concentration (composition)	
Metallurgical constituents See Sigma phase		Molarity See Concentration (composition)	
Metastability		Molten metals	
Calculations of Stable and Metastable Equilibrium Diagrams of the Ag—Cu and Cd—Zn Systems.	261-268A	See Liquid metals	
Meteorites, Crystal lattices Nucleation of Intragranular Ferrite in Fe—Ni—P Alloys.	861-865A	Molten salts See Fused salts	
Microalloyed steels See High strength low alloy steels	55 T 555 N	Molybdenum, Binary systems Solute Stabilization for H.C.PF.C.C. Transitions: Co—Mo.	67-72A
Microalloying Effect of Niobium on Austenite Recrystallization and Pearlite	.400 .4004	Molybdenum, Mechanical properties A Microstructural Investigation of the Origin of Brittle Behavior in the Transverse Direction in Molybdenum-Based Alloy	
Colony Size in a Microalloyed Eutectoid Steel.  Microparticles See Particles	1496-1499A	Bars.  Molybdenum, Powder technology Retarded Grain Boundary Mobility in Activated Sintered Mo-	1741-1752A
Microscopy			1103-1110A
See Electron microscopy Scanning electron microscopy		Molybdenum, Ternary systems Nickel-Miuminum-Molybdenum Phase Equilibria. Determination of Isothermal Sections of Nickel-Rich Portion	481-486A
Microshrinkage See Shrinkage		of Ni—Cr—Mo System by Analytical Electron Microscopy.	783-792A
Microstructure See also Fibrous structure Lamellar structure		Molybdenum base alloys, Mechanical properties  A Microstructural Investigation of the Origin of Brittle Behavior in the Transverse Direction in Molybdenum-Based Alloy	
Structure of Vacuum Brazed BNi-5 Joint of Inconel 718. Effects of Prior Cold Rolling and Post-Temper Rolling on the Properties of Continuously Annealed Low-Carbon Dual-	609-620A	Bars. Molybdenum chromium nickel steels	1741-1752A
Phase Steel.  Forced Velocity Pearlite in High-Purity Fe—C Alloys. I.—	671-678A	See Nickel chromium molybdenum steels  Molybdenum chromium steels	
Experimental.	1037-1045A	See Chromium molybdenum steels	
Carbide Composition Change During Liquid Phase Sintering of a Wear Resistant Alloy.	1099-1102A	Molybdenum nickel chromium steels See Nickel chromium molybdenum steels	
The Effect of Minor Alloying Elements on the Mechanical Properties of Al—Cu—Li Alloys. High-Temperature Phase Chemistries and Solidification	1209-1220A	Molybdenum steels See Chromium molybdenum steels	
Mode Prediction in Nitrogen-Strengthened Austenitic Stainless Steels.	1339-1351A	Chromium molybdenum vanadium steels Nickel chromium molybdenum steels	
The Microstructure and Tensile Properties of a Splat- Quenched Al—Cu—Li—Mg—Zr Alloy.	1367-1377A	Monocrystals	
Microstructure—Strength Relations in a Hardenable Stain- less Steel With 16% Chromium, 1.5% Molybdenum and 5%		See Single crystals Monotectic reactions	
Nickel. Structure and Properties of Rapidly Solidified Dispersion- Strengthened Titanium Alloys. I.—Characterization of Dis-	1379-1387A	The Solidification of Monotectic Alloys—Microstructures and Phase Spacings.	1003-1012A
persoid Distribution, Structure and Chemistry.	1451-1463A	Multiaxial stress See Axial stress	
Microstructure, Composition effects Interrelations of Cooling Rate, Microstructure and Mechani- cal Properties in Four HSLA Steels.	1807-1817A	Muriatic acid See Hydrochloric acid	
Microstructure, Cooling effects	1001 101111	Natural gas	
The Effect of Rapid Solidification Velocity on the Microstruc- ture of Ag—Cu Alloys.	55-66A	See Sour gas Necking	
The Effect of Quench Rate on the Microstructure, Mechanical Properties and Corrosion Behavior of U-6 Wt.% Nb.	1319-1330A	Localized Necking of Sheet at Negative Minor Strains.	323-329A
Cooling Rate Effects in Ti-6Al-2Sn-4Zr-2Mo Weld- ments.	1948-1952A	Neutral atmospheres See Inert atmospheres	
Microstructure, Deformation effects		Nickel, Alloying additive	
Microstructural Changes During Isothermal Forging of a Co—Cr—Mo Alloy.  The Effect of Hot Working on Structure and Strength of a Pre-	339-345A	Retarded Grain Boundary Mobility in Activated Sintered Mo- lybdenum.	1103-1110A
cipitation Strengthened Austenitic Stainless Steel. Microstructural Changes Produced in a Multifilamentary Nb / Ti Composite by Cold Work and Heat Treatment.	347-368A	Nickel, Alloying elements Nucleation of Intragranular Ferrite in Fe—Ni—P Alloys. Growth of Intragranular Ferrite in Fe—Ni—P Alloys.	861-865A 867-874A
Local Microstructural Modification in Dynamically Consolidated Metal Powders.		Measurement and Analysis of Distribution Coefficients in Fe—Ni Alloys Containing Sulfur and/or Phosphorus	
Modeling of Dynamic Material Behavior in Hot Deformation: Forging of Ti-6242.	1653-1664A 1883-1892A	<ul> <li>I.—K<sub>N</sub>, and K<sub>p</sub>.</li> <li>Isothermal Martensitic Transformation in Fe—Ni and Fe—Ni—C Alloys at Subzero Temperatures.</li> </ul>	1677-1685A
Microstructure, Heating effects  Modulated Microstructures in Copper—Zinc and Copper—		Nickel, Coatings	
Aluminum—Nickel.  Consequences of the Heterogeneous Nitriding of Alpha-Iron:	269-276A	Heat Transfer and Fluid Flow in Plasma Spraying.  Nickel, Composite materials	59-70B
Dislocation Production and Oriented Precipitation.	627-637A	Tensile Strength of Ni/Cu/(001)Ni Triple Layer Films.	1273-1280A

Nickel, Crystal growth Numerical Treatment of Rapid Solidification.	369-381B	Nickel chromium molybdenum steels, Welding Slag Metal Reactions During Submerged Arc Welding of	
Nickel, Diffusion		Alloy Steels.	217-227A
The Effect of Pressure Modulation on the Flow of Gas Through a Solid Membrane: Permeation and Diffusion of Hydrogen Through Nickel.	639-648A	Nickel chromium steels See also Nickel chromium molybdenum steels	
The Driving Force for Chemically Induced Migration of Molten	1503-1505A	Nickel chromium steels, Diffusion A Grain Boundary Etching Method for the Analysis of Intergranular Phosphorus-Segregation in Iron-Based Alloys.	563-1570A
Nickel, Extraction Control of Autoclave Scaling During Acid Pressure Leaching		Nickel chromium steels, Mechanical properties	
of Nickeliferous Laterite Ore. Hydrogen Reduction Kinetics of Nickel Sulfide in the Pres-	433-440B	Core Hardenability Calculations for Carburizing Steels.  Nickel compounds, Mechanical properties	173-1183A
ence of Calcium Oxide.  Nickel, Mechanical properties  Effects of the Additions of Boron, Phosphorus, Tin and Anti-	719-723B	The Mechanical Behavior of Nonstoichiometric Compounds Ni <sub>3</sub> Si, Ni <sub>3</sub> Ge and Fe <sub>3</sub> Ga. Improved Strength and Ductility in Ni <sub>3</sub> Al by Boron Modifica-	173-181A
mony on Oxygen-Assisted Hydrogen Embrittlement of Nick- el.	519-526A	tion and Rapid Solidification.	399-402A
Nickel, Oxidation The High-Temperature Oxidation of Metals Forming Cation-		Nickel compounds, Oxidation Oxidation of Nickel Sulfide.	127-133B
Diffusing Scales.  The High-Temperature Oxidation of Metals Forming Cation- Diffusing Scales.	195B 765-782A	Nickel compounds, Reduction (chemical) The Law of Additive Reaction Time Applied to the Hydrogen Reduction of Porous Nickel-Oxide Pellets.	403-406B
Nickel, Recovering The Precipitation of Ni <sub>3</sub> S <sub>2</sub> From Sulfate Solutions.	609-615B	Hydrogen Reduction Kinetics of Nickel Sulfide in the Presence of Calcium Oxide.	719-723B
Nickel, Refining The Interfacial Kinetics of the Reaction of CO <sub>2</sub> With Liquid	000-0100	Nickel mattes, Reduction (chemical) Oxidation of Nickel Sulfide.	127-133B
Nickel. Nickel, Solubility	655-661B	Nickel molybdenum chromium steels See Nickel chromium molybdenum steels	
Distribution of Nickel Between Copper—Nickel and Alumina- Saturated Iron Silicate Slags.	33-37B	Nickel molybdenum steels  See Nickel chromium molybdenum steels	
Nickel, Ternary systems Nickel—Aluminum—Molybdenum Phase Equilibria.	481-486A	Nickel plating Enhanced Tensile Strength for Electrodeposited Nickel/	
Zero-Flux Planes and Flux Reversals in the Cu—Ni—Zn System at 775°C.	649-659A	Copper Multilayer Composites.	2039-2040A
Determination of Isothermal Sections of Nickel-Rich Portion of Ni—Cr—Mo System by Analytical Electron Microscopy.  Miscibility Gap in Fe—Ni—Al and Fe—Ni—Al—Co Sys-	783-792A	Nickel steels  See also Nickel chromium molybdenum steels  Nickel chromium steels	
tems.  Nickel, Thermal properties	1819-1828A	Nickel steels, Mechanical properties Consideration on the Intergranular Tempered Martensite Em-	
Thermochemistry of Binary Liquid Gold Alloys: the Systems Au—Ni, Au—Co, Au—Fe and Au—Mn.	573-580B	brittlement.  The Role of the Constituent Phases in Determining the Low Temperature Toughness of 5.5Ni Cryogenic Steel.	393-395A 2213-2219A
Nickel base alloys, Brazing Structure of Vacuum Brazed BNi-5 Joint of Inconel 718.	609-620A	Niobium, Alloying additive Effect of Niobium on Austenite Recrystallization and Pearlite	
Nickel base alloys, Extrusion The Structure of Extruded NiAl.	1129-1136A	Colony Size in a Microalloyed Eutectoid Steel.  Niobium, Alloying elements	1496-1499A
Nickel base alloys, Mechanical properties  Behavior of Fe—Ni—Cr Alloys in a Complex Multioxidant Environment Under Conditions of Dynamic Straining.	11-22A	Grain Refinement of Niobium Steels by Control of Recrystall- ization During Hot Rolling.	87-98A
The Effects of a Liquid Sulfate / Chloride Environment on Su- peralloy Stress Rupture Properties at 704°C.	23-28A	Niobium, Powder technology The Influence of Gas Atmospheres on the First-Stage Sinter-	
The Effect of Protective Coatings on the High-Temperature Properties of a Gamma Prime-Strengthened Nickel-Base		ing of High-Purity Niobium Powders.  Niobium base alloys, Composite materials	1111-1116A
Superalloy.  Effect of Environment on Creep Crack Growth in PM/HIP René-95.	229-236A 381-388A	Microstructural Changes Produced in a Multifilamentary Nb/ Ti Composite by Cold Work and Heat Treatment.	843-852A
The High-Temperature Low-Cycle Fatigue Behavior of the Nickel-Base Alloy IN-617.	661-670A	Niobium base alloys, Mechanical properties Effects of Hydrogen on Mechanical Properties of	
Prior Deformation Effects on Creep and Fracture in Inconel Alloy X-750.		Vanadium—Niobium Alloys.	147-153A
Crack Growth in a Single-Crystal Superalloy at Elevated Temperature.		Niobium carbide, Solubility Solubility Product for Niobium Carbide in Austenite.	541-544A
Elevated-Temperature Compressive Steady State Deforma- tion and Failure in the Oxide Dispersion Strengthened Alloy MA 6000E.	1753-1762A	Solubility of Niobium Carbide and Niobium Carbonitride in Al- loyed Austenite and Ferrite.	545-553A
Tensile Behavior of Inconel Alloy X-750 in Air and Vacuum at Elevated Temperatures.		Niobium compounds See also Niobium carbide	
Effect of Oxidation Kinetics on the Near Threshold Fatigue Crack Growth Behavior of a Nickel-Base Superalloy.		Niobium compounds, Composite materials Effect of Tantalum Additions Upon In Situ Prepared Nb <sub>3</sub> Sn—	
Deformation and Fracture Behavior of Ni/Mo/Al (Gamma/ Gamma Prime-Alpha) In Situ Composite.	1905-1919A	Cu Superconducting Wire. Nitriding	283-286A
Nickel base alloys, Melting Observations of Melt Rate as a Function of Arc Power, CC		Consequences of the Heterogeneous Nitriding of Alpha-Iron: Dislocation Production and Oriented Precipitation.	627-637A
Pressure and Electrode Gap During Vacuum Consumable Arc Remelting of Inconel 718.		Resistometric Study of Fe—V and Fe—Mo Nitrided by Constant Activity Aging.	
Nickel base alloys, Phases (state of matter) "Premartensitic" Phase in Nickel—Aluminum Thin Foils.	1353-1357A	Nitrogen, Alloying elements	
Nickel base alloys, Powder technology Rapidly Soliditied Prealloyed Powders by Laser Spin Atom		Influence of Nitrogen Alloying on Hydrogen Embrittlement in AISI 304 Type Stainless Steels. The Wear Behavior of Nitrogen-Implanted Metals.	2205-2211A 2221-2229A
ization. The Fracture Behavior of Tungsten Wire-Reinforced Superal	149-153B	Nitrogen, Solubility Surface Interactions in the Iron—Nitrogen System.	199-202A
loy Composites During Isothermal Forging.  Nickel base alloys, Structural hardening	501-510A	Nitrogen compounds See Carbonitrides	
Precipitation of Beta Phase in the Gamma Prime Particles o Nickel-Base Superalloy.	1331-1334A	Nodular iron, Heat treatment Laser Processing of Cast Iron for Enhanced Erosion Resis	
Nickel chromium molybdenum steels, Mechanical properties		tance.	719-728A
Crack Paths and Hydrogen-Assisted Crack Growth Re sponse in AISI 4340 Steel. Core Hardenability Calculations for Carburizing Steels.	735-746A 1173-1183A	Nonferrous alloys, Phase transformations  The Nucleation Kinetics, Crystallography and Mechanism o the Massive Transformation.	427-435A
Hydrogen-Induced Interior Crack-Tip Morphologies in High Strength Steel. Low-Temperature Improvement of the Mechanical Propertie	1865-1871A	Nonferrous smelting See Smelting	
of 4340-Type Ultra-High-Strength Steel With Heat Treatin Techniques Using Interrupted Quenching Method. Nickel chromium molybdenum steels, Powder	2247-2249A	sion Spacings and on Directionality of Ductility in Ho	
technology Local Microstructural Modification in Dynamically Consol dated Metal Powders	i- 1653-1664A	Rolled C — Mn Steels.  Notch brittleness See Brittleness	1209/1204A

Notch ductility See Ductility		Oxides, Binary systems A Generalized Approach to the Flood—Knapp Structure	
Notch impact strength See Impact strength		Based Model for Binary Liquid Silicates: Application and Update for the PbO — SiO <sub>2</sub> System.	511-516B
Notched bar tensile test See Tension tests Nozzles		Oxides, Reduction (chemical) The Law of Additive Reaction Time Applied to the Hydrogen Reduction of Porous Nickel-Oxide Pellets. Whisker Growth in Reduction of Oxides.	403-406B 685-694B
Thermodynamics of Nozzle Blockage in Continuous Casting of Calcium-Containing Steels.	547-562B	Oxidizing See Oxidation	
Correction to Thermodynamics of Nozzle Blockage in Contin- uous Casting of Calcium-Containing Steels.	547-562B	Oxygen, Diffusion Isotope Exchange Studies of the Rate of Dissociation of CO <sub>2</sub>	
Nuclear reactors See Gas cooled reactors Sodium cooled reactors		on Liquid Iron Oxides and CaO-Saturated Calcium Ferrites.  Oxygen, Environment	563-571B
Nucleation		Chlorination of Cobalt in an Argon — 1% Oxygen — 1% Chlorine Mixture at 1000K.	403-405A
Recrystallization in Commercially Pure Aluminum. Numerical Treatment of Rapid Solidification. The Nucleation Kinetics, Crystallography and Mechanism of	287-297A 369-381B	Oxygen, Reactions (chemical) Activities of Oxygen in Liquid Bi—Pb and Bi—Sb Alloys.	141-147B
the Massive Transformation.  Nucleation of Intragranular Ferrite in Fe—Ni—P Alloys.  Solidification of Highly Undercooled Sn—Pb Alloy Droplets.	427-435A 861-865A 1303-1310A	Activity Coefficient of Oxygen in Copper—Sulfur Metts. Activity Coefficient of CuO <sub>0.5</sub> in Alumina-Saturated Iron Silicate Slags.	337-344B 345-349B
Nucleation of Recrystallization in a Co—Cr—Mo Alloy.  Nuclei (transformation)	1335-1338A	Discussion of "Calculation Method of Equilibrium Composi- tion in the Carbon—Hydrogen—Oxygen System and Its Application to Environments of a High-Temperature Gas	
See Nucleation Obstructing		Cooled Reactor"; Authors Reply.  Oxygen, Solubility	396-400B
See Blocking Open flame furnaces		Interactions of Gases in Molten Salts: Carbon Dioxide and Oxygen in Cryolite Alumina Melts.	39-46B
See Reverberatory furnaces Optical masers		Oxygen Solubility in Liquid Indium and Oxygen Diffusivity in Liquid Indium and Tin.	329-335B
See Lasers		Oxygen, Ternary systems Phase Relationships in the System Fe—Na—O.	319-327B
Order disorder  Some Effects of Parent Phase Aging on the Martensitic  Transformation in a Cu—Al—Ni Shape Memory Alloy.	621-626A	Oxygen blown converters See LD converters	
The Fracture of Ordered (Fe, Co) <sub>3</sub> V.  Order disorder, Heating effects Heating Rate Dependence of Disordering in Alpha-Cu—Al Al-	701-706A	Oxygen compounds, Oxidation Thermodynamics of the Oxidation of Rare Earth Oxysulfides at High Temperatures.	523-528B
loys.	1999-2008A	Oxygen conversion processes See Oxygen steel making	
Ordering See Order disorder		Oxygen steel making	74.750
Ores See Chalcopyrite Ilmenite		Mixing of Concentric Gas Jets Issuing Vertically Into a Liquid.  A New Approach to Investigate the Drop Size Distribution in Basic Oxygen Steelmaking.	71-75B 109-116B
Iron ores Laterites		Packing (crystal density) See Crystal structure	
Sphalerite		Parameters	
Organic compounds, Chemical analysis Electrochemical Determination of Thiourea and Glue in the Industrial Copper Electrolyte.	451-459B	See Lattice parameters  Particle shape, Diffusion effects	110 1501
Orientation See also Preferred orientation		Shape Changes During Dissolution of Theta Prime-CuAl <sub>2</sub> .  Particle size	449-458A
Consequences of the Heterogeneous Nitriding of Alpha-Iron: Dislocation Production and Oriented Precipitation.	627-637A	A New Approach to Investigate the Drop Size Distribution in Basic Oxygen Steelmaking. The Influence of Gas Atmospheres on the First-Stage Sinter-	109-116B
Direct Measurement of the Work of Fracture for Grain Bound- aries of Twist Misorientation About (100) in Tungsten. Tensile and Fatigue Behavior of Aluminum Oxide Fiber-	1289-1292A	ing of High-Purity Niobium Powders.	1111-1116A
Reinforced Magnesium Composites. I. — Fiber Fraction and Orientation.	1389-1396A	Particle size distribution  A New Approach to Investigate the Drop Size Distribution in Basic Oxygen Steelmaking.	109-116B
High-Temperature Oxidation of Iron at 1200°C in a Hot Stage Environmental Scanning Electron Microscope.	2231-2240A	Rapid Solidification of a Droplet-Processed Stainless Steel. Structure and Properties of Rapidly Solidified Dispersion-	819-833A
OSM process See Oxygen steel making		Strengthened Titanium Alloys. I.—Characterization of Dis- persoid Distribution, Structure and Chemistry.	1451-1463A
Overaging Temper-Aging of Continuously Annealed Low-Carbon Dual-		Particles, Diffusion Ostwald Ripening During Liquid Phase Sintering—Effect of Volume Fraction on Coarsening Kinetics.	1081-1088A
Phase Steel.  Oxidation	73-86A	Patterns	1001-1000A
Behavior of Fe—Ni—Cr Alloys in a Complex Multioxidant En- vironment Under Conditions of Dynamic Straining.	11-22A	See Diffraction patterns Pearlite	
The High-Temperature Oxidation of Metals Forming Cation- Diffusing Scales.	195B	A Review of the Data on the Interlamellar Spacing of Pearlite.  Pearlite, Alloying effects	1019-1036A
The High-Temperature Oxidation of Metals Forming Cation- Diffusing Scales. Effect of Oxidation Kinetics on the Near Threshold Fatigue	765-782A	Effect of Niobium on Austenite Recrystallization and Pearlite Colony Size in a Microalloyed Eutectoid Steel.	1496-1499A
Crack Growth Behavior of a Nickel-Base Superalloy. High-Temperature Oxidation of Iron at 1200°C in a Hot Stage		Pearlite, Crystal growth Forced Velocity Pearlite in High-Purity Fe—C Alloys. I.—	
Environmental Scanning Electron Microscope. Crystallographic and Morphological Characteristics of Oxi- dation Growth Pits in Wustite Grown at 1200°C.	2231-2240A 2241-2246A	Experimental.  Forced Velocity Pearlite in High-Purity Fe—C Alloys. II.— Theoretical.	1037-1045A 1047-1054A
Oxidation, High temperature effects		Penetration	1047-1054A
In Situ Observation of Copper Oxidation at High Tempera- tures.  A Collision Model for Fume Formation in Metal Oxidation.	573-586A 587-593A	The Effect of Pressure Modulation on the Flow of Gas Through a Solid Membrane: Permeation and Diffusion of Hydrogen Through Nickel.	639-648A
Oxidation rate Oxidation of Nickel Sulfide.	127-133B	Perforations See Holes	000 010/1
Oxide cathodes See Cathodes	.2. 1000	Peripheral speed	
Oxides See also Aluminum oxide		See Rotation Permeability, Coating effects The Effects Tip Register the Desceptibility of Hudsane	
See also Aluminum oxide Carbon dioxide Iron oxides		The Effect of a Tin Barrier on the Permeability of Hydrogen Through Mild Steel and Ferritic Stainless Steel.	2093-2095A
Magnesium oxide Silicon dioxide		Permeation See Penetration	
Titanium dioxide Wustite		Phase boundary The Gamma Phase Boundary of CuBe Alloys.	939-941A

Interphase Boundary Precipitation in Liquid Phase Sintered W—Ni—Fe and W—Ni—Cu Alloys.	1089-1098A	Physical metallurgy Process R & D—the Noranda Process.	411-432B
Phase decomposition, Alloying effects The Isothermal Decomposition of Austenite in Hot Rolled		Distribution of Lead Between Copper and Matte and the Ac- tivity of PbS in Copper-Saturated Mattes.	441-449B
Microalloyed Steels.  Phase decomposition, Stress effects Precipitation of Nb(CN) During High-Strain Rate Compres-	1137-1145A	Physical properties See Adhesion Diffusivity	
sion Testing of a 0.07% Niobium-Bearing Austenite.	241-243A	Heat of formation	
Phase diagram reactions See Austenitizing		Heat of mixing Heat of solution Magnetic properties	
Eutectoid reactions Martensitic transformations		Miscibility	
Monotectic reactions		Permeability Porosity	
Phase decomposition		Solid solubility Solubility	
Phase diagrams See also Pourbaix diagrams		Texture Thermal expansion	
Constitution of the Lead—Tin—Strontium. System Up to 36 Atomic Percent Strontium.	43-54A	Thermal stability	
Solute Stabilization for H.C.PF.C.C. Transitions: Co-Mo. Calculations of Stable and Metastable Equilibrium Diagrams	67-72A	Thermoelectricity	
of the Ag-Cu and Cd-Zn Systems.	261-268A	Piezoresistance See Electrical resistance	
The Grain Refining of Aluminum and Phase Relationships in the Al—Ti—B System.	277-282A	Pipe, Welding	
Phase Relationships in the System Fe—Na—O. Nickel—Aluminum—Molybdenum Phase Equilibria.	319-327B 481-486A		1165-1171A
Thermodynamic Properties of Liquid Mg—In—Cd Ternary Solutions.	543-546B	Plasma arc plating See Plasma spraying	
The Liquidus Surface for the AI-Li-Si System From 0.20%		Plasma arc spraying	
Lithium and 0.20% Silicon.  Phase Relationships in the Fe—Cr—C System at Solidifica-	595-597A	See Plasma spraying	
tion Temperatures.  Determination of Isothermal Sections of Nickel-Rich Portion	663-676B	Plasma jet spraying See Plasma spraying	
of Ni—Cr—Mo System by Analytical Electron Microscopy.  Miscibility Gap in Fe—Ni—Al and Fe—Ni—Al—Co Sys-	783-792A	Plasma spraying Heat Transfer and Fluid Flow in Plasma Spraying.	59-70B
tems. Thermodynamic Analysis of the Iron—Copper System.	1819-1828A	Plastic flow	29-10B
I.—The Stable and Metastable Phase Equilibria.  Phase stability	1921-1930A	A Generalized Quadratic Flow Law for Sheet Metals. Flow and Fracture of a Multiphase Alloy MP35N for Study of	129-132A
Metastable Phases in the Early Stage of Precipitation in Al— Mg Alloys.	835-842A	Workability.  Plastic flow, Microstructural effects	1837-1847A
The Role of the Constituent Phases in Determining the Low Temperature Toughness of 5.5Ni Cryogenic Steel.	2213-2219A	Slip Directions in B2 Fe—Al Alloys. High-Temperature Plastic-Flow Behavior of Mixtures of Aus-	395-399A
Phase stability, Heating effects The Stabilization of Martensite in Cu—Zn—Al Shape Memory Alloys.	1977-1986A	tenite, Cementite, Ferrite and Pearlite in Plain-Carbon Steels.	2041-2058A
Phase structure	1977-1900A	Plastic flow, Stress effects Strain-Rate Sensitivity of Zinc Sheet.	1265-1271A
See Solid phases Phase transformations		Plasticity See Superplasticity	
See also Austenitizing		Plating	
Martensitic transformations Massive type transformation		See Copper plating Duplex plating	
A Test for Randomness of Spatial Distribution of Particles During Phase Transformations. Interlamellar Spacing in Discontinuous Precipitation.	243-245A 1055-1062A	Nickel plating Polycrystals, Mechanical properties	
Phase transformations, Cooling effects Electron Microscopy Studies of Charge Density Wave (CDW) Transitions in a Ti <sub>58</sub> 7Ni <sub>37</sub> 6AI <sub>38</sub> Alloy.	1155-1163A	Dependence of Dynamic Fracture Resistance on Crack Ve- locity in Tungsten. II.—Bicrystals and Polycrystals.  Pore formation	1253-1258A
Phase transformations, Heating effects	110011	Pore Filling Process in Liquid Phase Sintering.	1075-1080A
Microstructure—Strength Relations in a Hardenable Stain- less Steel With 16% Chromium, 1.5% Molybdenum and 5% Nickel	1379-1387A	Pores See Porosity	
A Quantitative Assessment of the Hardenability Increase Re-		Porosity Sintering Atmosphere Effects on the Ductility of W—Ni—Fe	
sulting From a Superhardenability Treatment.  Phases (state of matter)  See also Sigma phase	2185-2191A	Heavy Metals.  Densification and Structural Development in Liquid Phase Sintering.	747-754A 1065-1074A
Solid phases	609-620A	Porosity, Composition effects	
Structure of Vacuum Brazed BNi-5 Joint of Inconel 718.  Phases (state of matter), Chemical analysis High-Temperature Phase Chemistries and Solidification		On the Effect of NaCl on Porosity in Elemental-Blend Powder Metallurgy Ti—5Al—2.5Sn.	248-249A
Mode Prediction in Nitrogen-Strengthened Austenitic		Postforming See Forming	
Stainless Steels.  Phosphates, Reactions (chemical) Thermodynamics of Phosphate and Phosphide in CaO—	1339-1351A	Potassium compounds, Reactions (chemical) Kinetic Study of Nonoxidative Leaching of Cinnabar Ore in	
CaF <sub>2</sub> Melts.	351-356B	Aqueous Hydrochloric Acid—Potassium Iodide Solutions.	13-18B
Phosphides, Reactions (chemical) Thermodynamics of Phosphate and Phosphide in CaO—CaF <sub>2</sub> Melts.	351-356B	Pots (electrolytic) See Electrolytic cells Pourbaix diagrams	
Phosphorus, Alloying elements		Relationships Between the Pourbaix Diagram for Ag-S- H <sub>2</sub> O and Electrochemical Oxidation and Reduction of	
Nucleation of Intragranular Ferrite in Fe—Ni—P Alloys.  Growth of Intragranular Ferrite in Fe—Ni—P Alloys.	861-865A 867-874A	Ag <sub>2</sub> S.	235-242B
Phosphorus, Diffusion		Powder compacts, Composite materials The Fracture Behavior of Tungsten Wire-Reinforced Superal-	
Grain Boundary Composition and Associated Hydrogen Cracking of Modified 4130 Steels.	565-572A	loy Composites During Isothermal Forging.	501-510A
A Grain Boundary Etching Method for the Analysis of Inter- granular Phosphorus-Segregation in Iron-Based Alloys. Measurement and Analysis of Distribution Coefficients in	1563-1570A	Powder compacts, Mechanical properties  The Microstructure and Tensile Properties of a Splat- Quenched AI—Cu—Li—Mg—Zr Alloy.	1367-1377A
Fe—Ni Alloys Containing Sulfur and/or Phosphorus i.— $K_{N_1}$ and $K_{\rm p}$ .		Powder compacts, Physical properties	
Phosphorus, Dopants	.011 1000A	On the Effect of NaCl on Porosity in Elemental-Blend Powder Metallurgy Ti—5Al—2.5Sn.	248-249A
Effects of the Additions of Boron, Phosphorus, Tin and Anti- mony on Oxygen-Assisted Hydrogen Embrittlement of Nick		Powder metallurgy See Sintering (powder metallurgy)	
el. Phosphorus, Impurities	519-526A	Powder metallurgy parts, Mechanical properties	
The Influence of Alloying Elements on Impurity-Induced Grain Boundary Embrittlement.	1415-1430A	Toughness Variation With Test Temperature and Cooling Rate for Liquid Phase Sintered W—3.5Ni—1.5Fe. Fracture Behavior of W—Ni—Fe Heavy Alloys.	121-128A 331-338A
Photo oxidation See Oxidation		Sintering Atmosphere Effects on the Ductility of W-Ni-Fe Heavy Metals.	747-754A

#### Powder metallurgy parts

Carbide Composition Change During Liquid Phase Sintering		Precipitation heat treatment	
of a Wear Resistant Alloy.  Powder metallurgy parts, Microstructure	1099-1102A	See Aging (artificial) Overaging Precipitation hardening	
Densification and Structural Development in Liquid Phase Sintering. Interphase Boundary Precipitation in Liquid Phase Sintered	1065-1074A	Preferred orientation Residual Stress Evaluation With X-Rays in Steels Having	
W—Ni—Fe and W—Ni—Cu Alloys.  Local Microstructural Modification in Dynamically Consoli-	1089-1098A 1653-1664A	Preferred Orientation. Influence of Texture on Fatigue Properties of Ti—6AI—4V.	1407-1414A 1597-1605A
Powder technology	1003-1004A	Pressing See Hot isostatic pressing	
See Sintering (powder metallurgy) Precious metal alloys		Pressure See Vacuum	
See Silver base alloys Precious metals		Prestressing Prior Deformation Effects on Creep and Fracture in Inconel	
See Gold Silver		Alloy X-750.	1437-1441A
Precipitates  Consideration on the Intergranular Tempered Martensite Embritlement.	393-395A	Probes, Design Velocity Measurement in Wood's Metal Using an Incorporated Magnet Probe.	734-736B
Solubility Product for Niobium Carbide in Austenite. Solubility of Niobium Carbide and Niobium Carbonitride in Al-	541-544A	Projection (forecasting) See Forecasting	
loyed Austenite and Ferrite.  The Influence of Microstructure on Brittle Fracture Tough-	545-553A	Propagation See Crack propagation	
ness. Microstructure—Strength Relations in a Hardenable Stain- less Steel With 16% Chromium, 1.5% Molybdenum and 5%	947-959A	Properzi process See Continuous casting	
Nickel.  Bismuth Precipitation in "Monocrystalline" InBi.	1379-1387A 1963-1967A	Prosthetics See Surgical implants	
Precipitates, Crystal growth Estimation of the Parabolic Growth Rate From the		Protective atmospheres See Controlled atmospheres	
Stereological Counting Measurements.  Dissolution Kinetics of Widmanstätten Gamma-Ag <sub>2</sub> Al Precip-	391-393A 1969-1975A	Punching Punch-Stretching Behavior of a 2014 Aluminum Alloy in the	
ritates. Precipitates, Crystal lattices	1969-1975A	Temperature Range 250 to 500°C.	923-929A
Interphase Boundary Precipitation in Liquid Phase Sintered W—Ni—Fe and W—Ni—Cu Alloys. Precipitation of Beta Phase in the Gamma Prime Particles of	1089-1098A	Quaternary systems, Phases (state of matter) Miscibility Gap in Fe—Ni—Al and Fe—Ni—Al—Co Systems.	1819-1828A
Nickel-Base Superalloy.  Precipitates, Heating effects	1331-1334A	Quench aging Kinetics of Precipitation From Quenched Low-Carbon Steel.	1147-1153A
Microstructural Changes Produced in a Multifilamentary Nb/ Ti Composite by Cold Work and Heat Treatment. Precipitates, Phase transformations	843-852A	Quenching (cooling)  See also Interrupted quenching  Quench aging	
Magnetization Measurement Associated With Gamma → Alpha Martensitic Transformation of Iron Particles in a Cu—1.59Fe Alloy.	755-756A	Rapid solidification Splat cooling Calorimetric Studies of AI—Cu Alloys: Quench Sensitivity	
Precipitates, Solubility Shape Changes During Dissolution of Theta Prime-CuAl <sub>2</sub> .	449-458A	and Sample Preparation.  The Effect of Quench Rate on the Microstructure, Mechanical Properties and Corrosion Behavior of U—6 Wt.% Nb.	389-391A 1319-1330A
Precipitates, Welding effects The Role of Alloy Composition on the Stability of Nitrides in	22.414	Quenching stresses See Residual stress	
Titanium-Microalloyed Steels During Weld Thermal Cycles.  Precipitates, X ray analysis	33-41A	Radiocrystallography See Crystallography	
Identification of Cu <sub>5</sub> Zr Phase in Cu—Zr Alloys.  Precipitation	1491-1493A	Rail steels, Crystal growth Effect of Nicbium on Austenite Recrystallization and Pearlite	
Consequences of the Heterogeneous Nitriding of Alpha-Iron: Dislocation Production and Oriented Precipitation. Kinetics of Precipitation From Quenched Low-Carbon Steel.	627-637A 1147-1153A	Colony Size in a Microalloyed Eutectoid Steel.  Raney nickel	1496-1499A
Precipitation of Beta Phase in the Gamma Prime Particles of Nickel-Base Superalloy. Precipitation in Rapidly Solidified Al—Mn Alloys.	1331-1334A 1987-1997A	See Catalysts Rapid solidification	
Precipitation, Alloying effects The Isothermal Decomposition of Austenite in Hot Rolled		The Effect of Rapid Solidification Velocity on the Microstruc- ture of Ag—Cu Alloys. Rapid Solidification Processing of Magnesium—Lithium Al-	55-66A
Microalloyed Steels. Precipitation, Stress effects	1137-1145A	loys. Numerical Treatment of Rapid Solidification. Improved Strength and Ductility in Ni₃Al by Boron Modifica-	237-240A 369-381B
Precipitation of Nb(CN) During High-Strain Rate Compression Testing of a 0.07% Niobium-Bearing Austenite.	241-243A	tion and Rapid Solidification.  Rapid Solidification of a Droplet-Processed Stainless Steel.	399-402A 819-833A
Hydride Precipitation and Dislocation Substructures in Ti— 5AI—2.5Sn.	813-817A	Solidification of Highly Undercooled Sn—Pb Alloy Droplets. Structure and Properties of Rapidly Solidified Dispersion-	1303-1310A
Precipitation hardening See also Aging (artificial) Calorimetric Studies of Al—Cu Alloys: Quench Sensitivity		Strengthened Titanium Alloys. I.—Characterization of Dis- persoid Distribution, Structure and Chemistry. Precipitation in Rapidly Solidified Al—Mn Alloys.	1451-1463A 1987-1997A
and Sample Preparation.  Some Effects of Parent Phase Aging on the Martensitic Transformation in a Cu—AI—Ni Shape Memory Alloy.	389-391A 621-626A	Rare earth compounds, Oxidation Thermodynamics of the Oxidation of Rare Earth Oxysulfides	
Metastable Phases in the Early Stage of Precipitation in Al— Mg Alloys.		at High Temperatures.  Rare earth metals	523-528B
Age Hardening in Cu-2.5%Ti. Kinetics of Aging in an Fe-12Ni-6Mn Maraging Alloy.	931-937A 1947-1948A	See also Lanthanide metals  Rare earth metals, Alloying elements	
Dissolution Kinetics of Widmanstätten Gamma-Ag <sub>2</sub> Al Precipitates.	1969-1975A	Structure and Properties of Rapidly Solidified Dispersion Strengthened Titanium Alloys. I.—Characterization of Dis	
Precipitation hardening, Cooling effects  The Effect of Quench Rate on the Microstructure, Mechanical Properties and Corrosion Behavior of U—6 Wt.% Nb.		persoid Distribution, Structure and Chemistry.  Structure and Properties of Rapidly Solidified Dispersion  Strengthened Titanium Alloys. II.—Tensile and Creep	)
Precipitation hardening alloys, Forging The Effect of Hot Working on Structure and Strength of a Pre cipitation Strengthened Austenitic Stainless Steel.	347-368A	Properties.  Reaction kinetics Reaction Kinetics of the Ferric Chloride Leaching o	1465-1474A
Precipitation hardening alloys, Mechanical properties		Sphalerite—an Experimental Study.  Kinetic Study of Nonoxidative Leaching of Cinnabar Ore in	5-12B
Effects of Fatigue on the G—P Zones in Al—Zn Alloys.  Precipitation hardening steels, Mechanical properties	1519-1529A	Aqueous Hydrochloric Acid—Potassium Iodide Solutions. The Dissolution of Titanium in Liquid Steel. Kinetics of Leaching of Zinc Ferrite in Aqueous Hydrochlori	13-18B 47-58B
Prevention of Hydrogen Embrittlement by a TiO <sub>2</sub> Surface Layer.	597-600A	Acid Solutions.  The Law of Additive Reaction Time Applied to the Hydrogen	221-228B
Precipitation hardening steels, Structural hardening Microstructure—Strength Relations in a Hardenable Stain less Steel With 16% Chromium, 1.5% Molybdenum and 5%	b	Reduction of Porous Nickel-Oxide Pellets. The Effect of Emergent Dislocations on the Kinetics of De composition of Solid Surfaces Under Conditions of Chemi	403-406B
Nickel.	1379-1387A	cal Reaction Control.	591-594B

The Interfacial Kinetics of the Reaction of CO <sub>2</sub> With Liquid		Reviews	
Nickel. The Breakdown of Dense Iron Layers on Wustite in CO/CO <sub>2</sub>	655-661B	A Review of the Data on the Interlamellar Spacing of Pearlite.	1019-1036A
and H <sub>2</sub> /H <sub>2</sub> O Systems. Establishment of Product Morphology During the Initial	701-708B	Rheological properties Compression of Semisolid Dendritic Sn—Pb Alloys at Low	170 1015
Stages of Wustite Reduction.  Hydrogen Reduction Kinetics of Nickel Sulfide in the Pres-	709-717B	Strain Rates. Ribbons (metallic)	173-181B
ence of Calcium Oxide. Recovery of Elemental Sulfur During the Oxidative Ammonia-	719-723B	See Tapes (metallic)	
cal Leaching of Chalcopyrite.  Kinetics of Aging in an Fe 12Ni-6Mn Maraging Alloy.	726-729B 1947-1948A	Roasting See also Sintering (roasting)	
Reaction sintering		Oxidation of Nickel Sulfide.  Roller hearth annealing	127-133 <b>B</b>
See Activated sintering Reactions (chemical)		See Continuous annealing	
See Carbothermic reactions Chemical attack		Rolling See Cold rolling	
Chlorination Desulfurizing		Controlled rolling Hot rolling	
Hydrogen reduction Oxidation		Rotating beam fatigue tests	
Reactivity (chemical)		See Fatigue tests Rotation	
See Activity (chemical) Reactors		The Effect of Fluid Flow on the Eutectic Lamellar Spacing.	307-312A
See Gas cooled reactors Sodium cooled reactors		Rotational velocity See Rotation	
Recovery See also Creep recovery		Rotational vibration See Rotation	
Precipitation of Nb(CN) During High-Strain Rate Compression Testing of a 0.07% Niobium-Bearing Austenite.	241-243A	Roughing (rolling) See Hot rolling	
Recrystallization See also Grain refinement Grain Refinement of Nichhim Steele by Control of Recrystall		Rupture strength See Creep rupture strength	
Grain Refinement of Niobium Steels by Control of Recrystall- ization During Hot Rolling. Precipitation of Nb(CN) During High-Strain Rate Compres-	87-98A	S N diagrams, Stress effects Existence of the Coaxing Effect and Effects of Small Artifi-	
sion Testing of a 0.07% Niobium-Bearing Austenite.  Nucleation of Recrystallization in a Co—Cr—Mo Alloy.	241-243A 1335-1338A	cial Holes on Fatigue Strength of an Aluminum Alloy and 70-30 Brass.	2029-2038A
Revealing Deformed and Recrystallized Structures in Beta Titanium Alloys.	1493-1496A	Saline water	
Recrystallization, Alloying effects	1493-1490A	See Salt water Salt (sodium chloride)	
Effect of Antimony on Recrystallization Behavior and Mag- netic Properties of a Nonoriented Silicon Steel.	257-260A	See Sodium chloride	
Effect of Niobium on Austenite Recrystallization and Pearlite Colony Size in a Microalloyed Eutectoid Steel.	1496-1499A	Salt roasting See Chloridizing	
Recrystallization, Composition effects		Salt water, Environment	
Effect of Composition and Initial Grain Size on the Dynamic Recrystallization of Austenite in Plain Carbon Steels.	2009-2019A	Near-Threshold Corrosion Fatigue Crack Growth Behavior of Type 422 Stainless Steel at Controlled Maximum Stress In-	
Recrystallization, Deformation effects Recrystallization in Commercially Pure Aluminum.	287-297A	tensities. Sandwich plating	693-699A
The Structure of Extruded NiAl.  Red hardness See Hardness	1129-1136A	See Duplex plating Sap process See Dispersion hardening	
Red shortness		Saws	
See Brittleness		See Hack saws	
Reduction (chemical) See Direct reduction Hydrogen reduction		Scale (corrosion) Control of Autoclave Scaling During Acid Pressure Leaching of Nickeliferous Laterite Ore.	433-440B
Reduction (electrolytic) See Electrowinning		Scale (corrosion), Crystal growth The High-Temperature Oxidation of Metals Forming Cation-	
Reduction (metal working) See Cold rolling		Diffusing Scales. In Situ Observation of Copper Oxidation at High Tempera-	195B
Hot rolling		tures. The High-Temperature Oxidation of Metals Forming Cation-	573-586A
See Electroslag refining		Diffusing Scales. Scale removal	765-782A
Vacuum refining Refractory alloys		See Descaling	
See Molybdenum base alloys Niobium base alloys		Scanning electron microscopy  In Situ Observation of Copper Oxidation at High Tempera-	
Tungsten base alloys Vanadium base alloys		tures.  A Collision Model for Fume Formation in Metal Oxidation.	573-586A 587-593A
Refractory metal compounds		Screw dislocations	
See Chromium carbide Niobium carbide Niobium compounds		High-Temperature Oxidation of Iron at 1200°C in a Hot Stage Environmental Scanning Electron Microscope.  Season cracking	2231-2240A
Vanadium compounds		See Stress corrosion cracking	
Refractory metals See Chromium		Seeding See Nucleation	
Molybdenum Niobium		Segregations	
Tantalum Tungsten		An Analytical Electron Microscope Study of the Kinetics of the Equilibrium Segregation of Bismuth in Copper.	99-105A
Vanadium Reinforcement		Convection in the Two-Phase Zone of Solidifying Alloys. Compression of Semisolid Dendritic Sn—Pb Alloys at Low	
See Fiber composites		Strain Rates.  Grain Boundary Composition and Associated Hydrogen	
Residual stress The Effect of Overload on the Fatigue Crack Propagation in		Cracking of Modified 4130 Steels.  Structural Effects and Band Segregate Formation During the	
Metastable Beta Ti-V Alloys. Residual Stress Evaluation With X-Rays in Steels Having	511-517A	Electromagnetic Stirring of Strand-Cast Steel.  The Influence of Alloying Elements on Impurity-Induced Grain Boundary Embrittlement.	581-589B 1415-1430A
Preferred Orientation. Resistance welds	1407-1414A	Segregation and Influence of Boron on the Impact Toughness to Ti-6AI-2Nb-1Ta-0.8Mo Welds and Castings.	1505-1507A
See Welded joints Revaporization		A Grain Boundary Etching Method for the Analysis of Inter- granular Phosphorus-Segregation in Iron-Based Alloys.	1563-1570A
See Vaporizing		Measurement and Analysis of Distribution Coefficients in Fe-Ni Alloys Containing Sulfur and/or Phosphorus	
Reverberatory furnaces The Nature and Source of Copper Smelter Particulate Emis		I.—K <sub>Ni</sub> and K <sub>p</sub> .  Effects of Gravity on Interdendritic Flow: an Analytical Ap-	1677-1685A
sions.	617-622B	proach.	2095-2097A

The Mechanisms of Formation and Prevention of Channel	2163-2173A	Silicon steels, Mechanical properties Fatigue Crack Propagation in Dual-Phase Steels: Effects of	
Segregation During Alloy Solidification.  Segregations, Heating effects Segregation of Manganese During Intercritical Annealing of	2163-2173A	Ferritic-Martensitic Microstructures on Crack Path Mor-	1193-1207A
Dual-Phase Steels. Self diffusion	1499-1502A	Silver, Alloying elements Dissolution Kinetics of Widmanstätten Gamma-Ag <sub>2</sub> Al Precipitates.	1969-1975A
See Diffusion		Silver, Binary systems	
Semicontinuous casting See Continuous casting		Thermochemistry of Binary Liquid Gold Alloys: the Systems Gold—Copper and Gold—Silver at 1379K. Calculations of Stable and Metastable Equilibrium Diagrams	203-208A
Sensitizing Chromium Depletion in the Vicinity of Carbides in Sensitized Austenitic Stainless Steels.	793-811A	of the Ag—Cu and Cd—Zn Systems.  Silver, Dopants	261-268A
Shape See Perticle chape		Metastable Alloys of Beryllium Prepared by Ion Implantation.	1787-1805A
See Particle shape Shape memory		Silver, Extraction Relationships Between the Pourbaix Diagram for Ag—S—	
Stress-Induced Martensitic Transformation Cycling and Two- Way Shape Memory Training in Cu—Zn—Al Alloys.	313-321A	${ m H_2O}$ and Electrochemical Oxidation and Reduction of ${ m Ag_2S}.$	235-242B
The Effect of Processing Conditions and Subsequent Heat Treatment on the Transformation Behavior of Some Rap- idly Solidified Copper-Base Shape Memory Alloys.	471-480A	Silver base alloys, Microstructure The Effect of Rapid Solidification Velocity on the Microstruc- ture of Ag—Cu Alloys.	55-66A
Some Effects of Parent Phase Aging on the Martensitic Transformation in a Cu—Al—Ni Shape Memory Alloy.	621-626A	Silver base alloys, Phase transformations	55 55%
Shape memory, Microstructural effects The Mechanical Properties of Grain-Refined Beta-CuAlNi		Growth Kinetics and Mechanism of the Massive Transforma- tion.	437-447A
Strain-Memory Alloys.	1613-1621A	Simulation See also Computer simulation	
Shear properties See Shear stress		Estimating Hardness Response of Hot Rolled Steel by Simu-	1507-1509A
Shear stress			2109-2115A
Critical Stress Intensity for Off-Axis Fracture of Al <sub>2</sub> O <sub>3</sub> Fiber- Reinforced Magnesium.	756-760A	Melt.	2117-2124A 2125-2137A
Sheet metal, Mechanical properties Localized Necking of Sheet at Negative Minor Strains. Tensile Properties of a 2014 Aluminum Alloy in the Tempera-	323-329A	Single crystals, Corrosion Stress-Corrosion Cracking of Copper Single Crystals.	1941-1946A
ture Range 250 to 500°C.	913-922A	Single crystals, Mechanical properties	
Strain-Rate Sensitivity of Zinc Sheet.  Sheet metal, Metal working	1265-1271A	Dependence of Dynamic Fracture Resistance on Crack Ve- locity in Tungsten. I.—Single Crystals.	1247-1251A
A Generalized Quadratic Flow Law for Sheet Metals.  An Analysis of Biaxial Stretching of a Flat Sheet.	129-132A 133-138A	Crack Growth in a Single-Crystal Superalloy at Elevated Temperature.	1711-1719A
Sheet steel See Strip steel		Single crystals, Phases (state of matter) Bismuth Precipitation in "Monocrystalline" InBi.	1963-1967A
Shielded arc welding		Single crystals, Reduction (chemical) Hydrogen Reduction of Wustite Single Crystals Doped With	
See Gas tungsten arc welding Submerged arc welding		Magnesium, Manganese, Calcium, Aluminum and Silicon.	383-391B
Shielding Mixing of Concentric Gas Jets Issuing Vertically Into a Liquid.	71-75B	Sinter (material), Chemical analysis Influence of MgO Addition on Mineralogy of Iron Ore Sinter.	23-34B
Shrinkage, Alloying effects Retarded Grain Boundary Mobility in Activated Sintered Mo-		Sintered metal See Powder metallurgy parts	
lybdenum.	1103-1110A	Sintering	
Sigma phase, Crystal growth  Correction to "The Kinetics of Sigma-Phase Precipitation in		See Sintering (powder metallurgy) Sintering (roasting)	
AISI 310 and AISI 316 Steels". Silica	406A	Sintering (powder metallurgy) See also Activated sintering	
See Silicon dioxide		Liquid phase sintering The Influence of Gas Atmospheres on the First-Stage Sinter-	
Silicates, Reactions (chemical) An Alternative Method for the Recovery of Lithium From Spodumene.	725-726B	ing of High-Purity Niobium Powders.  Sintering (roasting)	1111-1116A
Silicon, Alloying elements		Influence of MgO Addition on Mineralogy of Iron Ore Sinter.  Size distribution (particle)	23-34B
Modification in the Aluminum—Silicon System. Fatigue Threshold Studies in Iron, Fe—Si and HSLA Steel. I.—Effect of Strength and Surface Asperities on Closure.	459-469A 875-888A	See Particle size distribution	
Fatigue Threshold Studies in Iron, Fe—Si and HSLA Steel.  II.—Thermally Activated Behavior of the Effective Stress		The Formation of Oscillation Marks in the Continuous Casting of Steel Slabs.	493-509B
Intensity at Threshold. Silicon, Diffusion	889-900A	Slag fuming Injection Phenomena in Nonferrous Processes.	*
Reduction of Silica in Coke With Ash of Increased Basicity.	729-732B	Slags	77-89B
Silicon, Ternary systems The Liquidus Surface for the Al—Li—Si System From 0.20%		Activity Coefficient of CuO <sub>0.5</sub> in Alumina-Saturated Iron Sili- cate Slags.	345-349B
Lithium and 0.20% Silicon.  Silicon carbide, Composite materials	595-597A	Thermodynamics of Phosphate and Phosphide in CaO— CaF <sub>2</sub> Melts.	351-356B
Creep Rupture of a Silicon Carbide Reinforced Aluminum Composite.	139-146A	Slags, Diffusion	
Correction to "Effect of Lithium on the Mechanical Properties and Microstructure of SiC Whisker Reinforced Aluminum	3	Isotope Exchange Studies of the Rate of Dissociation of CO <sub>2</sub> on Liquid Iron Oxides and CaO-Saturated Calcium Ferrites.	563-571B
Alloys". Silicon compounds	406A	Slags, Solubility Distribution of Nickel Between Copper—Nickel and Alumina-	
See also Silicon carbide Silicon dioxide		Saturated Iron Silicate Slags.  Equilibria Between Silica-Saturated Iron Silicate Slags and Molten Cu—As, Cu—Sb and Cu—Bi Alloys.	33-37B 535-541B
Silicon compounds, Mechanical properties The Mechanical Behavior of Nonstoichiometric Compounds		Slip	330:3418
Ni <sub>3</sub> Si, Ni <sub>3</sub> Ge and Fe <sub>3</sub> Ga.	173-181A	See also Slip planes Mechanisms of Slow Fatigue Crack Growth in High-Strength	000 0704
Silicon dioxide, Binary systems A Generalized Approach to the Flood—Knapp Structure		Aluminum Alloys: Role of Microstructure and Environment. The Effect of Microstructure and Environment on Fatigue	
Based Model for Binary Liquid Silicates: Application and Update for the PbO—SiO <sub>2</sub> System.		Crack Closure of 7475 Aluminum Alloy.  Age Hardening in Cu—2.5%Ti.	555-563A 931-937A
Silicon iron See Silicon steels		Dependence of Dynamic Fracture Resistance on Crack Velocity in Tungsten. I.—Single Crystals.	1247-1251A
Silicon steels		Slip, Microstructural effects  The Effect of Microstructure on the Deformation Modes and	
See also Electrical steels Silicon steels, Crystal growth		Mechanical Properties of Ti-6Al-2Nb-1Ta-0.8Mo. I.—Widmanstätten Structures.	1229-1245A
Effect of Antimony on Recrystallization Behavior and Mag netic Properties of a Nonoriented Silicon Steel.	257-260A	Slip planes, Deformation effects Slip Directions in B2 Fe—Al Alloys.	395-399A

Smelter dust, Chemical analysis The Nature and Source of Copper Smelter Particulate Emis-		Solvus (metallurgical) See Solid solubility	
sions. Smelting	617-622B	Sorption See Absorption (material)	
Process R & D—the Noranda Process.	411-432B	Adsorption	
Smelting furnaces  The Nature and Source of Copper Smelter Particulate Emissions.	617-622B	Sour gas A Contribution to the Thermodynamics of High-Temperature Digenite $Cu_{2-\gamma}$ —S.	736-739B
Soaking Comparison of Numerical Modeling Techniques for Complex, Two-Dimensional, Transient Heat-Conduction Problems.	307-318B	Space environment  Heat and Fluid Flow Phenomena in a Levitation Melted Sphere Under Zero Gravity.	183-186B
Sodium, Reactions (chemical) The Determination of the Thermodynamics of the NaF—		Spark erosion machining See Electric discharge machining	
AIF <sub>3</sub> —AI <sub>2</sub> O <sub>3</sub> System With a Solid Electrolyte Cell.  Sodium, Ternary systems	135-139B	Spark machining See Electric discharge machining	
Phase Relationships in the System Fe—Na—O.  Sodium aluminum fluoride	319-327B	Specimen preparation Calorimetric Studies of Al—Cu Alloys: Quench Sensitivity	
See Cryolite  Sodium chloride, Environment  Discussion of "The Effect of Heat Treatments on the Corro-		and Sample Preparation.  Revealing Deformed and Recrystallized Structures in Beta Titanium Alloys.	389-391A 1493-1496A
sion Fatigue Properties of 13% Chromium Stainless Steel in 3% NaCl Aqueous Solution" (and Authors' Reply).	250-251A	Speed See Velocity	
Sodium chloride, Impurities On the Effect of NaCl on Porosity in Elemental-Blend Powder Metallurgy Ti—5AI—2.55n.	248-249A	Spelter See Zinc	
Sodium compounds See Sodium chloride	246-249A	Sphalerite, Reactions (chemical) Reaction Kinetics of the Ferric Chloride Leaching of Sphalerite—an Experimental Study.	5-12B
Sodium cooled reactors Phase Relationships in the System Fe—Na—O.	319-327B	Spheroidal iron See Nodular iron	
Soft annealing See Annealing		Splat cooling The Microstructure and Tensile Properties of a Splat-	1007 1079
Softening See Overaging		Quenched AI—Cu—Li—Mg—Zr Alloy.  Sponginess	1367-1377A
Solid phases A Test for Randomness of Spatial Distribution of Particles	242.2454	See Porosity Spraying	
During Phase Transformations.  Solid solubility Thermodynamics of the Massive Transformation.	243-245A 411-419A	See Plasma spraying  Squeezing See Compressing	
The Gamma Phase Boundary of CuBe Alloys.	939-941A	Stability	
Solid solutions, Diffusion Ternary Diffusion. Solutions With Diffusion Coefficients Linearly Dependent on Concentrations.	1359-1366A	See also Phase stability Thermal stability Morphological Stability in the Presence of Fluid Flow in the Melt.	2117-2124A
Solidification See also Directional solidification		Stainless steels	2117-2124A
Rapid solidification  Numerical Models for Casting Solidification. I.—The Cou- pling of the Boundary Element and Finite Difference Metit-		See also Austenitic stainless steels Ferritic stainless steels Martensitic stainless steels	
ods for Solidification Problems. Numerical Models for Casting Solidification. II. — Application of the Boundary Element Method to Solidification Prob-	91-99B	Stainless steels, Welding Slag Metal Reactions During Submerged Arc Welding of	0.17.0074
lems. Convection in the Two-Phase Zone of Solidifying Alloys.	101-107B 163-172B	Alloy Steels.  Metal Vaporization From Weld Pools.	217-227A 461-469B
The Movement of Particles in Liquid Metals Due to Gravity. Fluid Flow From a Low to a Higher Density Liquid. High-Temperature Phase Chemistries and Solidification	479-485B 681-684B	Static fatigue See Creep rupture strength	
Mode Prediction in Nitrogen-Strengthened Austenitic Stainless Steels.  The Breakdown of Fibrous Structures in Directionally Grown	1339-1351A	Statistical analysis Strain Hardening Behavior of Polycrystalline Iron and Low- Carbon Steels—a Statistical Analysis.	1185-1192A
Monotectic Alloys. Effects of Gravity on Interdendritic Flow: an Analytical Ap-	1626-1631A	Steel constituents See Austenite	
proach. Convection-Induced Distortion of a Solid/Liquid Interface.	2095-2097A 2109-2115A	Ferrite Martensite	
Morphological Stability in the Presence of Fluid Flow in the Melt. The Mechanisms of Formation and Prevention of Channel	2117-2124A	Pearlite  Steel converters See Bottom blown converters	
Segregation During Alloy Solidification.  Solidification, Deformation effects	2163-2173A	LD converters	
Compression of Semisolid Dendritic Sn—Pb Alloys at Low Strain Rates.	173-181B	See Oxygen steel making	
Solidification, Environmental effects The Effects of Water Vapor on Solidification of Galvanized Coatings.	393-395B	Steels See also Aluminum killed steels Austenitic stainless steels	
Solubility	300 3332	Bearing steels Carbon steels	
See also Solid solubility Oxygen Solubility in Liquid Indium and Oxygen Diffusivity in Liquid Indium and Tin.	329-335B	Chromium molybdenum steels Chromium molybdenum vanadium steels	
Solubility Product for Niobium Carbide in Austenite.  Solubility of Niobium Carbide and Niobium Carbonitride in Al-	541-544A	Chromium steels Dual phase steels	
loyed Austenite and Ferrite.  Determination of Isothermal Sections of Nickel-Rich Portion	545-553A	Electrical steels Ferritic stainless steels High speed tool steels	
of Ni—Cr—Mo System by Analytical Electron Microscopy.  Solubility. Composition effects	783-792A	High strength low alloy steels High strength steels	
Interactions of Gases in Molten Salts: Carbon Dioxide and Oxygen in Cryolite Alumina Melts.	39-46B	Low alloy steels Martensitic stainless steels Nickel chromium molybdenum steels	
Solubility, Cooling effects Precipitation in Rapidly Solidified Al—Mn Alloys.	1987-1997A	Nickel chromium steels Nickel steels Precipitation hardening steels	
Solubility, Deformation effects Surface Interactions in the Iron—Nitrogen System.	199-202A	Rail steels Silicon steels	
Solution hardening See Solution strengthening		Stainless steels Tool steels	
Solution strengthening Tensile and Fatigue Behavior of Aluminum Oxide Fiber-		Steels, Casting The Formation of Oscillation Marks in the Continuous Cast-	
Reinforced Magnesium Composites. II.—Alloying Effects.	1397-1405A	ing of Steel Slabs.	493-509B

Structural Effects and Band Segregate Formation During the Electromagnetic Stirring of Strand-Cast Steel.	581-589B	Effect of Tempering on Quasistatic and Impact Fracture Toughness and Mechanical Properties for 5140 H Steel.	901-911A
Strain Induced Cracking in Partially Solidified Tin—Lead Alloy.	739-741B	Stress relieving See Grain refinement	
Steels, Crystal growth Numerical Models for Casting Solidification. II.—Application of the Boundary Element Method to Solidification Prob-		Stress rupture strength See Creep rupture strength	
lems. Fluid Flow From a Low to a Higher Density Liquid.	101-107B 681-684B	Stress strain curves	
A Two-Dimensional Transient Model for Convection in Laser	2175-2184A	The High-Temperature Low-Cycle Fatigue Behavior of the Nickel-Base Alloy IN-617. Strain Hardening Behavior of Polycrystalline Iron and Low-	661-670A
Steels, Heat treatment Comparison of Numerical Modeling Techniques for Complex, Two-Dimensional, Transient Heat-Conduction Problems.	307-318B	Carbon Steels—a Statistical Analysis.  Stress strain curves, Heating effects  Effect of Tempering on Quasistatic and Impact Fracture	1185-1192A
Steels, Mechanical properties Localized Necking of Sheet at Negative Minor Strains.	323-329A	Toughness and Mechanical Properties for 5140 H Steel.  Stress strain curves, Microstructural effects	901-911A
Steels, Refining Charge Transfer at Fe/FeO(CaF <sub>c</sub> ) Electrodes at 1450°C: Exchange Current Density, Electrode Capacitance, Diffu-		The Mechanical Properties of Grain-Refined Beta-CuAlNi	1607-1612A
sivity. Thermodynamics of Phosphate and Phosphide in CaO—	281-288B	Interrelations of Cooling Rate, Microstructure and Mechani-	1613-1621A
CaF <sub>2</sub> Melts. Fluid Flow and Mass Transfer in an Inductively Stirred Four-	351-356B	cal Properties in Four HSLA Steels.  Stress strain curves, Temperature effects	1807-1817A
Ton Melt of Molten Steel: a Comparison of Measurements and Predictions.	633-640B	Elevated-Temperature Compressive Steady State Deforma- tion and Failure in the Oxide Dispersion Strengthened Alloy	1753-1762A
Steels, Solubility The Dissolution of Titanium in Liquid Steel.	47-58B	Stresses	1755-11024
Steels, Welding A New Finite Element Model for Welding Heat Sources.	299-305B	See Axial stress Residual stress	
Step quenching		Shear stress Stress intensity	
See Interrupted quenching Sticking (adhesion)		Stressing See Prestressing	
See Adhesion		Stretch forming	
Stirring See Electromagnetic stirring		Punch-Stretching Behavior of a 2014 Aluminum Alloy in the Temperature Range 250 to 500°C.	923-929A
Stora Kaldo process See Oxygen steel making		Stretching See Stretch forming	
Strain hardening Age Hardening in Cu—2.5%Ti.	931-937A	Strip See Strip steel	
Strain Hardening Behavior of Polycrystalline Iron and Low- Carbon Steels—a Statistical Analysis. Dislocation Substructure as a Function of Strain in a Dual-	1185-1192A	Strip steel, Coating The Effects of Water Vapor on Solidification of Galvanized	202 2058
Phase Steel.	1221-1228A	Coatings. Strontium, Ternary systems	393-395B
Strain hardening, Alloying effects Effects of Hydrogen on Mechanical Properties of Vanadium—Niobium Alloys.	147-153A	Constitution of the Lead—Tin—Strontium. System Up to 36 Atomic Percent Strontium.	43-54A
Strain rate  Tensile Properties of a 2014 Aluminum Alloy in the Temperature Range 250 to 500°C.  Strain-Rate Sensitivity of Zinc Sheet.	913-922A 1265-1271A	Structural hardening See Aging (artificial) Precipitation hardening Strain hardening	
The Influence of Deformation Path on the Slow Strain-Rate Stress Corrosion Cracking of Admiralty Brass Sheet.	1281-1286A	Structural steels See Rail steels	
Strength of materials See Mechanical properties		Structures (crystalline) See Banded structure	
Strengthening (solution)		Crystal structure Dendritic structure	
See Solution strengthening Stress analysis		Fibrous structure Grain structure	
See X ray stress analysis Stress concentration		Intergranular structure Lamellar structure	
Determination of Strain Distributions in Machined Chips.	1777-1779A	Macrostructure Microstructure	
Stress corrosion cracking Near-Threshold Corrosion Fatigue Crack Growth Behavior of		Substructures (crystalline) Widmanstatten structure	
Type 422 Stainless Steel at Controlled Maximum Stress In- tensities.	693-699A	Subgrain boundaries	
The Influence of Deformation Path on the Slow Strain-Rate Stress Corrosion Cracking of Admiralty Brass Sheet.	1281-1286A	See Grain sub boundaries Submerged arc welding	
Stress-Corrosion Cracking of Copper Single Crystals. Investigation of Stress Corrosion Cracking of Cast and	1941-1946A	The Role of Alloy Composition on the Stability of Nitrides in Titanium-Microalloyed Steels During Weld Thermal Cycles.	33-41A
Forged Steel in Water.  Stress corrosion cracking, Microstructural effects	2087-2092A	Slag Metal Reactions During Submerged Arc Welding of Alloy Steels.	217-227A
Effect of Retrogression and Reaging Treatments on the Mi- crostructure of Al-7075-T651.	1531-1543A	A New Finite Element Model for Welding Heat Sources.  Submerged arc welds	299-305B
Stress corrosion resistance See Corrosion resistance		See Welded joints Substructures (crystalline)	
Stress cracking Grain Boundary Composition and Associated Hydrogen		Dislocation Substructure as a Function of Strain in a Dual- Phase Steel.	1221-1228A
Cracking of Modified 4130 Steels.  Stress distribution	565-572A	On the Substructure of Athermal and Isothermal Martensites Formed in an Fe—21Ni—4Mn Alloy.	1555-1562A
See Stress concentration		Suction See Vacuum	
Stress intensity Fatigue in Binary Alloys of B.C.C. Iron. Near-Threshold Corrosion Fatigue Crack Growth Behavior of Type 422 Stainless Steel at Controlled Maximum Stress In-		Sulfates, Environment The Influence of Detormation Path on the Slow Strain-Rate Stress Corrosion Cracking of Admiralty Brass Sheet.	1281-1286A
tensities. Crack Paths and Hydrogen-Assisted Crack Growth Re-	693-699A	Sulfates, Reduction (chemical) The Precipitation of Ni <sub>2</sub> S <sub>2</sub> From Sulfate Solutions.	609-615B
sponse in AISI 4340 Steel.  Critical Stress Intensity for Off-Axis Fracture of Al <sub>2</sub> O <sub>3</sub> Fiber	735-746A	Sulfidation (corrosion)	003-0138
Reinforced Magnesium.  Fatigue Threshold Studies in Iron, Fe—Si and HSLA Steel	756-760A	See Sulfurization Sulfides	
I.—Effect of Strength and Surface Asperities on Closure. Fatigue Threshold Studies in Iron, Fe—Si and HSLA Steel	875-888A	See also Hydrogen sulfide	
II.—Thermally Activated Behavior of the Effective Stress Intensity at Threshold.	889-900A	Sulfides, Crystal growth  The Precipitation of $Ni_3S_2$ From Sulfate Solutions.	609-615B

Sulfides, Diffusion	505 500B	Superheating	
Activity of SnS in Copper-Saturated Matte.  Sulfides, Microstructure	595-598B		2185-2191A
Effect of Shape of Sulfide Inclusions on Anisotropy of Inclu- sion Spacings and on Directionality of Ductility in Hot Rolled C—Mn Steels.	1259-1264A	Superlattices Electron Microscopy Studies of Charge Density Wave (CDW) Transitions in a Ti <sub>58 7</sub> Ni <sub>37 5</sub> Al <sub>3 8</sub> Alloy.	1155-1163A
Sulfides, Oxidation Oxidation of Nickel Sulfide.	127-133B	Superplasticity Effect of Cavitation on Post-Deformation Tensile Properties	
Thermodynamics of the Oxidation of Rare Earth Oxysulfides at High Temperatures.	523-528B	of a Superplastic Copper-Base Alloy.  Supersonic nozzles	1443-1450A
Sulfides, Reduction (chemical) Cell Measurements of the Reduction Potentials of Gas- Phase Emanating From PbS/CaO/C at Elevated Tempera-		See Nozzies Surface alloying	
tures.  Relationships Between the Pourbaix Diagram for Ag—S— H <sub>2</sub> O and Electrochemical Oxidation and Reduction of	19-22B	Metastable Alloys of Beryllium Prepared by Ion Implantation.  Surface chemistry  An Electron Microscope Study of the Featureless Zone Ob-	1787-1805A
Ag.S. Electrodissolution of Lead Sulfide in Different Acidic Media. Hydrogen Reduction Kinetics of Nickel Sulfide in the Pres-	235-242B 605-608B	tained During Rapid Solidification.  Surface defects, Composition effects The Formation of Oscillation Marks in the Continuous Cast-	29-31A
ence of Calcium Oxide.  Sulfides, Reduction (electrolytic) New Hydrometallurgical Process for Obtaining Mercury From	719-723B	ing of Steel Slabs. Surface diffusion	493-509B
Cinnabar Ore.	229-233B	See Diffusion	
Sulfides, Sorption Distribution of Lead Between Copper and Matte and the Activity of PbS in Copper-Saturated Mattes.	441-449B	Surface energy A Numerical Finite Difference Model of Steady State Cellular and Dendritic Growth. The Solidification of Monotectic Alloys—Microstructures	983-994A
Sulfur, Diffusion Reduction of Silica in Coke With Ash of Increased Basicity.	729-732B	and Phase Spacings. Further Considerations on the Thermodynamics of the	1003-1012A
Measurement and Analysis of Distribution Coefficients in Fe—Ni Alloys Containing Sulfur and/or Phosphorus. I.—K <sub>N</sub> , and K <sub>0</sub> .	1677-1685A	Proeutectoid Ferrite Reaction in Fe—C Alloys.  Surface finishing	1287-1288A
Sulfur, Recovering Recovery of Elemental Sulfur During the Oxidative Ammonia-		See also Descaling Surface Interactions in the Iron—Nitrogen System.	199-202A
cal Leaching of Chalcopyrite.	726-729B	Surface hardening See Carburizing	
Sulfur compounds See also Hydrogen sulfide		Laser beam hardening Nitriding	
Sulfur compounds, Reactions (chemical) A Contribution to the Thermodynamics of High-Temperature Digenite Cu <sub>2-y</sub> —S.	736-739B	Surface layer, Chemical analysis An Electron Microscope Study of the Featureless Zone Obtained During Rapid Solidification.	29-31A
Sulfuric acid leaching Control of Autoclave Scaling During Acid Pressure Leaching of Nickeliferous Laterite Ore.	433-440B	Surface properties See Surface structure	
The Precipitation of $Ni_3S_2$ From Sulfate Solutions. Sulfurization	609-615B	Surface temperature Surface structure	
The Sulfidation Attack of a Nickel-Base Alloy at Intermediate Temperatures.  Behavior of Fe—Ni—Cr Alloys in a Complex Multioxidant En-	5-10A	Surface Interactions in the Iron—Nitrogen System. Surface Relief Produced by Diffusion-Induced Boundary Mi- gration in Cu—Zn.	199-202A 495-499A
vironment Under Conditions of Dynamic Straining.	11-22A	Laser Processing of Cast fron for Enhanced Erosion Resistance.	719-728A
Sulphur See Sulfur		Fatigue Behavior of Carburized Steel With Internal Oxides and Nonmartensitic Microstructure Near the Surface. Dislocation-Depth Distribution in High-Temperature Creep.	1431-1436A 1571-1577A
Superalloys, Brazing Structure of Vacuum Brazed BNi-5 Joint of Inconel 718.  Superalloys, Mechanical properties	609-620A	Surface structure, Heating effects Resistometric Study of Fe—V and Fe—Mo Nitrided by Constant Activity Aging.	1545-1554A
The Sulfidation Attack of a Nickel-Base Alloy at Intermediate Temperatures.	5-10A	Surface temperature	1010 100111
Behavior of Fe—Ni—Cr Alloys in a Complex Multioxidant En- vironment Under Conditions of Dynamic Straining. The Effects of a Liquid Sulfate / Chloride Environment on Su-	11-22A	Forced Velocity Pearlite in High-Purity Fe—C Alloys. I.— Experimental.	1037-1045A
peralloy Stress Rupture Properties at 704°C.  The Effect of Protective Coatings on the High-Temperature Properties of a Gamma Prime-Strengthened Nickel-Base		Surgical implants, Materials selection Microstructural Changes During Isothermal Forging of a Co—Cr—Mo Alloy.	339-345A
Superalloy. Effect of Environment on Creep Crack Growth in PM/HIP	229-236A	Synthetic coke See Coke	
René-95. Fatigue Crack Growth Behavior of an Oxide Dispersion-	381-388A	Systems (metallurgical) See Binary systems	
Strengthened MA 956 Alloy. The High-Temperature Low-Cycle Fatigue Behavior of the Nickel-Base Alloy IN-617.	527-539A 661-670A	Quaternary systems Ternary systems	
Prior Deformation Effects on Creep and Fracture in Inconel Alloy X-750.	1437-1441A	Tanks (electrolytic) See Electrolytic cells	
Crack Growth in a Single-Crystal Superalloy at Elevated Temperature. Elevated-Temperature Compressive Steady State Deforma-	1711-1719A	Tantalum, Alloying additive  Effect of Tantalum Additions Upon In Situ Prepared Nb <sub>3</sub> Sn— Cu Superconducting Wire.	283-286A
tion and Failure in the Oxide Dispersion Strengthened Alloy MA 6000E. Tensile Behavior of Inconel Alloy X-750 in Air and Vacuum at Elevated Temperatures.	1753-1762A	Tapes (metallic), Casting Ribbon—Substrate Adhesion Dynamics in Chill Block Melt-	
Effect of Oxidation Kinetics on the Near Threshold Fatigue Crack Growth Behavior of a Nickel-Base Superalloy.		Spinning Processes. Temper brittleness	155-161B
Superalloys, Melting Observations of Melt Rate as a Function of Arc Power, CO Pressure and Electrode Gap During Vacuum Consumable		Discussion of "The Effect of Heat Treatments on the Corro- sion Fatigue Properties of 13% Chromium Stainless Steel in 3% NaCl Aqueous Solution" (and Authors' Reply).	
Arc Remelting of Inconel 718.  Superalloys, Metal working Flow and Fracture of a Multiphase Alloy MP35N for Study of	117-125B	Temper brittleness, Microstructural effects Consideration on the Intergranular Tempered Martensite Embrittlement.	393-395A
Workability.  Superalloys, Powder technology The Fracture Behavior of Tungsten Wire-Reinforced Superal-	1837-1847A	Temperature See Critical temperature Surface temperature	
loy Composites During Isothermal Forging.  Carbide Composition Change During Liquid Phase Sintering	501-510A	Temperature distribution Temperature distribution	
of a Wear Resistant Alloy.  Superalloys, Structural hardening Precipitation of Beta Phase in the Gamma Prime Particles of	1099-1102A	Heat Transfer and Fluid Flow in Plasma Spraying.  Temperature distribution, Environmental effects Heat and Fluid Flow Phenomena in a Levitation Melter	
Nickel-Base Superalloy. Supercooling	1331-1334A	Sphere Under Zero Gravity.  Temperature field	183-186B
Solidification of Highly Undercooled Sn—Pb Alloy Droplets.	1303-1310A	See Temperature distribution	

Tempering Temper-Aging of Continuously Annealed Low-Carbon Dual- Phase Steel. Discussion of "The Effect of Heat Treatments on the Corro- sion Fatigue Properties of 13% Chromium Stainless Steel	73-86A	Ternary systems, Diffusion Zero-Flux Planes and Flux Reversals in the Cu—Ni—Zn System at 775°C. Ternary Diffusion. Solutions With Diffusion Coefficients Linearly Dependent on Concentrations.	649-659A 359-1366A
in 3% NaCl Aqueous Solution" (and Authors' Reply). Effect of Tempering on Quasistatic and Impact Fracture Toughness and Mechanical Properties for 5140 H Steel. Microstructure—Strength Relations in a Hardenable Stain-	250-251A 901-911A	Ternary systems, Phases (state of matter) Constitution of the Lead—Tin—Strontium. System Up to 36 Atomic Percent Strontium.	43-54A
less Steel With 16% Chromium, 1.5% Molybdenum and 5% Nickel. Effect of Tempering on the Carbon Activity and Hydrogen At-	1379-1387A	The Grain Refining of Aluminum and Phase Relationships in the Al—Ti—B System. Phase Relationships in the System Fe—Na—O. Nickel—Aluminum—Molybdenum Phase Equilibria.	277-282A 319-327B 481-486A
The Role of the Constituent Phases in Determining the Low	2021-2027A 2213-2219A	Thermodynamic Properties of Liquid Mg—In—Cd Ternary Solutions.  The Liquidus Surface for the AI—Li—Si System From 0.20%	543-546B
Tenacity See Tensile strength		Lithium and 0.20% Silicon.  Phase Relationships in the Fe—Cr—C System at Solidifica-	595-597A
Tensile modulus See Modulus of elasticity		tion Temperatures.  Determination of Isothermal Sections of Nickel-Rich Portion of Ni—Cr—Mo System by Analytical Electron Microscopy.	663-676B 783-792A
Tensile properties See also Elongation		Crystallization Studies in the Aluminum-Rich Corner of the Aluminum—Iron—Manganese System.	1311-1317A
Tensile strength Yield strength Fatigue in Binary Alloys of B.C.C. Iron.	679-691A		1819-1828A
The Microstructure and Tensile Properties of a Splat- Quenched Al—Cu—Li—Mg—Zr Alloy.	1367-1377A	Testing equipment, Automation A Study of Creep Crack Growth in 2219-T851 Aluminum Alloy Using a Computerized Testing System.	107-120A
Embrittlement of Types 316L and 347 Weld Overlay by Post- Weld Heat Treatment and Hydrogen. Influence of Nitrogen Alloying on Hydrogen Embrittlement in	1475-1484A	Texture Biaxial Deformation of 70-30 Brass: Flow Behaviors, Tex-	
AISI 304 Type Stainless Steels.	2205-2211A	ture, Microstructures.  Texture, Alloying effects	1607-1612A
Tensile properties, Alloying effects  The Effect of Minor Alloying Elements on the Mechanical  Properties of Al—Cu—Li Ailoys.  Tensile and Fatigue Behavior of Aluminum Oxide Fiber-	1209-1220A	Effect of Antimony on Recrystallization Behavior and Mag- netic Properties of a Nonoriented Silicon Steel.	257-260A
Reinforced Magnesium Composites. II. — Alloying Effects.  Tensile properties, Deformation effects	1397-1405A	Thermal analysis Modification in the Aluminum—Silicon System.	459-469A
The Effect of Hot Working on Structure and Strength of a Pre- cipitation Strengthened Austenitic Stainless Steel.	347-368A	Thermal EMF See Thermoelectricity	
Effects of Prior Cold Rolling and Post-Temper Rolling on the Properties of Continuously Annealed Low-Carbon Dual- Phase Steel.	671-678A	Thermal expansion, Cooling effects Isothermal Martensitic Transformation in Fe—Ni and Fe—Ni—C Alloys at Subzero Temperatures.	2193-2203A
Tensile properties, Environmental effects Tensile Behavior of Inconel Alloy X-750 in Air and Vacuum at		Thermal flux See Heat transmission	
Elevated Temperatures.  Tensile properties, Heating effects	1763-1767A	Thermal power See Thermoelectricity	
Temper-Aging of Continuously Annealed Low-Carbon Dual- Phase Steel. Microstructure—Strength Relations in a Hardenable Stain-	73-86A	Thermal properties See Heat of formation Heat of mixing	
less Steel With 16% Chromium, 1.5% Molybdenum and 5% Nickel.  Tensile properties, Microstructural effects	1379-1387A	Heat of solution Thermal expansion Thermal stability	
Sintering Atmosphere Effects on the Ductility of W—Ni—Fe Heavy Metals. Tensile and Fatigue Behavior of Aluminum Oxide Fiber-	747-754A	Thermoelectricity  Thermal stability Rapid Solidification of a Droplet-Processed Stainless Steel.	819-833A
Reinforced Magnesium Composites. I. — Fiber Fraction and Orientation. Effect of Cavitation on Post-Deformation Tensile Properties	1389-1396A	Thermoanalysis See Thermal analysis	
of a Superplastic Copper-Base Alloy.  Structure and Properties of Rapidly Solidified Dispersion- Strengthened Titanium Alloys. II.—Tensile and Creep	1443-1450A	Thermochemistry Thermochemistry of Binary Liquid Gold Alloys: the Systems Au—Ni, Au—Co, Au—Fe and Au—Mn.	573-580B
Properties. Influence of Texture on Fatigue Properties of Ti—6AI—4V. A Microstructural Investigation of the Origin of Brittle Behav-	1465-1474A 1597-1605A	Thermodynamics The Determination of the Thermodynamics of the NaF—AIF <sub>3</sub> —AI <sub>2</sub> O <sub>3</sub> System With a Solid Electrolyte Cell.	135-139B
ior in the Transverse Direction in Molybdenum-Based Alloy Bars. Interrelations of Cooling Rate, Microstructure and Mechani-	1741-1752A	Thermodynamics of the Massive Transformation.  Distribution of Lead Between Copper and Matte and the Activity of PbS in Copper-Saturated Mattes.	411-419A
cal Properties in Four HSLA Steels.  The Effect of Microstructure on the Deformation Modes and Mechanical Properties of Ti—6AI—2Nb—0.8Mo.	1807-1817A	High-Temperature Thermodynamic Properties of the Chro- mium Carbides Cr <sub>7</sub> C <sub>3</sub> and Cr <sub>3</sub> C <sub>2</sub> Determined Using a Gal-	441-449B
II.—Equiaxed Structures. Deformation and Fracture Behavior of Ni/Mo/Al (Gamma/		vanic Cell Technique. Thermodynamics of the Oxidation of Rare Earth Oxysulfides	517-521B
Gamma Prime-Alpha) In Situ Composite.  Cooling Rate Effects in Ti—6AI—2Sn—4Zr—2Mo Weldments.	1905-1919A 1948-1952A	at High Temperatures.  Thermodynamic Properties of Liquid Mg—In—Cd Ternary Solutions.	523-528B 543-546B
Tensile properties, Size effects Tensile Strength of Ni/Ou/(001)Ni Triple Layer Films.	1273-1280A	On the Relationship Between Interaction Coefficients.  A Contribution to the Thermodynamics of High-Temperature	677-680B
Tensile properties, Temperature effects Tensile Properties of a 2014 Aluminum Alloy in the Tempera-		Digenite $Gu_{2-y}$ —S.  Ostwald Ripening and Relaxation in Dendritic Structures.  Further Considerations on the Thermodynamics of the	736-739B 995-1001A 1287-1288A
ture Range 250 to 500°C. Elevated-Temperature Compressive Steady State Deforma- tion and Failure in the Oxide Dispersion Strengthened Alloy	/	Proeutectoid Ferrite Reaction in Fe—C Alloys. Hydrogen Attack in an Austenitic Stainless Steel. Thermodynamics of Several Lewis-Acid-Base Stabilized Transition Metal Alloys.	1485-1490A
MA 6000E. Tensile strength	1753-1762A	Thermoelastic properties	2013-2003A
Enhanced Tensile Strength for Electrodeposited Nickel Copper Multilayer Composites.	2039-2040A	See Internal friction Shape memory	
Tensile strength, Heating effects  Low-Temperature Improvement of the Mechanical Properties	s	Thermoelectric effect See Thermoelectricity	
of 4340-Type Ultra-High-Strength Steel With Heat Treating Techniques Using Interrupted Quenching Method.	2247-2249A	Thermoelectric EMF See Thermoelectricity	
Tensile strength, Microstructural effects The Mechanical Properties of Grain-Refined Beta-CuAIN Strain-Memory Alloys.	i 1613-1621A	Thermoelectricity  Thermoelectric and Morphological Effects of Peltier Pulsing on Directional Solidification of Eutectic Bi/Mn.	2147-2154A
Tensile tests See Tension tests		Thermomechanical treatment See Controlled rolling	
Tensile yield strength See Yield strength		Thermostability See Thermal stability	
Tension tests Strain-Rate Sensitivity of Zinc Sheet.	1265-1271A	Thickness Tensile Strength of Ni/Cu/(001)Ni Triple Layer Films.	1273-1280A

Thin films, Diffusion The Driving Force for Chemically Induced Migration of Molten Nickel Films Between Tungsten Grains.	1503-1505A	Titanium base alloys, Metal working Modeling of Dynamic Material Behavior in Hot Deformation: Forging of Ti-6242.	883-1892A
Thin films, Directional solidification Interlamellar Spacing in Directionally Solidified Eutectic Thin Films.	1013-1017A	Titanium base alloys, Metallography Revealing Deformed and Recrystallized Structures in Beta Titanium Alloys.	1493-1496A
Tig arc welding See Gas tungsten arc welding	.010101111	Titanium base alloys, Phase transformations Electron Microscopy Studies of Charge Density Wave (CDW)	1493-1490A
Tilting furnaces See Bottom blown converters Copper converters LD converters		Titanium base alloys, Powder technology Rapidly Solidified Prealloyed Powders by Laser Spin Atom-	1155-1163A
Time quenching		ization. On the Effect of NaCl on Porosity in Elemental-Blend Powder Metallurgy Ti—5AI—2.5Sn.	149-153B 248-249A
See Interrupted quenching  Tin, Alloying elements  The Mechanisms of Formation and Prevention of Channel Segregation During Alloy Solidification.	2163-2173A	Structure and Properties of Rapidly Solidified Dispersion- Strengthened Titanium Alloys. I.—Characterization of Dis-	1451-1463A
Tin, Coatings The Effect of a Tin Barrier on the Permeability of Hydrogen		Strengthened Titanium Alloys. II.—Tensile and Creep Properties.	1465-1474A
Through Mild Steel and Ferritic Stainless Steel.  Tin, Crystal growth The Movement of Particles in Liquid Metals Due to Gravity.	2093-2095A 479-485B	Titanium base alloys, Sorption Hydride Precipitation and Dislocation Substructures in Ti— 5AI—2.5Sn.	813-817A
Tin, Dopants  Effects of the Additions of Boron, Phosphorus, Tin and Anti- mony on Oxygen-Assisted Hydrogen Embrittlement of Nick- el.	519-526A	Titanium base alloys, Welding Microstructure and Mechanical Properties of a Welded (Alpha + Beta) Titanium Alloy. Cooling Rate Effects in Ti-6AI-2Sn-4Zr-2Mo Weld-	1589-1596A
Tin, Solubility	319-320A	ments. Titanium compounds	1948-1952A
Oxygen Solubility in Liquid Indium and Oxygen Diffusivity in Liquid Indium and Tin.	329-335B	See also Titanium dioxide	
Tin, Ternary systems  Constitution of the Lead—Tin—Strontium. System Up to 36  Atomic Percent Strontium.	43-54A	Titanium compounds, Mechanical properties Deformation in Ti <sub>3</sub> Al Fatigued at Room and Elevated Temperatures.	1721-1729A
Tin base alloys, Crystal growth Convection in the Two-Phase Zone of Solidifying Alloys. Solidification of Highly Undercooled Sn—Pb Alloy Droplets.	163-172B 1303-1310A	<b>Titanium dioxide, Coatings</b> Prevention of Hydrogen Embrittlement by a TiO <sub>2</sub> Surface Layer.	597-600A
Tin base alloys, Metal working Compression of Semisolid Dendritic Sn—Pb Alloys at Low		Titanium ores See Ilmenite	
Strain Rates.  Tin compounds, Composite materials  Effect of Tantalum Additions Upon In Situ Prepared Nb <sub>3</sub> Sn— Cu Superconducting Wire.	173-181B 283-286A	Tool life, Heating effects Microstructure and its Effect on Toughness and Wear Resistance of Laser Surface Melted and Post-Heat Treated High-Speed Steel.	1829-1835A
Tin compounds, Diffusion Activity of SnS in Copper-Saturated Matte.	595-598B	Tool steels See also High speed steel tools	
Titanium, Acoustic properties Determination of the Sources of Acoustic Emission Gener-		High speed tool steels  Tool steels, Mechanical properties	
ated During the Deformation of Titanium.  Titanium, Alloying elements	1849-1853A	Hot Workability of Three Grades of Tool Steels.  Tools  See High speed steel tools	1855-1864A
Grain Refinement of Niobium Steels by Control of Recrystall- ization During Hot Rolling. Microstructural Changes Produced in a Multifilamentary Nb/	87-98A	High speed tool steels Top blown converters	
Ti Composite by Cold Work and Heat Treatment.  Titanium, Dopants	843-852A	See LD converters Toughness	
Metastable Alloys of Beryllium Prepared by Ion Implantation.  Titanium, Machining	1787-1805A	See also Fracture toughness Toughness, Cooling effects	
Formation of Metal Carbide Powder by Spark Machining of Reactive Metals.	1117-1127A	Toughness Variation With Test Temperature and Cooling Rate for Liquid Phase Sintered W—3.5Ni—1.5Fe.	121-128A
Titanium, Solubility The Dissolution of Titanium in Liquid Steel.  Titanium, Ternary systems	47-58B	Toughness, Microstructural effects The Role of the Constituent Phases in Determining the Low Temperature Toughness of 5.5Ni Cryogenic Steel.	2213-2219A
The Grain Refining of Aluminum and Phase Relationships in the Al—Ti—B System.	277-282A	Transferring See Heat transfer	
Titanium base alloys, Composite materials Environmentally Influenced Mixed Mode Fatigue Crack Prop- agation of Titanium Metal/Matrix Composites.	209-215A	Mass transfer  Transformations (materials)  See Martensitic transformations	
Titanium base alloys, Machining Determination of Strain Distributions in Machined Chips.	1777-1779A	Massive type transformation Phase transformations	
Titanium base alloys, Mechanical properties The Role of Alpha and Beta Phases in Fatigue Crack Propa-		Transformer steels See Electrical steels	
gation of Ti—Mn Alloys.  Effect of Microstructure, Strength and Oxygen Content on Fatigue Crack Growth Rate of Ti—4.5AI—5.0Mo—1.5Cr	155-171A	Transition metal alloys See also Cobalt base alloys	
(CORONA 5).  Localized Necking of Sheet at Negative Minor Strains.  The Effect of Overload on the Fatigue Crack Propagation in	183-197A 323-329A	Ferrous alloys Molybdenum base alloys Nickel base alloys	
Metastable Beta Ti — V Alloys.  The Effect of Microstructure on the Deformation Modes and Mechanical Properties of Ti — 6AI — 2Nb — 1Ta — 0.8Mo.	511-517A	Niobium base alloys Titanium base alloys Tungsten base alloys	
I. — Widmanstätten Structures. Segregation and Influence of Boron on the Impact Toughness	1229-1245A	Vanadium base alloys Transition metal alloys, Atomic properties	
to Ti—6AI—2Nb—17a—0.8Mo Welds and Castings. Influence of Texture on Fatigue Properties of Ti—6AI—4V. The Effect of Microstructure and Deformation Behavior or	1505-1507A 1597-1605A	Thermodynamics of Several Lewis-Acid-Base Stabilized Transition Metal Alloys.	2075-2085A
the Hot Ductility of Ti—6AI—2Nb—1Ta—0.8Mo.  The Effect of Microstructure on the Deformation Modes and Mechanical Properties of Ti—6AI—2Nb—0.8Mo	1687-1698A	Transition metal compounds See Chromium carbide Cobalt compounds	
II.—Equiaxed Structures.  Fatigue Crack Growth Mechanics for Ti—6AI—4V (RA) in		Iron compounds Iron oxides	
Vacuum and Humid Air. The Influence of Hydrogen and the Interface Phase on Frac	1931-1940A	Nickel compounds Nicobium carbide	
ture in Ti Code 12.  Yield Loci of HY80, HY100 Steels and		Niobium compounds Titanium compounds	
Ti—6AI—2Nb—1Ta—0.8Mo. The Wear Behavior of Nitrogen-Implanted Metals.	2097-2101A 2221-2229A	Titanium dioxide Vanadium compounds	

#### Transition metals

Transition metals See also Chromium		Vanadium, Alloying elements The Effect of Overload on the Fatigue Crack Propagation in	
Cobalt		Metastable Beta Ti—V Alloys.	511-517A
Manganese Molybdenum		Vanadium base alloys, Mechanical properties  Effects of Hydrogen on Mechanical Properties of  Vanadium—Niobium Alloys.	147-153A
Nickel Niobium		Vanadium compounds, Mechanical properties	
Tantalum Tilanium		The Fracture of Ordered (Fe, Co) <sub>3</sub> V.  Vanadium steels	701-706A
Tungsten Vanadium		See Chromium molybdenum vanadium steels	
Zirconium  Transition metals, Alloying elements		Vaporizing Metal Vaporization From Weld Pools.	461-469B
The Influence of Alloying Elements on Impurity-Induced Grain Boundary Embrittlement.	1415-1430A	Alloying Element Vaporization and Weld Pool Temperature During Laser Welding of AISI 202 Stainless Steel.	641-644B
Transition metals, Thermal properties Thermochemistry of Alloys of Transition Metals. IV.—Alloys of Copper With Scandium, Yttrium, Lanthanum and Lute-		Vapors See Water vapor Veining (structure)	
tium.	357-368B	See Preferred orientation	
Transmission See Conduction Heat transmission		Forced Velocity Pearlite in High-Purity Fe—C Alloys. II.—	
Triaxial stress		Dependence of Dynamic Fracture Resistance on Crack Ve-	1047-1054A
See Axial stress		Dependence of Dynamic Fracture Resistance on Crack Ve-	1247-1251A
Tubular goods See Pipe		locity in Tungsten. II.—Bicrystals and Polycrystals.  Volatilizing	1253-1258A
Tungsten, Composite materials The Fracture Behavior of Tungsten Wire-Reinforced Superal-		See Vaporizing	
loy Composites During Isothermal Forging.	501-510A	Water See also Salt water	
Tungsten, Machining Formation of Metal Carbide Powder by Spark Machining of Reactive Metals.	1117-1127A	Water, Environment Investigation of Stress Corrosion Cracking of Cast and Forged Steel in Water.	2087-2092A
Tungsten, Mechanical properties  Dependence of Dynamic Fracture Resistance on Crack Velocity in Tungsten. I.—Single Crystals.	1247-1251A	Water vapor The Effects of Water Vapor on Solidification of Galvanized Coatings.	393-395B
Dependence of Dynamic Fracture Resistance on Crack Ve- locity in Tungsten. II.—Bicrystals and Polycrystals. Direct Measurement of the Work of Fracture for Grain Bound-	1253-1258A	Water vapor, Environment Environmentally Influenced Mixed Mode Fatigue Crack Prop-	
aries of Twist Misorientation About (100) in Tungsten.  Tungsten, Powder technology	1289-1292A	agation of Titanium Metal/Matrix Composites.  Mechanisms of Slow Fatigue Crack Growth in High-Strength	209-215A
The Driving Force for Chemically Induced Migration of Molten Nickel Films Between Tungsten Grains.	1503-1505A	Aluminum Alloys: Role of Microstructure and Environment.  Wear	369-379A
Tungsten arc welding See Gas tungsten arc welding		See Hot gas corrosion  Wear resistance	
Tungsten base alloys, Powder technology		Carbide Composition Change During Liquid Phase Sintering of a Wear Resistant Alloy.	1099-1102A
Toughness Variation With Test Temperature and Cooling Rate for Liquid Phase Sintered W—3.5Ni—1.5Fe. Fracture Behavior of W—Ni—Fe Heavy Alloys.	121-128A 331-338A	Wear resistance, Alloying effects	2221-2229A
Sintering Atmosphere Effects on the Ductility of W—Ni—Fe Heavy Metals. Interphase Boundary Precipitation in Liquid Phase Sintered W—Ni—Fe and W—Ni—Cu Alloys.	747-754A 1089-1098A	Wear resistance, Heating effects Microstructure and Its Effect on Toughness and Wear Resistance of Laser Surface Melted and Post-Heat Treated	
Turbine blades, Heat treatment	1009-10968	High-Speed Steel.	1829-1835A
Discussion of "The Effect of Heat Treatments on the Corro- sion Fatigue Properties of 13% Chromium Stainless Steel in 3% NaCl Aqueous Solution" (and Authors' Reply).	250-251A	Weld deposited coatings, Mechanical properties Embritlement of Types 316L and 347 Weld Overlay by Post- Weld Heat Treatment and Hydrogen.	1475-1484A
Turbine blades, Mechanical properties The Effect of Protective Coatings on the High-Temperature		Weld metal Metal Vaporization From Weld Pools.	461-469B
Properties of a Gamma Prime-Strengthened Nickel-Base Superalloy.	229-236A	Weld metal, Crystal growth A Two-Dimensional Transient Model for Convection in Laser	
Tuyeres Mixing of Concentric Gas Jets Issuing Vertically Into a Liquid.	71-75B	Melted Pool.  Weld metal, Reactions (chemical)	2175-2184A
High-Pressure Injection of Air Into a Peirce—Smith Copper Converter.	243-250B	Slag Metal Reactions During Submerged Arc Welding of Alloy Steels.	217-227A
Tuyeres, Corrosion Injection Phenomena in Nonferrous Processes.	77-89B	Welded joints, Microstructure Microstructure and Mechanical Properties of a Welded	
Twinning  Nucleation of Recrystallization in a Co—Cr—Mo Alloy.	1335-1338A	(Alpha + Beta) Titanium Alloy. Cooling Rate Effects in Ti—6Al—2Sn—4Zr—2Mo Weld-	1589-1596A
Ultimate tensile strength See Tensile strength		ments. Welding	1948-1952A
Undercooling See Supercooling		See Electron beam welding Electroslag welding Gas tungsten arc welding	
Uranium base alloys, Microstructure  The Effect of Quench Rate on the Microstructure, Mechanical Properties and Corrosion Behavior of U—6 Wt.% Nb.	1319-13304	Laser beam welding Submerged arc welding	
Vacuum		Welds See Welded joints	
The Effect of Microstructure and Environment on Fatigue Crack Closure of 7475 Aluminum Alloy. The Influence of Gas Atmospheres on the First-Stage Sinter-	555-563A	Whiskers (metals), Composite materials Creep Rupture of a Silicon Carbide Reinforced Aluminum Composite.	139-146A
ing of High-Purity Niobium Powders.  Vacuum arc melting	1111-1116A	Whiskers (metals), Crystal growth Whisker Growth in Reduction of Oxides.	685-694B
Observations of Melt Rate as a Function of Arc Power, CO Pressure and Electrode Gap During Vactium Consumable Arc Remelting of Inconel 718.		Widmanstatten structure The Effect of Microstructure on the Deformation Modes and	
Vacuum brazing Structure of Vacuum Brazed BNi-5 Joint of Inconel 718.	609-620A	Mechanical Properties of Ti-6Al-2Nb-1Ta-0.8Mo. I.—Widmanstätten Structures. Grain Boundary Widmanstätten Ferrite Spacings in 0.2%	1229-1245A
Vacuum melting See Vacuum arc melting		Carbon Steel.  The Effect of Microstructure and Deformation Behavior on	1643-1651A
Vacuum refining		the Hot Ductility of Ti-6Al-2Nb-1Ta-0.8Mo.  The Effect of Microstructure on the Deformation Modes and	1687-1698A
Vacuum Refining Copper Melts to Remove Bismuth, Arsenic and Antimony.	251-257B	Mechanical Properties of Ti-6AI-2Nb-0.8Mo. II.—Equiaxed Structures.	1873-1881A

Wire, Superconductivity Effect of Tantalum Additions Upon In Situ Prepared Nb <sub>3</sub> Sn— Cu Superconducting Wire.	283-286A	Z
Nire bar See Billets		2
Nolfram See Tungsten		2
Work hardening		
See Strain hardening Work strengthening		Z
See Strain hardening Workability		Z
See Formability Hot workability		2
Crystallographic and Morphological Characteristics of Oxi-	2231-2240A 2241-2246A	
Wustite, Reduction (chemical) Hydrogen Reduction of Wustite Single Crystals Doped With		
Magnesium, Manganese, Calcium, Aluminum and Silicon. The Breakdown of Dense Iron Layers on Wustite in CO/CO <sub>2</sub>	383-391B	
and H <sub>2</sub> /H <sub>2</sub> O Systems. Establishment of Product Morphology During the Initial	701-708B 709-717B	
Stages of Wustite Reduction.  X ray analysis	709-7176	
See X ray stress analysis X ray diffraction		
See X ray stress analysis		
X ray stress analysis Residual Stress Evaluation With X-Rays in Steels Having Preferred Orientation.	1407-1414A	
Yield strength An Analysis of Biaxial Stretching of a Flat Sheet.	133-138A	
Age Hardening in Cu—2.5%Ti. Fatigue Crack Propagation in Dual-Phase Steels: Effects of Ferritic—Martensitic Microstructures on Crack Path Mor-	931-937A	
phology. Hot Workability of Three Grades of Tool Steels.	1193-1207A 1855-1864A	
Yield strength, Alloying effects  Effects of Hydrogen on Mechanical Properties of Vanadium—Niobium Alloys.	147-153A	
Yield strength, Anisotropy A Generalized Quadratic Flow Law for Sheet Metals.	129-132A	
Yield strength, Cooling effects Improved Strength and Ductility in Ni <sub>3</sub> Al by Boron Modifica-		
tion and Rapid Solidification.  Yield strength, Deformation effects The Effect of Hot Working on Structure and Strength of a Pre-	399-402A	
cipitation Strengthened Austenitic Stainless Steel.  Yield strength, Microstructural effects	347-368A	
The Role of Alpha and Beta Phases in Fatigue Crack Propa- gation of Ti—Mn Alloys.	155-171A	
The Mechanical Behavior of Nonstoichiometric Compounds Ni <sub>3</sub> Si, Ni <sub>3</sub> Ge and Fe <sub>3</sub> Ga.  The Effect of Microstructure on the Deformation Modes and	173-181A	
Mechanical Properties of Ti—6Al—2Nb—1Ta—0.8Mo. I.—Widmanstätten Structures. Biaxial Deformation of 70-30 Brass: Flow Behaviors, Tex-	1229-1245A	
ture, Microstructures. Yielding Anisotropy From the Bauschinger Effect and Crys-	1607-1612A	
tallographic Texture in Drawn HSLA Steel Sheet. High-Temperature Plastic-Flow Behavior of Mixtures of Austenite, Cementite, Ferrite and Pearlite in Plain-Carbon	1699-1710A	
Steels. Yield Loci of HY80, HY100 Steels and	2041-2058A	
Ti-6AI-2Nb-1Ta-0.8Mo.  Yield strength, Stress effects	2097-2101A	
Strain-Rate Sensitivity of Zinc Sheet.  Yield strength, Temperature effects	1265-1271A	
Elevated Temperature Compressive Steady State Deforma- tion and Failure in the Oxide Dispersion Strengthened Alloy MA 6000E.	1753-1762A	
Yield stress See Yield strength		
Youngs modulus		
See Modulus of elasticity  Zinc, Alloying elements		
Surface Relief Produced by Diffusion-Induced Boundary Mi- gration in Cu—Zn.	495-499A	
Zinc, Binary systems Calculations of Stable and Metastable Equilibrium Diagrams of the Ag—Cu and Cd—Zn Systems.	261-268A	
Zinc, Dopants Metastable Alloys of Beryllium Prepared by Ion Implantation.	1787-1805A	
Zinc, Extraction  Reaction Kinetics of the Ferric Chloride Leaching of Sphalerite—an Experimental Study.	5-12B	
Kinetics of Leaching of Zinc Ferrite in Aqueous Hydrochloric Acid Solutions.	221-228B	
Fluidized-Bed Electrodeposition of Zinc.  Zinc, Mechanical properties	623-631B	
Strain-Rate Sensitivity of Zinc Sheet.	1265-1271A	

Zinc, Ternary systems Zero-Flux Planes and Flux Reversals in the Cu—Ni—Zn System at 775°C.	649-659A
Zinc compounds, Reduction (chemical)  Kinetics of Leaching of Zinc Ferrite in Aqueous Hydrochloric Acid Solutions.	221-228B
Zinc ores See Sphalerite	
Zinc plating See Hot dip galvanizing	
Zirconium, Alloying elements Identification of Cu <sub>2</sub> Zr Phase in Cu—Zr Alloys.	1491-1493A
Zirconium, Machining Formation of Metal Carbide Powder by Spark Machining of Reactive Metals.	1117-1127A